

**Influence of morphology on the relaxation behavior of  
*vulcanized PB-SBR diblock copolymers***

DISSERTATION

zur Erlangung des akademischen Grades

doctor rerum naturalium

(Dr. rer. nat.)

genehmigt durch

die Naturwissenschaftliche Fakultät II

Institut für Physik

der Martin-Luther-Universität

Halle-Wittenberg

vorgelegt von

M. Sc. Cecilia Aguiar da Silva

geboren am 19.12.1986 in Recife, Brazil

Halle (Saale), October 12<sup>th</sup>, 2016

Gutachter:

1. Prof. Dr. Mario Beiner
2. Prof. Dr. Gert Heinrich
3. Prof. Dr. Michael Bartke

Öffentliche Verteidigung: November 4<sup>th</sup>, 2016

*Our Father, who art in heaven,  
hallowed be Thy name;  
Thy kingdom come;  
Thy will be done,  
On earth as it is in heaven.  
Give us this day our daily bread.  
And forgive us our trespasses,  
as we forgive those who trespass against us.  
And lead us not into temptation;  
but deliver us from evil.  
[For Thine is the kingdom,  
the power, and the glory,  
forever.  
Amen.*

# Contents

<b>1</b>	<b>Introduction</b>	<b>1</b>
<b>2</b>	<b>Aim of the work</b>	<b>4</b>
<b>3</b>	<b>Theoretical background</b>	<b>5</b>
3.1	Living anionic polymerization of block copolymers.....	5
3.1.1	Polybutadiene stereochemistry depending on the living anionic polymerization conditions.....	6
3.1.2	Living anionic polymerization of styrene-butadiene random copolymer.	8
3.2	Phase separation of block copolymers.....	9
3.2.1	Phase separation of diblock copolymers.....	10
3.2.2	Influence of segregation strength.....	12
3.2.3	Dependence of morphology on block copolymer composition.....	14
3.2.4	Phase diagram of diblock copolymers.....	15
3.3	Thermal and dynamic glass transition.....	16
3.3.1	Thermal glass transition.....	16
3.3.2	The dynamic glass transition.....	18
3.3.3	Special factors influencing the alpha dynamics of diblock copolymers..	22
<b>4</b>	<b>Living anionic polymerization of PB-SBR diblock copolymers</b>	<b>25</b>
4.1	Chemicals.....	25
4.1.1	Polymerization of symmetric and asymmetric PB-SBR diblock copolymers with low <i>1,2-vinyl</i> contents in both blocks.....	25
4.1.2	Polymerization of symmetric PB-SBR diblock copolymers with systematically varied <i>1,2-vinyl</i> contents either in the PB or SBR block...	27
4.2	Molecular characterization.....	28
4.2.1	Gel permeation chromatography (GPC).....	28
4.2.1.1	<sup>1</sup> H nuclear magnetic resonance (NMR).....	29
4.3	PB-SBR diblock copolymer samples.....	29
<b>5</b>	<b>Mixing and vulcanization</b>	<b>32</b>

5.1 Non-filled PB-SBR diblock copolymers.....	32
1.1 Silica-filled PB-SBR composites.....	32
<b>6 Characterization methods</b>	<b>34</b>
6.1 Differential Scanning Calorimetry (DSC).....	34
6.2 Small Angle X-ray Scattering (SAXS).....	35
6.3 Atomic Force Microscopy (AFM).....	38
6.4 Dynamic mechanical analysis (DMA).....	38
<b>7 Results</b>	<b>41</b>
7.1 Non-crosslinked PB-SBR diblock copolymer samples.....	41
7.1.1 Structural analysis by small angle X-ray scattering.....	41
7.1.2 Information about the softening behavior from Differential Scanning Calorimetry.....	44
7.2 PB-SBR diblock copolymers in the crosslinked state.....	52
7.2.1 Structural information from Atomic Force Microscopy (AFM).....	52
7.2.2 Relaxation dynamics from dynamic shear measurements.....	57
7.3 Mechanical performance of silica-filled PB <sub>50</sub> -S <sup>45</sup> B <sup>55</sup> R <sub>50</sub> diblock copolymer composites.....	68
<b>8 Discussion</b>	<b>74</b>
8.1 Order-disorder-transition and interfacial width from thermodynamic models.....	74
8.2 Correlations between block copolymer microstructure, self-assembled morphology and segmental $\alpha$ dynamics.....	81
8.3 Relaxation behavior of silica-filled diblock copolymer composites.....	92
<b>9 Conclusions</b>	<b>94</b>
<b>References</b>	<b>98</b>

# Chapter 1

## Introduction

Since the early years of the 20<sup>th</sup> century, elastomer-nanoparticle composites are commonly used in tire treads.<sup>1</sup> The first reinforcing filler to be used was zinc oxide, however it was replaced by carbon black, around the 1910s, as reinforcement requirement changed. Later, in the 1990s precipitated silica has been introduced as reinforcing filler because its composites have superior wet skid and rolling resistance performance compared to carbon black with similar filler content. From a polymer point of view, natural rubber was the first elastomer used for making tires. However, later during the World War I, synthetic rubber has been developed in Germany due to cut off of natural rubber suppliers. Hence, the possibility to synthesize different elastomers and consequently the use of blends composed of these elastomers opened new opportunities to fine tune tire mechanical performances.

BR/SBR polymer blends are commonly used as elastomeric matrices in composites for passenger tire treads.<sup>2</sup> Depending on the microstructure of the butadiene units in both polymeric units, on the BR/SBR blend ratio and on the styrene content in the SBR copolymer, different phase separation behavior is observed.<sup>3</sup> From a dissipation point of view, the phase separation phenomenon is advantageous in this particular case since contribution from the individual phases superimpose and tire performance parameters, like grip and rolling resistance can be fine-tuned. These are important properties in applications since they are indicators for safety and fuel consumption of the vehicle, respectively. An optimum compromise between these two quantities would be a material having as low as possible rolling resistance combined with high wet grip. Unfortunately, this optimum is hard to obtain and it is a complex fine-tuning problem since rolling resistance is commonly lowered if wet grip is diminished, and vice versa. A commonly used wet grip indicator from the lab experiments is  $\tan\delta$  at 10 Hz and 0°C while the rolling resistance is related to  $\tan\delta$  at 10 Hz and 60°C.<sup>4,5,6</sup> However, one should be aware that this remains a crude approximation based on the time-temperature-superposition principle, since tires are normally used under (more or less) isothermal conditions. The truly application relevant variable determining the wet grip and rolling resistance performances are frequency-dependent dissipation. Low frequencies (in the Hz range)

are related to the rolling resistance while high frequencies (in the kHz range) are responsible for the wet grip.<sup>7,8</sup>

A major drawback of blend-based composites is that the morphology of the polymer matrix and the control over phase dispersion is determined mainly by the processing steps. For instance, a reasonably good phase dispersion with domain size  $\approx 100$  nm can be eventually obtained by shearing the polymer blend-based composites for a longer time and at high speed. However, a coalescence process, i.e. the loss of phase dispersion, take place over time after the processing steps.<sup>9</sup> Therefore, the application of polymer blends as tire tread elastomeric matrices has remaining disadvantages since their morphology is not stable over time and also processing conditions dependent. A direct consequence is an influence on the final tire tread properties.<sup>10</sup>

An alternative concept to overcome these disadvantages of elastomer blends as tire tread matrices would be the use of self-assembled block copolymers of similar chemical composition. This approach allows to control the dissipation behavior and to combine the contributions of two polymeric components in the relaxation spectrum.<sup>11,12,13</sup> The morphology of self-assembled block copolymers is usually well reproducible, tunable and weakly affected by the processing conditions. Therefore, the use of block copolymers has significant advantages compared to blends composed of similar components. The phase separation behavior of block copolymers is broadly investigated and well understood.<sup>14,15,16</sup>

In case of microphase-separated diblock copolymers, different nanostructures like spherical, cylindrical, or lamellar morphologies as well as bicontinuous gyroidal phases can be obtained by varying parameters such as the volume fraction ( $\phi$ ) of individual components and the order parameter  $\chi N$ , where  $\chi$  and  $N$  are the Flory-Huggins segmental interaction parameter and the total length chain, respectively. The value of  $\chi N$  itself is temperature dependent leading in many cases to disorder and miscibility at high temperatures. The relaxation dynamics of well microphase-separated block copolymers is in a first approximation a superposition of those of their components.<sup>17,18</sup> However, many aspects of the relaxation dynamics can depend on details of the block copolymer structure like morphology, domain size or amount of interfacial material. Underlying structure-property relations in block copolymers have not been systematically studied so far. However, these aspects are related to fundamental questions in the field of glass transition research, which are still controversially debated, like those about the influence of (i) domain size and geometrical confinement,<sup>19-27,31</sup> (ii) constraints at interfaces,<sup>31-32,36</sup> (iii) local chemical

composition<sup>37</sup> and (iv) local density<sup>38</sup> on the segmental  $\alpha$  dynamics in amorphous systems with a complex internal structure. Hence, a detailed study of interrelations between block copolymer structure and the segmental  $\alpha$  dynamics in different states seems to be very interesting from the scientific point of view as well as application relevant.

A prominent example of microphase-separated systems is PB-SBR diblock copolymers composed of a styrene-*stat*-butadiene rubber (SBR) block with a butadiene (PB) block. In this particular case, PB-SBR diblock copolymers are an interesting class of materials based on the fact that BR and SBR copolymer are typical polymer components used in tire tread matrices.

The aim of this work is to investigate the interrelations between structure and dynamics of four distinct PB-SBR diblock copolymer series in the non-crosslinked and crosslinked states. This study is important to optimize tire performance such as wet skid and rolling resistance, for example. Some scientific questions will be addressed and discussed in details in **Chapter 8**.

## Chapter 2

### Aim of the work

The aim of this work is to investigate four distinct PB-SBR diblock copolymer series with an average molecular weight of 200 kg/mol. These model systems will be used to study:

- Morphology and dynamic behavior of PB-SBR diblock copolymers in the non-crosslinked as well as in the crosslinked state as a function of: styrene content in the SBR block, volume fraction of the blocks and *1,2-vinyl* contents in the SBR or PB block.
- Phase separation of symmetric PB-SBR diblock copolymers depending on the segregation strength between SBR and PB block due to variation of styrene or *1,2-vinyl* contents in either the SBR or PB block. A thermodynamic model, originally developed for PB/SBR blends, will be applied in order to calculate the effective interaction parameter,  $\chi_{eff}$ , and thus predicting the miscibility behavior of these symmetric PB-SBR diblock copolymers under investigation.
- The dependence of the glass transition of the PB and SBR phases on the *1,2-vinyl* and styrene content, respectively.
- About cooperatively rearranging region (CCRs) in block copolymers and amorphous polymers in general by an experimental approach based on the influence of interfacial material on the  $\alpha$  relaxation dynamics.
- Relaxation behavior and morphology of one series of diblock copolymer based composites. The results will be used in order to learn more about potential advantages of diblock copolymer based composites for their use in tire treads.

## Chapter 3

### Theoretical background

#### 3.1 Living anionic polymerization of block copolymers

Since the early discovery of living anionic polymerization in the mid-1950s, it has become one of the most applied synthesis routes to prepare block copolymers due to its unique ability to yield macromolecules of well-defined molecular architecture and block composition.<sup>39</sup> The anionic polymerization is mostly initiated by an alkyl metal species and featuring: fast initiation, limited promptness to side and/or transfer reactions, no termination, possibility of sequential addition of monomers to the “living chain” and narrow polydispersity of the final block copolymer. The sequential addition of monomers is just possible because the carbanion active center, the only site where chain propagation takes place, remains “alive” and chain growth will continue upon further monomer addition. In order to maintain the “living” center active, i.e. not allowing termination reactions to take place, the reaction medium has to be free of any impurity and moisture (i.e. must be anhydrous) and the polymerization must be carried out under inert atmosphere (i.e. oxygen free). Obviously, the solvent used must be inert and aprotic, otherwise the initiator is deactivated or else termination occurs by the transfer of protons from the solvent to the growing chain.

Among the large amount of block copolymer structures available so far, A-B diblock and A-B-C triblock copolymers are the most exploited ones towards scientific and industrial applications, respectively. A-B diblock copolymers are obtained by first synthesizing the A block, upon complete consumption of all A monomers. The B monomers are subsequently added to the “living A site” and finally when the copolymerization of B monomers reaches about 100% yield, the reaction is terminated by the addition of a hydrogen donor reagent, usually methanol. Besides, copolymerization of A/B random copolymers instead of A-B diblock copolymers is also possible by copolymerizing both monomers simultaneously rather than sequentially adding the monomers B, as previously described. Typical monomer classes suitable for performing living anionic polymerization are acrylates, dienes and styrene.<sup>40</sup>

The possibility of sequential addition of different monomers to the “living chain” enables the access to block copolymers with a variety of molecular structures as illustrated below.<sup>9</sup>

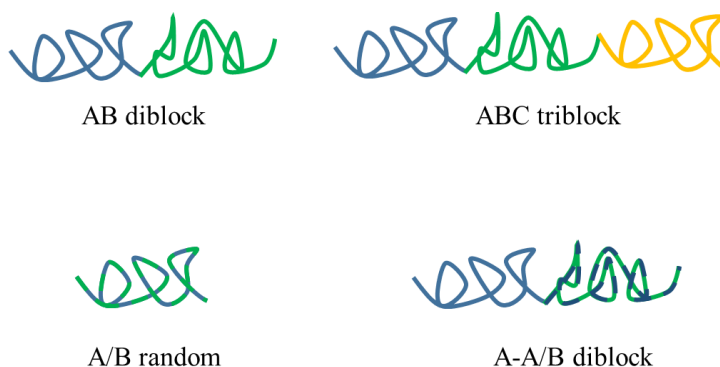


**Figure 1:** Molecular architectures of linear block copolymers.

### 3.1.1 Polybutadiene stereochemistry depending on the living anionic polymerization conditions

The polybutadiene microstructure can be controlled by changing the polymerization conditions such as the solvent polarity, the presence of a Lewis base or temperature.<sup>41</sup> For instance, the formation of a high *1,2-vinyl* content is expected in the presence of a Lewis base and this effect is further enhanced as the polarity as well as the concentration of the Lewis base increases. This phenomenon can be explained by the fact that the Lewis base solvates the lithium ion like a strong coordinating ligand favoring the insertion of butadiene units with *1,2* addition mode. Apart from the regioselectivity contributions, the presence of the Lewis base also influences the reaction kinetics and faster reaction are expected as the concentration of the Lewis base increases. Strong commonly used bases are TMEDA (N,N,N',N'-tetramethylethylene-diamine), diglyme and DIPIP (1,2-dipiperidinoethane). Temperature also influences the regioselectivity of the butadiene addition reaction, and high *1,2-vinyl* contents are favored at low temperatures. Moreover, the contribution of temperature on formation of *1,2-vinyl* is intensified in the presence of a the Lewis base. Notwithstanding, although *1,2-vinyl* contents can be varied by adjusting the concentration/effectiveness of Lewis base and/or temperature, the content *1,4 cis/trans* ratio is kept almost constant. The table below illustrates the influence of Lewis bases as well as temperature on the formation of *1,2-vinyl* content according to the Ref. 41

**Table 1:** Effect of temperature and concentration of Lewis base on *1,2-vinyl* content of butadiene units in hexane.<sup>41</sup>

Base	[Base]/[Li <sup>+</sup> ]	1,2 microstructure (wt %)			
		5°C	30°C	50°C	70°C
Triethylamine	30	-	21.0	18.0	14.0
	270	-	37.0	33.0	25.0
Diethyl ether	12	-	22.0	16.0	14.0
	180	-	38.0	29.0	27.0
Tetrahydrofuran	5.0	-	44.0	25.0	20.0
	85.0	-	73.0	49.0	46.0
Diglyme	0.1	-	51.0	24.0	14.0
	0.8	-	78.0	64.0	40.0
TMEDA <sup>a</sup>	0.6	-	73.0	47.0	30.0
	0.4	78.0	-	-	-
	6.7	85.0	-	-	-
	1.14	-	76.0	61.0	46.0
DIPIP <sup>b</sup>	0.5	91.0	50.0	44.0	21.0
	1.0	99.99	99.0	68.0	31.0
BME <sup>c</sup>	1.0	88.0	62.0	34.0	17.0
	4.0	98.0	86.0	63.0	28.0
DIDIOX <sup>d</sup>	0.2	85.0	-	-	-
	1.0	95-96.0	-	-	-
	0.5	97.0	91.0	80.0	63.0
TMDC <sup>e</sup>	0.7	69.0	-	-	-
	3.0	71.0	-	-	-

<sup>a</sup> N,N,N',N'-tetramethylethylene-diamine

<sup>b</sup> Bispiperidinoethane

<sup>c</sup> Bismorpholinoethane

<sup>d</sup> 2,2'-Bis(4,4,6-trimethyl-1,3-dioxane)

<sup>e</sup> *cis*-N,N,N',N'-Tetramethyl-1,2-diaminocyclopentane

### 3.1.2 Living anionic polymerization of styrene-butadiene random copolymer

During the anionic copolymerization of styrene and butadiene initiated by alkyl lithium in hydrocarbon solvent, butadiene monomers are first consumed at a slower reaction rate and after their complete consumption styrene monomers start reacting. The latter has a faster kinetic rate compared to the former one. This finding is contradictory based on the individual homopolymerization rates of butadiene and styrene. Because, under the same reaction conditions styrene has a faster homopolymerization rate.<sup>42,43</sup> Different theoretical approaches have been developed in order to explain this non trivial kinetic behavior. Korotkov et al. treated this controversial result about the kinetic rates between butadiene and styrene, during their copolymerization, by considering butadiene as being a stronger Li<sup>+</sup> solvating agent, making the active center more reactive towards butadiene compared to styrene monomers.<sup>44</sup> On the other hand, O'Driscoll and Kuntz believe this difference in kinetic rates is related to the cross over rate constant. According to this hypothesis, the polystyryllithium species have a faster reaction rate towards butadiene compared to the homopolymerization rate of styrene, and after the insertion of butadiene units, the polybutadienyllithium starts polymerizing slowly, since the cross over reaction towards styrene insertion is slower.<sup>45</sup>

A Lewis base, also known as randomizer or modifier, is used in the copolymerization of butadiene and styrene in order to obtain styrene-butadiene random copolymers with constant styrene composition through the polymer chain.<sup>43</sup> The role of the Lewis base in this case is to facilitate a homogeneous successive insertion of both monomers in the growing chain. The Lewis base acts as a solvating agent as explained previously in **section 2.1.1**. There are two classes of randomizers which are defined based on their effectiveness: weak and strong randomizers. The first ones are able of maintaining styrene composition constant throughout the polymer chain and of maintaining low *1,2-vinyl* contents, which is sometimes desired. However, these randomizers are effective only for low styrene contents, otherwise PS blockiness is obtained at the end of the chain. Examples of weak randomizers are: diphenyl ether, diethyl ether, methyl *tert*-butyl ether (MTBE) and sodium dodecylbenzene sulfonate (SDBS).<sup>46-49</sup> Although the latter can yield styrene-butadiene random copolymers, with a total styrene concentration up to 36 wt% and *1,2-vinyl* content of 16.6 mol%, PS blockiness of 4.4 wt% is still present. Furthermore, the solubility of SDBS in hydrocarbon solvents is rather poor, making it difficult to be used.<sup>48</sup> Therefore, in case one has to synthesize

SBR with a high concentration of styrene, the use of a strong modifier is needed in order to avoid PS blockiness. However, as a direct consequence high *1,2-vinyl* contents are expected in this case. Examples of strong modifiers are: TMEDA (N,N,N',N'-tetramethylethylene-diamine), THF (tetrahydrofuran) and DIPIP (1,2-dipiperidinoethane) which are widely used for the copolymerization of SBR.<sup>50</sup> The randomizer effectiveness is enhanced by increasing its concentration, and it is in most cases applied to avoid PS blockiness when high styrene composition or if high *1,2-vinyl* contents is desired. Another factor influencing the stereochemistry of butadiene units is temperature and, whose effect is more pronounced in the presence of stronger modifiers.<sup>46</sup>

### 3.2 Phase separation of block copolymers

Block copolymers are macromolecules composed of covalently bonded homopolymers, which tend to microphase separate due to chemical incompatibility between the distinct blocks as well as due to the low entropy of mixing associated with their high molecular weights.<sup>51</sup> Whereas homopolymer blends macrophase separate, block copolymers of similar chemical composition microphase separate with domain sizes comparable to the radius of gyration of the individual blocks (5-100 nm).<sup>52</sup> Different phase separation states can be accessed by changing the block copolymer composition or the segregation strength between the blocks. Most important is the order parameter  $\chi N$ ; where  $\chi$  and  $N$  are the Flory-Huggins segmental interaction parameter and the total degree of polymerization, respectively. The value of  $\chi N$  itself is temperature dependent leading in most of the cases to disorder and miscibility at high temperatures. By varying the volume fractions of the components, different morphologies can be obtained. Domain size, domain shape and interfacial curvature are governed by the competing effects between interfacial tension and entropic penalty for stretching polymer coils at the interface. It means that the block copolymers tend to self-assemble into domains with a minimum surface area and to accommodate the chains at the interface in a coil configuration.<sup>53</sup>

### 3.2.1 Phase separation of diblock copolymers

Among the block copolymers the A-B diblock copolymers have the simplest molecular architecture and are extensively studied. Their phase separation behavior can be described by well-established and proven thermodynamic models.<sup>52</sup>

Phase separation behavior is dictated by the sign of the Gibbs free energy ( $G$ ) which incorporates enthalpic ( $H$ ) and entropic ( $S$ ) contributions according to <sup>54,55</sup>

$$G = H - TS \quad (1)$$

Single phase, equilibrium and phase separated states are obtained for  $G < 0$ ,  $G = 0$  and  $G > 0$ , respectively. Flory<sup>56</sup> and Huggins<sup>57,58</sup> developed independently the expression for the free energy of mixing  $\Delta G_m$  (based on Gaussian) polymeric chains on an incompressible lattice. This thermodynamic model was developed for binary mixtures of homopolymers A and B. One gets

$$\frac{\Delta G_m}{k_b T} = \underbrace{\frac{\phi_A}{N_A} \ln \phi_A + \frac{(1 - \phi_A)}{N_B} \ln(1 - \phi_A)}_{\Delta S_m} + \underbrace{\phi_A(1 - \phi_A)\chi}_{\Delta H_m} \quad (2)$$

where:  $K_b$  is the Boltzmann constant;  $\phi_A$  and  $\phi_B$  are the volume fractions of the homopolymer A and B, respectively;  $N_A$  and  $N_B$  are the corresponding degrees of polymerization of homopolymers A and B;  $\Delta S_m$  and  $\Delta H_m$  are the entropy and enthalpy of mixing, respectively. The Flory-Huggins interaction parameter,  $\chi$ , is temperature dependent according to<sup>59,54</sup>

$$\chi_{AB} = \frac{1}{k_B T} \left[ \epsilon_{AB} - \frac{1}{2}(\epsilon_{AA} - \epsilon_{BB}) \right] \quad (3)$$

In this equation  $\epsilon_{ij}$  represents the contact energy between the segments  $i$  and  $j$ .

According to **Eq. 3**, repulsive forces between monomers A and B lead to negative  $\chi_{AB}$ , meaning that both homopolymers are phase separated. On the other hand, attractive forces between monomers A and B result in positive  $\chi_{AB}$ , indicating that homopolymers A and B are miscible. Moreover, one can clearly see that  $\chi_{AB}$  is inversely proportional to temperature. Phase separation is favored at lower temperatures. Based upon the assumption that polymer chains can just assume few mixing configurations due to their high molecular weight, the contribution of entropy of mixing,  $\Delta S_m$ , to the free energy of mixing is rather negligible. Therefore, the energy of mixing can be approximated by the Flory-Huggins interaction parameter,  $\chi_{AB}$ . In reality the assumption previously made that the polymer chains are on an incompressible lattice is not completely fulfilled. Therefore, an equation-of-state to describe  $\chi_{AB}$  is needed in order to compensate this deviation. Thus,  $\chi_{AB}$  can be described according to

$$\chi_{AB} = A + \frac{B}{T} \quad (4)$$

where A and B are experimentally determined enthalpy and excess entropy coefficients for a particular composition. In general, the parameters A and B are depended on  $\phi$ , N and T. Although, it has been assumed before that the contribution of entropy to the free energy of mixing is negligible, entropic effects have to be accounted for in **equation 4** (enthalpic contribution) due to the violation of the incompressible lattice assumption.

The phase separation state is in principle controlled by the volume fraction, total degree of polymerization and the Flory-Huggins interaction parameter. Therefore, based on **equation (4)** it is possible to predict the phase separation behavior of block copolymers, although it was originally developed for binary homopolymer mixtures. Nevertheless, it is noteworthy that this model does not take into consideration that the chain segments close to the interface adopt a chain stretching configuration in case of block copolymers in the strong segregation state.<sup>52</sup> For symmetric binary blends in equilibrium, an order-disorder transition (ODT) is expected for  $(\chi N)_c = 2$ .<sup>52</sup> The influence of the order parameter  $\chi N$  on the phase separation behavior of block copolymers will be discussed in the next subsection.

### 3.2.2 Influence of segregation strength

The  $\chi$  and  $N^{-1}$  parameters represent basically the enthalpic and entropic contributions to the free energy density, respectively. Therefore, the order parameter  $\chi N$  defines the block segregation strength and consequently the diblock copolymer phase separation state.<sup>14</sup> According to Leibler's weak segregation theory, an order-disorder transition (ODT) is expected if the order parameter is approaching  $(\chi N)_c=10.5$  for A-B diblock copolymers at the critical composition ( $\phi = 0.5$ ).<sup>14</sup> **Figure 2** illustrates the chain segments configuration in the ordered and disordered states in case of diblock copolymers with symmetric composition ( $\phi = 0.5$ ) according to Leibler's weak segregation theory. A disordered state (absence of long range order) is predicted for  $\chi N < 10.5$  while a microphase-separated state with long range ordered morphology is expected for  $\chi N > 10.5$ .

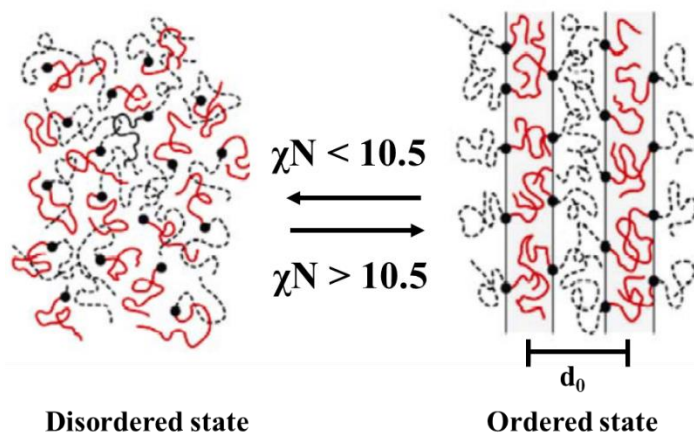


**Figure 2:** Schematic illustration of the order-disorder transition for diblock copolymer with symmetric composition ( $\phi=0.5$ ) explained by Leibler.<sup>14</sup> Disordered state (left side) is observed for  $\chi N < 10.5$  and ordered state with lamellar morphology with periodicity  $d_0$  (right side) for  $\chi N > 10.5$ . This figure is adapted from Ref.15.

In the microphase-separated state different segregation strengths related to different interfacial situations can be distinguished depending on the  $\chi N$  value. The stages are straightforwardly classified based on the corresponding  $\chi N$  values: strong (e.g.  $\chi N = 60$ ),<sup>60</sup> intermediate ( $\chi N \sim 15 - 60$ )<sup>60</sup> and weak segregation ( $10.5 < \chi N < 15$ ). **Figure 3** shows the dependence of structure and concentration profile on the  $\chi N$  values for block copolymer with symmetric composition ( $\phi=0.5$ ).

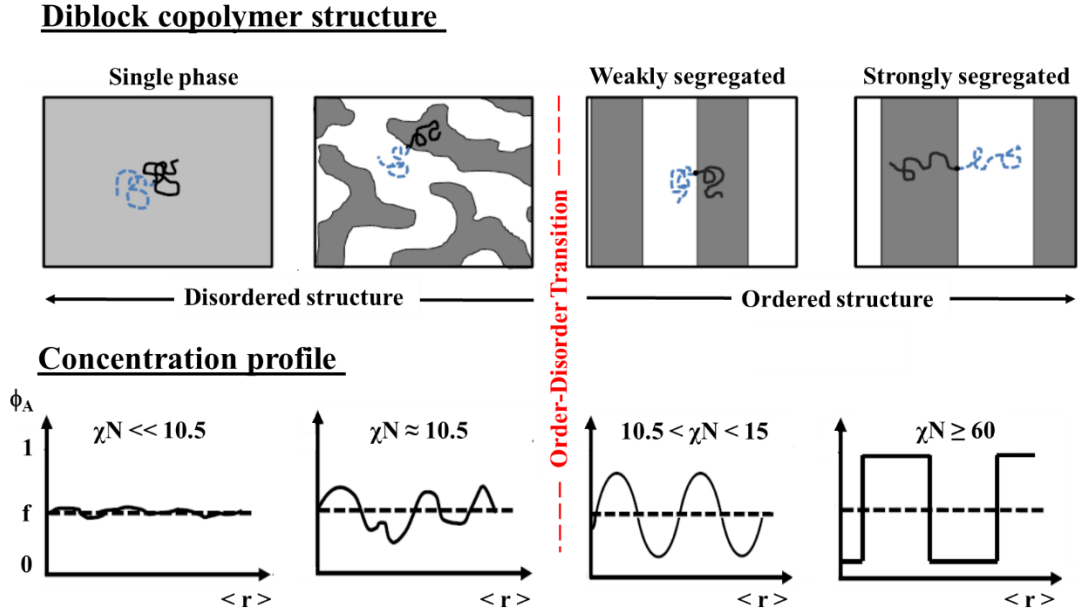


**Figure 3:** Dependence of structure (upper part) and concentration profile (lower part) on the  $\chi N$  values for A-B diblock copolymer with  $\phi = 0.5$ . Depending on the segregation strengths ( $\chi N$  values) different phase separation states are described: strong ( $\chi N \geq 60$ ), intermediate ( $15 < \chi N < 60$ ), or single phase ( $\chi N \ll 10.5$ ). This figure was adapted from Ref. 52.

Differences regarding phase separation behavior and interfacial situation depending on the segregation strengths can be explained based on a competition of entropic and enthalpic effects. If the entropic factor dominates a single phase ( $\chi N \ll 10.5$ ) is observed and the chain segments of both blocks are homogeneously distributed.<sup>14</sup> If  $\chi N \approx 10.5$  is reached by increasing  $\chi$  and/or  $N$  the enthalpic and entropic contributions are comparable and as a direct consequence, local concentration fluctuation takes place close to the ODT (Order Disorder Transition) as shown in **Figure 3**.<sup>61</sup> A first transition from disordered to ordered state is obtained when  $\chi N \geq 10.5$ , because in this case there is a fine balance between the enthalpic and entropic effects. Here the concentration profile can be approximated by a sinusoidal as shown in **Figure 3** and the microdomain period size is proportional to  $N^{1/2}$ . This scenario is the well-known *weak segregation limit* (WSL) and the chain segments are not fully stretched at the interface.<sup>61</sup> A fourth phase behavior is accessed by further increasing  $\chi N$  up to 60 where the enthalpic contribution is greater than the entropic effect, consequently the chains located at the interface are stretched, the interface width is sharper compared to the WSL state and a nearly square wave composition profile is

observed. This phase separation state is defined as *strong segregation limit* (SSL) and has a microdomain dimensions that scales as  $N^{2/3}\chi^{1/6}$ .<sup>14</sup> The dependence of the periodicity on  $\chi$  is due to the entropic penalty of having the chains stretched at the interface.<sup>14</sup>

Phase separation behavior as well as morphology can be fine-tuned by varying block copolymer composition as it will be discussed in details in the next subsection.

### 3.2.3 Dependence of morphology on block copolymer composition

For A-B diblock copolymers with a fixed  $\chi N$  value well above the order-disorder transition a variety of morphologies can be accessed by changing the volume fraction of the blocks,  $\phi_A$  and  $\phi_B$ . Lamellar morphologies are observed if the volume fractions of both blocks are comparable ( $\phi_A \sim \phi_B$ ). If the volume fraction of one of the blocks become sufficiently larger compared to that of the other one, the minority component tends to form cylinders packing in a hexagonal arrangement embedded in the majority phase. By further increasing asymmetry, the minority phase is observed, at similar  $\chi N$  values, to form spheres packing in a body-centered cubic arrangement. According to the free energy expression developed for diblock copolymer in the strong segregation (SSL) limit, lamellar, cylinders and spheres phases are stable for  $0.299 < \phi < 0.701$ ,  $0.117 < \phi < 0.299$  and  $\phi < 0.117$ , respectively. In SSL state complex morphologies, such as gyroid phase, are reported to be not stable, therefore it cannot be predicted by using this model.<sup>60</sup>

These are the commonly observed morphologies for A-B diblock copolymers. Later other morphologies were identified, among them the most frequently reported is the bicontinuous gyroidal structure, which occurs between lamellar and cylindrical morphologies. In this case, the minority component forms two interpenetrating lattices which are threefold coordinated.<sup>62</sup> The real space representation of the different equilibrium morphologies described above as well as their dependence on volume fraction for A-B diblock copolymers in the ordered state with a fixed  $\chi N$  are shown below (**Figure 4**).<sup>63</sup>

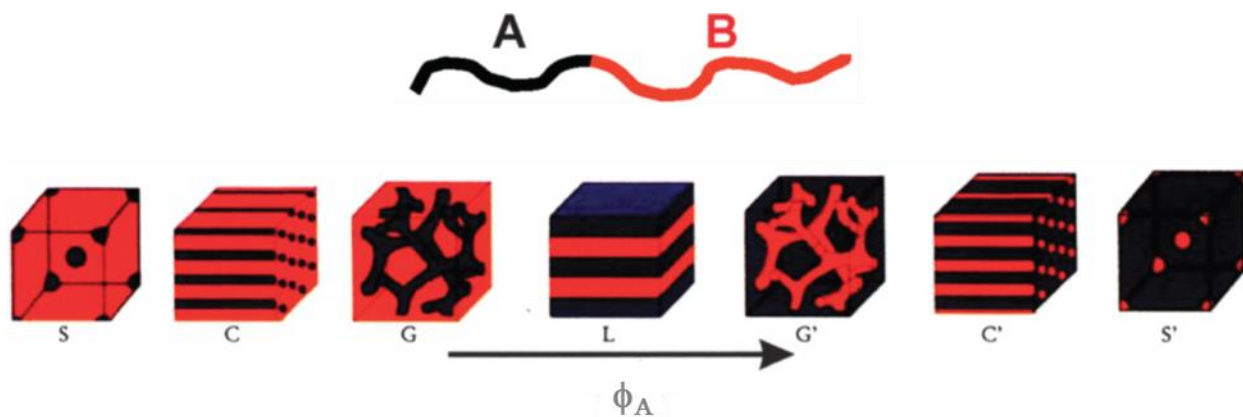


**Figure 4:** Dependence of the equilibrium morphologies on the volume fraction ( $\phi_A$ ) of block A for A-B diblock copolymers in the ordered state. According to the self-consistent mean field theory, spherical (S and S'), cylindrical (C and C'), gyriodal (G and G') and lamellar (L and L') morphologies are predicted based on  $\phi_A$  for a fixed  $\chi N$  value. The scheme was taken from Ref. 63.

Extensive experimental studies carried out on various diblock copolymers have confirmed the theoretical predictions regarding the morphology dependence on block copolymer composition.<sup>64,65</sup> Certain discrepancies between the experimental and theoretical phase behaviors occur due to the assumption, in the model used, that a A-B diblock copolymer has a symmetric conformation. However, depending on the chosen monomers a slightly different conformational symmetry is observed since each monomer has a specific Kuhn length.

The influence of  $\chi N$  and  $\phi_A$  or  $\phi_B$  on the phase separation behavior of A-B diblock copolymers will be explained in the following subsection.

### 3.2.4 Phase diagram of diblock copolymers

Phase separation behavior is controlled by the volume fraction of one of the blocks as well as by the order parameter  $\chi N$ . **Figure 5** shows the theoretical phase diagram of a classical A-B diblock copolymer calculated using self-consistent field theory. It clearly illustrates the effects of  $\chi N$  and  $\phi$  on the phase behavior.

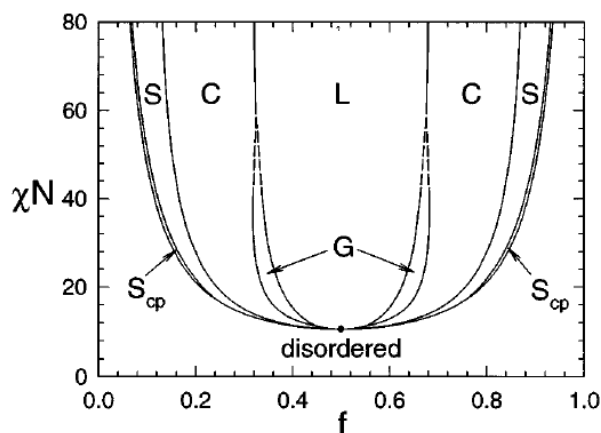


**Figure 5:** Mean field phase diagram of a A-B diblock copolymer calculated in Ref. 66 showing the stability regions of the ordered lamellar (L), gyroidal (G), cylindrical (C), spherical (S) and close-packed spherical ( $S_{cp}$ ) phases depending on the volume fraction and on the  $\chi N$  order parameter. Disordered phase is observed below the critical  $\chi N = 10.5$ . The dashed curves denote extrapolated phase boundaries, which could not be calculated due to numerical limitations.

The phase diagram displayed above is able to predict both the classical morphologies such as lamellar, cylindrical and spheres as well as the complex gyroidal phase structure. The changes in the morphology with volume fraction are due to the competing effects of interfacial tension and the degree of stretching of polymer coils at the interface. The latter prefers the formation of domains with constant thickness in order to avoid packing frustration. On the other hand, contribution constant mean curvature (CMC) surface tends to be formed due to the interfacial tension in order to reduce interfacial area. In case of diblock copolymers in the WSL, polymer stretching contribution at the interface can be neglected whereas it is present and relevant in the SSL, as reported by Semenov.<sup>53,67</sup>

### 3.3 Thermal and dynamic glass transition

#### 3.3.1 Thermal glass transition

Glasses are amorphous solids having an internal structure without long range order similar to the situation in conventional liquids. Glasses are formed if a liquid is (rapidly) cooled to a sufficiently

low temperature where the liquid-like motions ( $\alpha$  dynamics) slow down to such an extent that they freeze in. This phenomenon is called **thermal glass transition** and occurs at the glass temperature  $T_g$ , which depends on cooling rate. In case of crystallizable materials, the cooling rate must be sufficiently high to prevent crystallization above  $T_g$ . The glassy state below  $T_g$  is a non-equilibrium vitrified state and the thermal glass transition corresponds to the temperature interval in which the liquid falls out of equilibrium, i.e. represents an equilibrium-to-non-equilibrium transition. This phenomenon is usually accompanied by a step-like change in the heat capacity  $c_p(T)$  due to freezing-in of entropy fluctuations and high viscosity values approaching usually  $10^{13}$  poise at  $T_g$ . For full specification of the thermal glass transition, the cooling rate must be specified. Other experimental parameters like pressure, mechanical and electrical fields can also influence  $T_g$ . This rate-dependence is a clear indication that the thermal glass transition represents the transition to a non-equilibrium glassy state, which is characterized by slow equilibration processes towards the equilibrium liquid state called physical aging or structural relaxation.

The thermal glass transition can be visualized using volume (from classical dilatometric measurements), or enthalpy curves (from conventional thermal analysis methods like differential scanning calorimetry) vs temperature as shown in **Figure 6**. At high temperature, an isotropic liquid state exists. On cooling the liquid at a specific rate, the volume decreases first linearly but deviates at temperatures below  $T_g$  clearly from the extrapolated equilibrium line due to vitrification. For conventional cooling rates ( $\sim 10\text{K/min}$ ), the characteristic time of the  $\alpha$  motions in the liquid approaches at the glass transition temperature approximately 100s. On cooling at a relatively slower rate, liquid is given longer time to achieve the desired structural arrangements towards equilibrium resulting in lowering of the glass temperature.

Due to the relevance of glasses and glass transition in many applications various models exist in the literature aimed to describe the thermal glass transition at  $T_g$  as well as the  $\alpha$  dynamics in the equilibrium state above  $T_g$  which is often called  $\alpha$  relaxation or dynamic glass transition. Examples are free-volume approach,<sup>68,69</sup> configuration entropy-based thermodynamic models,<sup>70</sup> cooperativity approaches,<sup>71,72</sup> mode coupling theory,<sup>73</sup> coupling model,<sup>74</sup> fragility concept,<sup>75</sup> etc. Despite of that there is still no generally accepted model describing phenomenology and molecular background of the glass transition. Hence, the physical origin of the glass transition is still understood as one of the most fundamental open questions in soft matter science.<sup>76</sup>

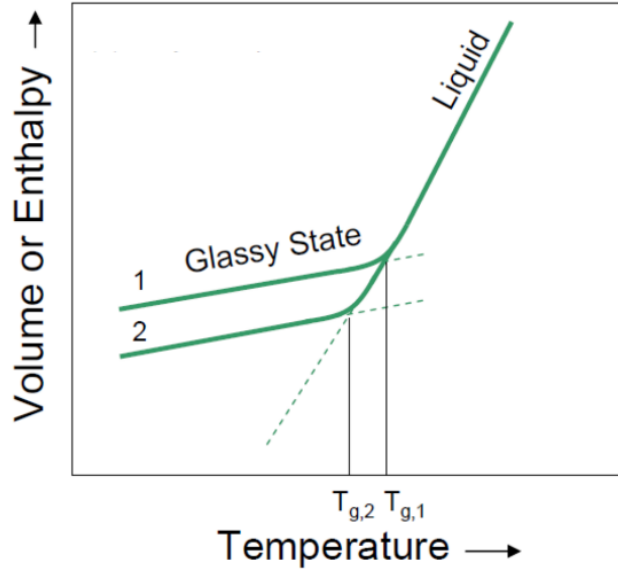


**Figure 6:** Volume  $V$  or enthalpy  $H$  vs temperature under isobaric conditions.  $T_{g,1}$  and  $T_{g,2}$  represent the glass transitions produced at the cooling rates of  $Q_1$  and  $Q_2$ , with  $Q_2 < Q_1$ .

### 3.3.2 The dynamic glass transition

The dynamic glass transition or  $\alpha$  relaxation process is the most prominent dynamics in an equilibrium liquid above  $T_g$ . These cooperative dynamics are strongly temperature dependent and due to slow fluctuations responsible for the time and temperature dependent softening behavior.

The  $\alpha$  relaxation can be measured by linear response methods detecting the response of macroscopic samples to small external perturbations. Depending on the perturbation used, such linear response experiments result in different susceptibilities such as shear compliance  $J(t)$  or dielectric permittivity  $\epsilon(t)$ . Characteristic for a relaxation process is a non-exponential time dependence and a non-Arrhenius like temperature dependence of the average  $\alpha$  relaxation time. In time dependent measurement the dynamic glass transition  $\alpha$  can often be approximated by the empirical Kohlrausch-Williams-Watts (KWW) function<sup>77</sup>

$$\phi(t) = \exp[-(t/\tau)^{\beta_{KWW}}] \quad (5)$$

where  $\phi(t)$ ,  $\tau$  and  $\beta_{KWW}$  are the relaxation function, the relaxation time and the Kohlrausch exponent, respectively.  $\beta_{KWW}$  has typical values between 0 and 1.  $\beta_{KWW}$  equals to 1 means that

there is just a single Debye relaxator, indicating the single exponential function. However, for conventional  $\alpha$  relaxation processes  $\beta_{\text{KWW}} < 1$  is typically observed. Whether this is a consequence of a superposition of different spatially distributed Debye relaxators or due to intrinsic broadening of all relaxing entities is remaining a point of debate although the latter version seems to be more likely.<sup>78,79</sup> The existence of dynamic heterogeneities is one model, among many others in the literature, used to understand the non-exponential behavior of the dynamic glass transition.<sup>37</sup> This approach will be described in more detail below and adopted in the discussion (**section 8.2**) in order to explain the dynamic behaviors of interfacial material observed in block copolymers.

The Arrhenius plot or relaxation map (**Figure 7**) illustrates the typical temperature dependence of the average  $\alpha$  relaxation time  $\tau_\alpha$  or  $\alpha$  relaxation frequency  $\omega_\alpha = \tau_\alpha^{-1}$ , usually obtained from linear response measurements. The typical non-Arrhenius like temperature dependence of the average  $\alpha$  relaxation frequency can be commonly described by Vogel-Fulcher-Tammann-Hesse (VFTH) equation.<sup>37</sup>

$$\log(\omega_\alpha) = \log(\omega_0) - B/(T - T_v) \quad (6)$$

where  $\omega_0$ ,  $B$  and  $T_v$  represent limiting frequency, curvature and Vogel temperature respectively. According to the  $\alpha$ -trace temperature dependence shown in **Figure 7**, one can observe that the  $\alpha$  dynamics has a stronger temperature dependence compared to that of simply activated more local, non-cooperative motions seen in glasses as Johari-Goldstein relaxation processes ( $\beta$ -relaxations).<sup>80</sup> As already mentioned above, the relaxation time of the dynamic glass transition at  $T_g$  is about 100s. Below  $T_g$ , i.e. in the glassy state, experimentally measured  $\alpha$  traces will deviate from the VFTH prediction due to non-equilibrium effects. Note that the average  $\alpha$  relaxation time will diverge at  $T_v$  a few 10K below  $T_g$  according the VFTH prediction. Since it is impossible to measure such long relaxation times in equilibrium there is still an ongoing discussion whether or not this prediction is reasonable. The temperature dependence of  $\omega_\alpha = \tau_\alpha^{-1}$  in the experimentally accessible temperature range above  $T_g$  is usually quite well described by the VFTH equation. In contrast, the temperature dependence of the relaxation frequency  $\omega_\beta$  of secondary relaxation processes ( $\beta$ ) has an Arrhenius like temperature dependency expressed as

$$\log(\omega_\beta) = \log(\omega_0) - E_A/(RT) \quad (7)$$

where  $E_A$  is the activation energy and  $R$  is the gas constant.

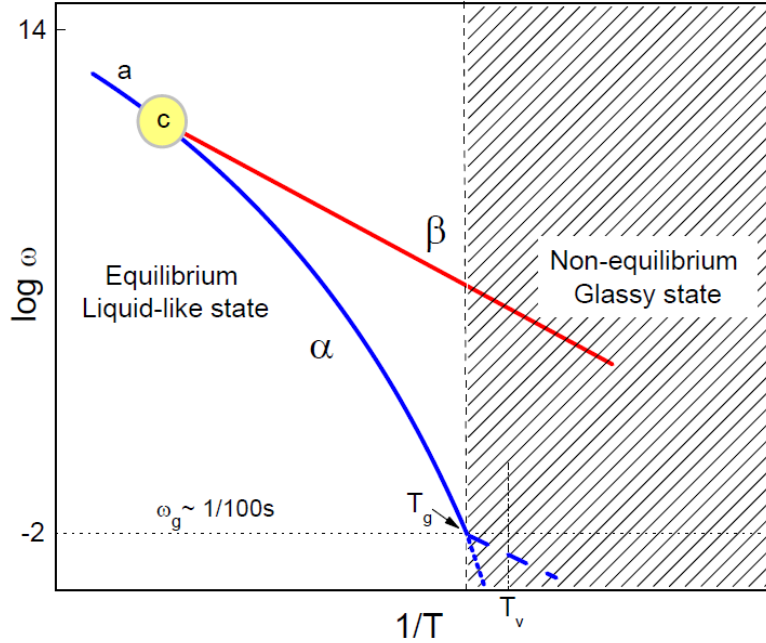


**Figure 7:** Arrhenius plot  $\log \omega$  vs  $1/T$  showing dynamic glass transition process ( $\alpha$ ), local dynamics ( $\beta$ ), crossover region (c) where temperature dependence of  $\alpha$  and  $\beta$  approach each other and high temperature process (a).  $T_v$  corresponds to the Vogel temperature. Taken from Ref. 81.

Among the various models reported in the literature used to explain the  $\alpha$  dynamics and the related softening process in liquids, the Free-volume concept is often used. According to this concept, the mobility of molecules (monomer units in case of polymers) are controlled by the free volume ( $V_f$ ) or the unoccupied volume under isothermal conditions. Basic assumptions behind this theory are that (i) free volume is continuously redistributed without any expense of local free energy for this redistribution and (ii) molecular mobility is realized by movement of atoms or molecules into voids of approximately equal or greater than that of molecular dimensions.<sup>82,83</sup>

The free volume is temperature dependent and it is correlated according Doolittle with the viscosity by<sup>84,85</sup>

$$\eta = A \exp[b(V - V_f)/V_f] \quad (8)$$

where  $V_f$  is the available volume or free volume and  $V_0 = V - V_f$  being the limiting volume of the liquid or Van der Waals volume of the molecules at 0K. The packing density increase is temperature controlled, resulting in slower molecular mobility as well as in reduction of free volume at lower temperatures. At the glass transition, these translational diffusive motions freeze. Only localized relaxational motions seen as Johari-Goldstein  $\beta$  process are still possible.<sup>86</sup> The free volume approach has been used to explain the strong temperature dependent changes in the  $\alpha$  relaxation frequencies in equilibrium liquids based on the Williams-Landel-Ferry relation (WLF)<sup>87</sup>

$$\log(\omega_\alpha/\omega_0) = \frac{(B/2.303f_0)(T - T_0)}{\left(\frac{f_0}{\alpha_f}\right) + (T - T_0)} \quad (9)$$

where  $f_0$  is the fractional free volume ( $V_f/V_0$ ) at the reference temperature  $T_0$  and  $\alpha_f$  is the thermal expansion coefficient. Note that the WLF equation is mathematically equivalent to the VFTH like equation as shown in **equation 6**.

Another widely used approach to understand the dynamic glass transition are cooperativity concepts. Adam and Gibbs have postulated in their famous paper in 1965 that there are cooperatively rearranging regions (CRRs) being of major relevance for the (dynamic) glass transition.<sup>88</sup> Later, the characteristic length  $\xi_\alpha$  of glass transition corresponding to the size of cooperatively rearranging regions CRR was defined by  $V_\alpha = \xi_\alpha^3$ .<sup>71</sup> Moreover,  $\xi_\alpha$  was experimentally quantified based on the fluctuation approach by Donth combining calorimetric results and Nyquist-type equation.<sup>89</sup> This equation was derived from the fluctuation dissipation theorem (FDT), applied to the dynamic glass transition, and no molecular estimation or microscopic models are necessary for obtaining the length according to<sup>37</sup>

$$V_\alpha = \xi_\alpha^3 = k_B T^2 \Delta(1/C_v) / \rho \partial T^2 \quad (10)$$

where  $\Delta(1/C_v)$  is the step in the reciprocal heat capacity at constant volume,  $\rho$  is the mass density ( $\text{g/cm}^3$ ) and  $\partial T^2 \equiv (\partial T)^2$  is the mean-square temperature fluctuation of one average CRR.

**Equation 10** answers the question about that subsystem size whose fluctuations are determined via the FTD by linear response across the glass transition. Therefore, the subsystem defined by **eq. 10** is the CRR. Typical characteristic length scale  $\xi_\alpha$  in the order of 1-3 nm have been reported for a variety of glass forming materials.<sup>37</sup> Alternative concepts giving slightly different  $\xi_\alpha$  values have been reported but will be not discussed here in detail.<sup>71,89</sup> According to the cooperative rearranging regions (CRRs) concept,  $\xi_\alpha$  can be accessed in an indirect way also by experiments on nanostructured materials like block copolymers as it will be shown in more details in the discussion part of this work.

### 3.3.3 Special factors influencing the alpha dynamics of diblock copolymers

The dynamic glass transition of the individual phases of A-B diblock copolymers may be influenced by special factors which are absent in bulk samples. There are mainly three influencing factors:<sup>90</sup> **(1)** geometrical confinement, **(2)** changes due to differences in chemical composition, i.e. interfacial material and **(3)** constraints at interfaces resulting in density changes. In particular, the question whether or not and at which length scale true geometrical confinement effects exist seems to be of major importance for the discussion about the nature of the dynamic glass transition  $\alpha$  since it is related to the discussion about the CRR size. Hence, the three different influencing factors mentioned above, **(1)-(3)**, to the  $\alpha$  dynamics should be discussed in connection with the CRR concept in more detail. In particular, it will be considered how the softening response of block copolymer based systems can be represented by the superposition of subsystems composed of specific chemical composition with characteristic length  $\xi_\alpha$  near the glass temperature.

**Geometrical confinement effects.** According to the hindered glass transition picture<sup>91</sup> the  $\alpha$  dynamics of polymers under confinement should be different from that of the bulk as soon as the domain size  $d$  approaches the characteristic length of the glass transition  $\xi_\alpha$ . Cooperativity concepts commonly postulate that  $\alpha$  motions are cooperative in nature involving many “particles” (being monomeric units in case of polymers). If the domain is too small the CRR size is not reached and the number of “particles” available is not reaching that needed for a bulk-like glass transition. Hence, it is assumed that polymers confined in extremely small domains should show a reduction

in the glass transition temperature compared to the bulk state. The influence of domain size on the softening behavior has been extensively investigated for glass-forming materials confined in nanopores,<sup>19,21,22,24</sup> in thin polymeric films with nanoscopic dimensions,<sup>30,92</sup> or in amorphous domains of semi-crystalline polymers.<sup>24,25</sup> Confinement effects on the  $\alpha$  segmental dynamics has been reported for many nanophase-separated side chain polymers with domain sizes in the range 1-5 nm.<sup>27,38,93,94</sup> Besides, confinement was also observed for block copolymers with ordered cylindrical morphology with domain size of 8 nm.<sup>95</sup> On the other hand, microphase-separated diblock copolymers with domain sizes of the order of 25 nm show commonly no confinement effects, as confirmed by dielectric and dynamic mechanical data.<sup>81,96</sup> Several studies carried out on block copolymers with distinct morphologies such as lamellar,<sup>97,98</sup> cylinder<sup>82</sup> and spheres<sup>82</sup> showed that the softening behavior of the individual phases are comparable to the response of their corresponding homopolymers in the bulk.

**Interfacial material effects.** As previously discussed, there are basically three main states for block copolymers regarding segregation strength: **(a)** weak or **(b)** strong segregation of the phases as well as **(c)** disordered state.<sup>36</sup> Depending on the segregation strength ( $\chi N$ ), specific relaxation dynamics scenario will be observed. In the case of strongly segregated block copolymers **(a)**, the  $\alpha$  relaxation dynamics related to the individual phases corresponds to that of corresponding homopolymers.<sup>14,99</sup> On the other hand, weakly segregated block copolymers **(b)** are composed of pure domains of both components surrounded by a large amount of interfacial material with gradient chemical composition. Block copolymers in this state are long-range ordered but have significantly larger interfacial width and interphase fraction compared to strongly segregated systems. Their  $\alpha$  relaxation dynamics is essentially composed of two main  $\alpha$  processes,  $\alpha_A$  and  $\alpha_B$ , combined with pronounced  $G''(T,\omega)$  contributions in the region between them.<sup>99</sup> The latter is due to the contribution from an interfacial material being a mixture of both components. This  $G''(T,\omega)$  dependence may be interpreted as the superposition of many  $\alpha$  relaxators, representing different chemical compositions.<sup>99</sup> Extreme examples with comparable structure and  $\alpha$  dynamics are the gradient block copolymers,<sup>100</sup> which contain no pure phases but practically only interfacial material although they are long range ordered. In case of well disordered A-B diblock copolymers **(c)** significantly above the ODT a single phase should occur. The  $\alpha$  relaxation dynamics should then be similar to random copolymers. In this case, the polymer segments are homogeneously

distributed and just one single  $\alpha$  relaxation process between the  $\alpha_A$  and  $\alpha_B$  of the pure components will be observed.<sup>99,101</sup>

It will be demonstrated in this work that the different  $\alpha$  relaxation scenarios seen in block copolymers described above, depending on the segregation strength  $\chi N$ , can be explained based on the cooperativity concepts considering the existence of CRRs.<sup>37</sup> It is assumed that differences in the local chemical composition, on the CRR's length scale, should have an effect in the softening behavior.

**Constraints at interfaces.** Changes related to the segmental  $\alpha$  dynamics also appear in polymer nanoparticle composites with small compartment sizes and huge fractions of polymer material at the interface. The  $\alpha$  dynamics of such composite materials has been heavily investigated experimentally as well as via numerical simulations. The segmental dynamics of interfacial material can be either faster or slower than in the bulk depending on the interaction.<sup>31,34,35</sup> Hence, broader glass transition intervals are observed. For attractive interaction between polymer and filler an increase in  $T_g$  has been commonly reported. A possible reason for that is an increase in density close to the interface.<sup>102</sup>

A detailed study of the  $\alpha$  relaxation behavior of S-SBR matrices, systematically filled with different silica loadings, revealed the existence of an “immobilized layer” having a higher glass transition temperature compared to the polymer bulk,<sup>6</sup> This immobilized fraction is detected by shear and Double Quantum NMR measurements.<sup>103</sup> Its estimated thickness is 1-3 nm. On the other hand, there are also observations that the segmental dynamics ( $\alpha$ -relaxation) and glass transition temperature ( $T_g$ ) are not significantly affected by the presence of filler, despite of significant levels of “bound” polymer from chemically modified polymer–filler interfaces and from well dispersed particles with high surface area.<sup>104</sup> Hence, the extent to which these localized effects translate into modification of the viscoelastic  $T_g$  of the polymer matrix in general is relatively unclear and it has to be clarified for each individual composite how large the fraction of polymer influenced by the filler is. To what extent similar effects exist in filled block copolymers will be discussed shortly in **Section 7.3.**

## Chapter 4

### Living anionic polymerization of PB-SBR diblock copolymers

#### 4.1 Chemicals

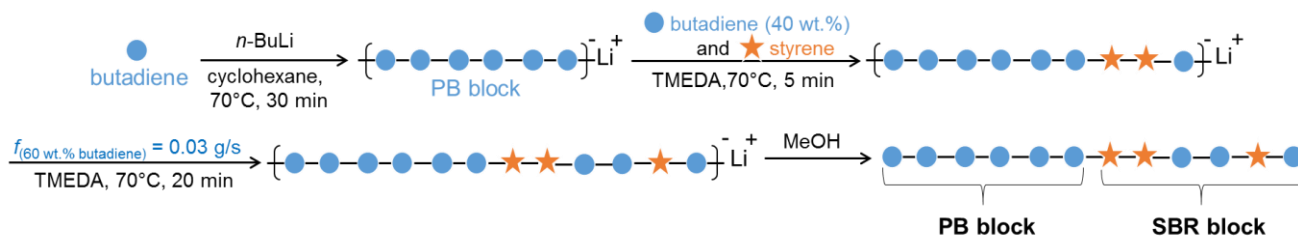
Cyclohexane and 1,3-butadiene were obtained from Dow Chemical Schkopau (Germany) and used without further purification. *N*-butyl lithium (Sigma Aldrich, 2.5 M in *n*-hexane) was diluted in cyclohexane to 0.8 M. Styrene (Chemievertrieb Magdeburg, Germany) was destabilized with sodium hydroxide (NaOH) (Merck), stirred over hydrate calcium (CaH<sub>2</sub>) under nitrogen (N<sub>2</sub>) atmosphere overnight, and afterwards distilled under reduced pressure. *N,N,N',N'*-Tetramethylethylenediamine (TMEDA) (Merck) was stirred over CaH<sub>2</sub> for one day, distilled under nitrogen atmosphere, and afterwards a solution of 3 wt% was prepared in cyclohexane. Methanol (Chemievertrieb Magdeburg, Germany) was used as received without further purification. All glassware utilized was always blanket with nitrogen and dried under vacuum prior to use.

##### 4.1.1 Polymerization of symmetric and asymmetric PB-SBR diblock copolymers with low *1,2-vinyl* contents in both blocks

After preparing a 5L stainless steel reactor equipped with an electromagnetic induction stirrer for performing a living anionic polymerization, cyclohexane and butadiene were charged into the vessel and stirred with 200 rpm under N<sub>2</sub> atmosphere (~ 1.5 bar). The synthesis of PB-SBR diblock copolymers was carried out in a two-stage procedure at 70°C. The first stage was aimed at polymerizing the PB block. The vessel temperature was set to 70°C (bath temperature) and *n*-BuLi was added by means of a bomb so as to initiate the polymerization of the first butadiene block (PB). The outer wall temperature was controlled by a water heater thermostat. The PB block was synthesized without modifier in order to achieve as low as possible a *1,2-vinyl* content. This initial polymerization step consists of a typical batch polymerization, without further charges of any additional reactants, and its reaction time was about 0.5 h with 100% yield. An aliquot of the

reaction mixture was collected immediately, prior to the second monomer charge to permit characterization of this first PB block.

For the synthesis of the second SBR block, styrene-*stat*-butadiene copolymer; TMEDA (with molar ratio  $n\text{-BuLi}/\text{TMEDA}$  1:0.4), styrene and 40 wt% of the total 1,3-butadiene needed for the preparation of the SBR block were added by means of a bomb to the living polybutadienyl-lithium. After 5 min, the remaining 1,3-butadiene (60 wt%) was metered by means of a pump with a continuous flow rate of 0.03g/s. Once 1,3-butadiene was completely added, the reaction mixture was stirred for an additional 20 min until conversion approached 100%. The remaining pressure was released and the polymerization was terminated with methanol. It is important to highlight that low *1,2-vinyl* contents were aimed for in both blocks, therefore a low TMEDA concentration was used for the synthesis of the SBR block. However, PS blockiness tends to appear at the end of the chain as a direct consequence of this low TMEDA concentration. Thus, a semi-batch concept was applied in this case in which 1,3-butadiene monomers were continuously added in order to control the reaction kinetics between 1,3-butadiene and styrene monomers. The final solid concentration was in average 12 wt%. Stabilizer (Irganox 1330) was dissolved in cyclohexane and added to the polymer solution with a final mass concentration of 0.5 phr (parts per hundred rubbers). Afterwards, this polymer mixture was discharged from the reactor and cyclohexane was removed via steam stripping. The final diblock copolymers were collected and dried by means of a circulation air dryer at 60°C until the mass was constant. The **Scheme 1** illustrates the stepwise copolymerization of the PB-SBR diblock copolymers with low *1,2-vinyl* content in both blocks.



**Scheme 1:** Stepwise anionic copolymerization of the PB-SBR diblock copolymers with low *1,2-vinyl* contents in both blocks.

### 4.1.2 Polymerization of symmetric PB-SBR diblock copolymers with systematically varied *1,2-vinyl* contents either in the PB or SBR block

A similar synthesis procedure to the one previously explained in **section 4.1.1** was used for the polymerization of the series of symmetric PB-SBR diblock copolymers having systematically varied *1,2-vinyl* contents in the SBR block. In this case due to the necessity to access higher *1,2-vinyl* contents in the SBR block, the concentration of TMEDA was adjusted accordingly. Besides, for the highest *1,2-vinyl* content the reaction temperature had to be lowered to 50°C. It is important to highlight that these were the only modifications made compared to the synthesis procedure described in **section 4.1.1**.

On the other hand, in order to polymerize the series of symmetric PB-SBR diblock copolymers having systematically varied *1,2-vinyl* content in the PB block, two main modifications compared to the synthesis route described **section 4.1.1** were made. They were: (1) the polymerization started with SBR block using the same *n*-BuLi:TMEDA ratio of 1:0.4 and (2) the TMEDA concentration was adjusted for the PB block polymerization depending on the *1,2-vinyl* content desired. Moreover, for the highest *1,2-vinyl* content the reaction temperature had to be lowered to 40°C. The modification (1) was adopted in order to keep low *1,2-vinyl* content in the SBR block and independently vary it in the PB block. Higher *1,2-vinyl* content was achieved by adjusting TMEDA concentration accordingly.

**Table 2** indicates *n*-BuLi:TMEDA ratio as well as the reaction temperature required to obtain the targeted *1,2-vinyl* contents in the independent blocks. For the highest *1,2-vinyl* contents the reaction temperature needed to be lowered since a higher *1,2-vinyl* content was not achieved by further increasing *n*-BuLi:TMEDA ratio at 70°C.

**Table 2:** The ratios of *n*-BuLi:TMEDA and the respective reaction temperature used for the polymerization of the individual PB and SBR block.

PB block			SBR block		
<i>l,2-vinyl</i> , mol%	<i>n</i> -BuLi: TMEDA	Temp., °C	<i>l,2-vinyl</i> , mol%	<i>n</i> -BuLi: TMEDA	Temp., °C
8.40	Without TMEDA	70	16.0	1:0.4	70
27.0	1:0.6	70	29.0	1:1	70
37.0	1:1	70	43.0	1:1.4	70
40.0	1:1.4	70	46.0	1:2	70
51.0	1:1.6	70	59.0	1:2	50
74.0	1:2.2	40			

## 4.2 Molecular characterization

### 4.2.1 Gel permeation chromatography (GPC)

Gel Permeation Chromatography (GPC) (SECcurity GPC System) was carried out at 35°C using two columns (PSS SDV linear XL 5µm) and a Waters 410 refractive index detector. Tetrahydrofuran (THF) was the mobile phase at flow rate of 1 ml/min. Calibration was carried out based on polystyrene (PS) standards with narrow molecular weight distribution and sample concentration of 1.0 mg/ml. The “polystyrene-equivalent” number average molecular weight ( $M_n$ ) and polydispersities ( $M_w/M_n$ ) of the PB block and the entire block copolymers PB-SBR were determined. The volume fractions ( $\Phi_{SBR}$ ) were calculated based on the  $M_n(SBR)$ ,  $M_n(PB)$ ,  $M_n(PB-SBR)$  and on the respective densities of the individual blocks, SBR and PB, obtained by the interpolation of  $\rho_{PB} = 0.89 \text{ g/cm}^3$  and  $\rho_{PS} = 1.05 \text{ g/cm}^3$ <sup>105</sup>

## 4.2.2 $^1\text{H}$ nuclear magnetic resonance (NMR)

*1,2-vinyl* (mol%) and styrene (wt%) contents were measured by  $^1\text{H}$  nuclear magnetic resonance (NMR) (Varian 400 MHz) according to the British Standard - BS ISO 21561:2005 +A1: 2010. The relative amount of styrene sequences longer than six units was determined based on the ratio of the phenyl *ortho* proton peak (6.5 ppm) and the total phenyl protons signal (6.1 – 7.7 ppm).<sup>106</sup> The samples were dissolved in deuterated chloroform containing 0.03% TMS at room temperature.

## 4.3 PB-SBR diblock copolymer samples

Four distinct series of PB-SBR diblock copolymers combining a polybutadiene (PB) block with a poly(styrene-*stat*-butadiene) (SBR) block were obtained. **Series I** consists of six symmetric ( $\sim 50$  vol%) PB-SBR diblock copolymers with low *1,2-vinyl* amount in both blocks and styrene contents in the SBR range of  $21 \leq x_{S,SBR} \leq 52$  mol% (in steps of  $\sim 5$  mol%). **Series II** contains in total six asymmetric samples with variable volume fraction ( $\Phi_{SBR}$ ) ranging from 20 to 69 vol% and low *1,2-vinyl* amounts in both blocks. The styrene content in the SBR varies only slightly ( $x_{S,SBR} = 32 \pm 4$  mol%). **Series III** is composed of five symmetric ( $\Phi_{PB} \approx \Phi_{SBR} \approx 50$  vol%) PB-SBR copolymer samples with low *1,2-vinyl* content in the PB block ( $\approx 8.0$  mol%), an average styrene content of  $39 \pm 4$  mol% and a *1,2-vinyl* content range of  $14.0 \text{ mol}\% \leq \textit{1,2-vinyl}(\text{SBR}) \leq 59.0 \text{ mol}\%$  in the SBR block. **Series IV** consists of six symmetric ( $\Phi_{PB} \approx \Phi_{SBR} \approx 50$  vol.%) PB-SBR copolymer samples with low *1,2-vinyl* content ( $\approx 16$  mol%), an average styrene concentration of  $32 \pm 4$  mol% in the SBR block and a *1,2-vinyl* content range of  $8.0 \text{ mol}\% \leq \textit{1,2-vinyl}(\text{PB}) \leq 74.0 \text{ mol}\%$  in the PB block.

The PB-SBR diblock copolymers in all series have a similar molecular weight of  $\underline{M}_n \sim 200$  kg/mol. Low *1,2-vinyl* contents are targeted for all samples of **Series I** and **Series II** in order to minimize known shifts in  $T_g$ <sup>107,108</sup> and changes in compatibility<sup>3</sup> caused by the microstructure of butadiene sequences. These diblock copolymers of **Series I** and **Series II** are labeled as  $\text{PB}_{\Phi_{PB}}\text{-S}^x\text{B}^y\text{R}_{\Phi_{SBR}}$ , where  $x = x_{S,SBR}$  and  $y = x_{B,SBR}$  are the approximated mole percentages of styrene (S) and butadiene (B) in the random block. On the other hand, PB-SBR diblock copolymers of **Series III** and **Series**

**IV** are labeled as  $\text{PB}^{1,2\text{-vinyl PB}}\text{-S}^x\text{B}^y\text{R}^{1,2\text{-vinyl SBR}}$ , where *1,2-vinyl* PB and *1,2-vinyl* SBR are the approximated *1,2-vinyl* contents in the PB and SBR, respectively; *x* and *y* are the mole percentages of styrene (S) and butadiene (B) in the random block.

Details on the microstructure of the diblock copolymer samples of all series are given in **Table 3**.

A polybutadiene homopolymer (PB,  $\underline{M}_w = 86.95$  kg/mol;  $\underline{M}_w/\underline{M}_n = 1.10$ ;  $c_{1,2\text{vinyl}} = 8.50$  mol%) and a random poly(styrene-*stat*-butadiene) copolymer ( $\text{S}^{30}\text{B}^{70}\text{R}$ ,  $\underline{M}_w = 81.98$  kg/mol;  $\underline{M}_w/\underline{M}_n = 1.04$ ;  $c_{1,2\text{vinyl}} = 17.63$  mol%;  $x_{\text{S,SBR}} = 29.84$  mol%) were synthesized in addition as reference materials.

**Table 3:** Molecular characteristics of all PB-SBR diblock copolymers.

Label	PB block			SBR block		PB-SBR diblock copolymer			
	$M_n$ ,	$M_w/M_n$	$C_{1,2-vinyl}$ ,	$x_{S,SBR}$ ,	$C_{1,2-vinyl}$ ,	$\Phi_{SBR}$	$M_n$ ,	$M_w/M_n$	$D$ , <sup>a</sup>
	kg mol <sup>-1</sup>		mol%	mol%	mol%	vol.%	kg mol <sup>-1</sup>		nm
<b>Series I</b>									
PB <sub>50</sub> -S <sup>52</sup> B <sup>48</sup> R <sub>50</sub>	110.75	1.06	8.39	52.15	15.74	46	214.76	1.04	69.0
PB <sub>50</sub> -S <sup>45</sup> B <sup>55</sup> R <sub>50</sub>	135.44	1.06	8.33	45.60	14.57	46	264.79	1.10	80.5
PB <sub>50</sub> -S <sup>40</sup> B <sup>60</sup> R <sub>50</sub>	108.85	1.06	8.72	40.41	15.05	46	210.88	1.05	63.4
PB <sub>50</sub> -S <sup>35</sup> B <sup>65</sup> R <sub>50</sub>	112.38	1.06	8.40	34.81	14.22	47	222.14	1.06	63.4
PB <sub>50</sub> -S <sup>27</sup> B <sup>73</sup> R <sub>50</sub>	103.24	1.06	8.60	27.38	16.15	48	206.98	1.05	53.2
PB <sub>50</sub> -S <sup>21</sup> B <sup>79</sup> R <sub>50</sub>	123.19	1.07	8.60	20.76	19.40	49	251.58	1.06	(51.5)
<b>Series II</b>									
PB <sub>80</sub> -S <sup>30</sup> B <sup>70</sup> R <sub>20</sub>	147.81	1.07	8.50	27.90	23.63	20	188.46	1.08	47.2
PB <sub>70</sub> -S <sup>30</sup> B <sup>70</sup> R <sub>30</sub>	123.22	1.07	8.50	32.64	18.96	30	179.73	1.09	62.8
PB <sub>62</sub> -S <sup>30</sup> B <sup>70</sup> R <sub>38</sub>	133.64	1.07	8.50	30.76	18.30	38	221.35	1.08	66.1
PB <sub>50</sub> -S <sup>35</sup> B <sup>65</sup> R <sub>50</sub>	112.38	1.06	8.40	34.81	14.22	47	222.14	1.06	63.4
PB <sub>40</sub> -S <sup>35</sup> B <sup>65</sup> R <sub>60</sub>	87.48	1.09	8.50	36.30	20.25	60	233.08	1.15	68.3
PB <sub>31</sub> -S <sup>35</sup> B <sup>65</sup> R <sub>69</sub>	50.76	1.18	8.37	34.35	16.54	69	173.71	1.06	49.5
<b>Series III</b>									
PB <sup>8</sup> -S <sup>35</sup> B <sup>65</sup> R <sup>14</sup>	112.38	1.06	8.40	34.81	14.22	47	222.14	1.06	62.8
PB <sup>8</sup> -S <sup>41</sup> B <sup>59</sup> R <sup>29</sup>	93.62	1.07	8.42	40.76	28.83	42	169.18	1.07	46.2
PB <sup>8</sup> -S <sup>44</sup> B <sup>56</sup> R <sup>43</sup>	107.85	1.10	8.40	44.18	42.85	38	181.81	1.11	45.8
PB <sup>8</sup> -S <sup>40</sup> B <sup>60</sup> R <sup>46</sup>	91.94	1.06	8.40	49.96	45.97	43	167.01	1.05	(36.9)
PB <sup>8</sup> -S <sup>34</sup> B <sup>66</sup> R <sup>59</sup>	102.83	1.06	8.40	33.73	58.69	46	197.23	1.06	(46.5)
<b>Series IV</b>									
PB <sup>8</sup> -S <sup>35</sup> B <sup>65</sup> R <sup>14</sup>	112.38	1.06	8.40	34.81	14.22	47	222.14	1.06	62.8
PB <sup>27</sup> -S <sup>30</sup> B <sup>70</sup> R <sup>18</sup>	86.24	1.08	26.91	29.63	17.91	51	182.28	1.03	62.8
PB <sup>37</sup> -S <sup>30</sup> B <sup>70</sup> R <sup>17</sup>	87.93	1.09	37.41	30.61	16.92	50	183.41	1.04	62.8
PB <sup>45</sup> -S <sup>27</sup> B <sup>73</sup> R <sup>16</sup>	101.02	1.04	45.51	27.19	15.64	43	185.31	1.07	68.7
PB <sup>51</sup> -S <sup>29</sup> B <sup>71</sup> R <sup>17</sup>	87.29	1.08	51.50	29.02	17.19	52	188.54	1.04	68.7
PB <sup>74</sup> -S <sup>27</sup> B <sup>73</sup> R <sup>16</sup>	105.21	1.04	73.67	27.20	17.34	54	188.13	1.04	68.7

<sup>a</sup> Periodicity calculated based on room temperature SAXS data for non-crosslinked samples using Bragg's law (details in **section 6.1.1**). Styrene sequences longer than six units were absent in all SBR blocks except for the sample with the highest styrene content in the SBR block (52 mol% S) which contains 8 wt% of such sequences.

## Chapter 5

### Mixing and vulcanization

#### 5.1 Non-filled PB-SBR diblock copolymers

An internal mixer (Brabender Plasticorder) of 83 cm<sup>3</sup> volume with two tangential rotors and a fill factor of 0.8 was used in order to incorporate the crosslinking additives into the polymer matrices. Polymer strips were added at low rotor speed of ~ 26 rpm, within this mixing time the temperature rose from 70 to 80°C. The material was further mixed until it looked homogenous, which took approximately 1 min. Afterwards, zinc oxide (2.5 phr), stearic acid (2 phr), N-cyclohexyl-2-benzothiazole sulfenamide (CBS, 2.5 phr), diphenylguanidine (DPG, 0.5 phr), N-(1,3-Dimethylbutyl)-N'-phenyl-p-phenylenediamine (6-PPD, 0.5 phr) and sulfur (1.5 phr) were added, and in order to further incorporate them into the polymer matrix the rotor speed was increased to 40 rpm. This mixing step has taken about 3 min and temperature reached about 90°C. To further enhance dispersion of those additives in the matrix and likewise melt them, the rotor speed was increased to 60 rpm for about 1 min and temperature reached about 110°C. Thereafter, the mixed batch was discharged and taken to the mill. It was passed through the roll mill four times with the back and front rotor speeds of 21 and 25 rpm, respectively, and a gap between them of 1.65 mm. Temperature in the roll mill was 50°C. The milled sheet was vulcanized in a rectangular frame of 110x160x2 mm<sup>3</sup> at 150°C applying a hydraulic pressure of 40 bar for 32 min. The chosen cure time was for all crosslinked samples larger than  $t_{90}$ .

#### 5.2 Silica-filled PB<sub>50</sub>-S<sup>45</sup>B<sup>55</sup>R<sub>50</sub> diblock copolymer composites

Among the PB-SBR diblock copolymer samples synthesized, PB<sub>50</sub>-S<sup>45</sup>B<sup>55</sup>R<sub>50</sub>, was selected in order to prepare a series of silica filled composites. The silica loading was varied from 20 to 80 phr in steps of 20 phr corresponding to filler volume fractions ( $\phi_{\text{sil}}$ ) of 0.082, 0.152, 0.212 and 0.264, respectively. The mixing was carried out in three main stages: 1) incorporation of silica into

the polymer matrix, 2) further mixing followed by the silanization reaction and at the end 3) the addition of the curatives. In the first stage, the initial mixing temperature was set to 80°C with a rotor speed of 19 rpm. Here, polymer strips, silica (Zeosil 1165MP from Solvay with surface area of 165 m<sup>2</sup>/g), anti-oxidant (0.75 phr, 6-PPD), oil (TDAE oil) and silane (Si 266 from EVONIK) were mixed. The oil to silica and silane to silica ratios used was 0.25 and 0.08 phr per 1 phr filler, respectively. Upon complete filler and additives incorporation, the temperature rose to about 110°C. After that, the rotor speed was increased to 40 rpm for 2 min until the temperature reached about 130°C. Consecutively, the rotation was increased to 60 rpm and consequently an increase in temperature up to few Kelvins was observed depending on the silica loading. Afterwards, the rotor speed was set to 80 rpm for 1 min and finally to 100 rpm for more 1 min. In this last step the mixing temperature was approximately 150°C at which silanization reaction takes place. Thereafter, the mixed batch was discharged and a relaxation time of about 1.5h was given prior to the second non-productive stage. This batch was further mixed at comparable conditions. Later, the curatives were added using the same chemicals and their respective concentration described in **section 5.1**. In this mixing step, temperature was not higher than 110°C in order to avoid premature vulcanization. Thereafter, the mixed batch was discharged and taken to the mill. It was passed through the roll mill four times with the back and front rotor speeds of 21 and 25 rpm, respectively, and a gap between them of 1.65 mm. Temperature in the roll mill was 50°C. The milled sheet was vulcanized in a rectangular frame of 110x160x2 mm<sup>3</sup> at 150°C applying a hydraulic pressure of 40 bar for 32 min. The chosen cure time was for all crosslinked samples larger than  $t_{90}$ .

## Chapter 6

### Characterization methods

#### 6.1 Differential Scanning Calorimetry (DSC)

Calorimeters are designed to determine phase transitions like crystallization, melting and glass transitions. Differential scanning calorimetry is one favored method providing qualitative and quantitative information about heat capacity or enthalpy.<sup>109</sup>

The principle of differential scanning calorimetry (DSC) is the measurement of the difference in the heat flow rate from/to the sample compared to a reference sample, being normally an empty pan. The main advantage of the difference principle is that the random external disturbances affect the two measuring system (sample and reference) in the same way, and therefore they will not significantly influence the difference signal. According to the working principle, DSC instruments are classified into two main types: (a) Heat Flux DSC and (b) Power Compensation DSC. In the latter, the difference in heating power is proportional to the heat flow released or consumed by the sample, while the characteristic feature of Heat Flux DSC is a symmetric heat flow from the furnace to the samples. As sample and reference behave thermally differently, the heat flow that goes through them causes a difference in temperature, which is proportional to the difference between the relevant heat flows.

The softening behavior of all samples was investigated in the non-crosslinked state by DSC experiments. The measurements on Series I, II and IV were performed using a METTLER TOLEDO DSC 821 instrument being a heat flow DSC at heating and cooling rates of  $|dT/dt| = 20$  K/min. The samples were first annealed at 130°C for 5 min, afterwards cooled down to -130°C and held at this temperature for 5 min before the heating scan was started. Sample masses were between 10 and 20 mg. The thermal glass transition temperature  $T_g$  and the related heat capacity step  $\Delta c_p$  were calculated according to ASTM E1269-05. For samples of **Series IV**, DSC specific heat curves were measured using a Perkin Elmer DSC 7 being a power compensation DSC with a heating rate of  $|dT/dt| = 10$  K/min. Samples with a mass of about 10 mg have been used.  $T_{g,PB}$  and  $T_{g,SBR}$  as well as the specific heat capacity steps related to the glass transition in the PB and SBR

phases,  $\Delta C_{p,PB}$  and  $\Delta C_{p,SBR}$ , were obtained by two individual tangent constructions for the PB and SBR glass transitions, respectively.

## 6.2 Small Angle X-ray Scattering (SAXS)

The SAXS technique is a useful tool to investigate long range ordered structures on a mesoscopic scale in the range from 10 Å up to 100 nm. Hence, it is possible to evaluate the periodicity of self-assembled block copolymers when there is sufficient electron density contrast between the two phases. **Figure 8** schematically illustrates a typical scattering set up. There is an incident beam of monochromatic radiation with wavelength  $\lambda$  and intensity  $I_0$ , which hits the sample. Whereas, the elastically scattered radiation ( $I(q)$ ) is measured by a detector (D) placed at a scattering angle  $2\theta$  to the sample. The typical wavelength  $\lambda$  used for SAXS measurements carried out on polymers is about 1Å. <sup>110</sup>

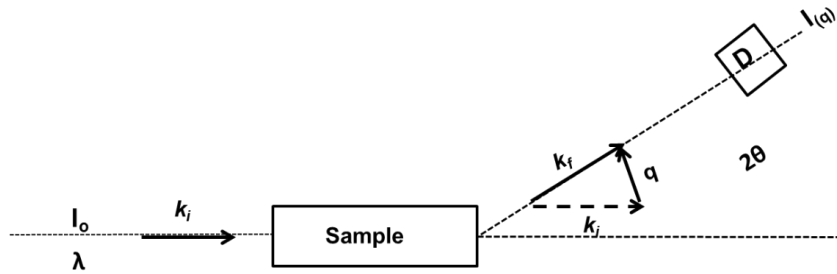


**Figure 8:** Typical small angle X-ray scattering set-up.

The scattering vector  $q$  shown in the sketch above describes the scattering geometry and it is represented by

$$\vec{q} = \vec{k}_f - \vec{k}_i \quad (11)$$

where  $k_f = 2\pi/\lambda$  and  $k_i = 2\pi/\lambda$  represent the wave vectors of the incident and scattered wave planes, respectively. In general, the final result of a scattering experiment is expressed by the scattered intensity as function of  $q$ -space,  $I(q)$ . In case of elastic scattering (frequency of the incident beam and scattered waves are identical) we have

$$|\vec{k}_f| = |\vec{k}_i| = \frac{2\pi}{\lambda} \quad (12)$$

Thus, by combining **Eq. (11)** and **(12)** one can obtain the absolute value of the scattering vector  $q$  as follows

$$|\vec{q}| = \frac{4\pi}{\lambda} \sin(\theta) \quad (13)$$

For materials containing periodic structures peaks occur in the scattering intensity  $I(q)$  due to constructive interference. A maximum in the scattered intensity  $I(q)$  occurs if the scattered waves from different planes, belonging to the same set of lattice planes, are “in-phase”. Constructive interference is obtained if an optical path difference  $2d\sin\theta$  between neighboring planes is an integral multiple of the wavelength  $n\lambda$  (**Figure 9**). Based on this condition one can calculate the periodicity for a given set of lattice planes or spacing  $d$  from the  $q$  value at the maximum of the corresponding scattering peak ( $q_{\max}$ ) using Bragg’s law

$$d = \frac{2\pi}{q_{\max}} \quad (14)$$

Note that Bragg’s equation is only applicable for isotropic materials. If  $\theta$  is small ( $\theta \leq 5^\circ$ ; Small angle x-ray scattering, SAXS), mesoscopic spacing  $d$  is accessible (1nm to 100nm). The vectorial nature of the relevant quantities has to be considered in case of anisotropic materials, and therefore the more complex Laue condition has to be applied for such materials.<sup>111</sup>

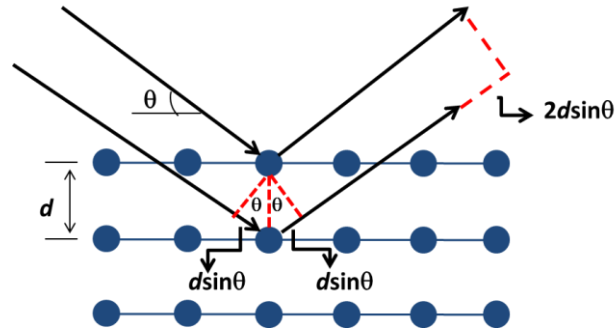


**Figure 9:** Scheme showing the derivation of Bragg’s law with  $d$  being the spacing describing the shown set of lattice planes (horizontal lines). The arrows indicate incoming waves and scattered waves.

Additional information about the morphology of microphase-separated block copolymers can be obtained from small angle X-ray scattering (SAXS) experiments by analyzing the peak positions in the scattering pattern. This method is based on the fact that different morphologies (lattices) result in the occurrence of different sets of lattice planes having a fixed relation of their  $d$  values. Hence, the higher order peaks for different morphologies such as lamellar (LAM), gyroid (GYR), cylinders (HPC) and spheres (FCC or BCC) appear at predefined multiples of the first Bragg reflection at  $q_1$  (**Table 4**).<sup>105</sup> This allows to determine the morphology of microphase-separated block copolymers directly from their scattering pattern  $I(q)$ .

**Table 4:** Peak positions (expressed as  $q/q_1$ ) of Bragg's reflections of various structures.

Morphology	Ratio of $q/q_1$
LAM	1, 2, 3, 4, 5, ...
HPC	1, $\sqrt{3}$ , $\sqrt{4}$ , $\sqrt{7}$ , $\sqrt{9}$ , $\sqrt{12}$ , ...
BCC	1, $\sqrt{2}$ , $\sqrt{3}$ , $\sqrt{4}$ , $\sqrt{5}$ , $\sqrt{6}$ , ...
FCC	1, $\sqrt{4/3}$ , $\sqrt{8/3}$ , $\sqrt{11/3}$ , $\sqrt{12/3}$ , $\sqrt{16/3}$ , ...
GYR	1, $\sqrt{4/3}$ , $\sqrt{7/3}$ , $\sqrt{8/3}$ , $\sqrt{10/3}$ , $\sqrt{11/3}$ , ...

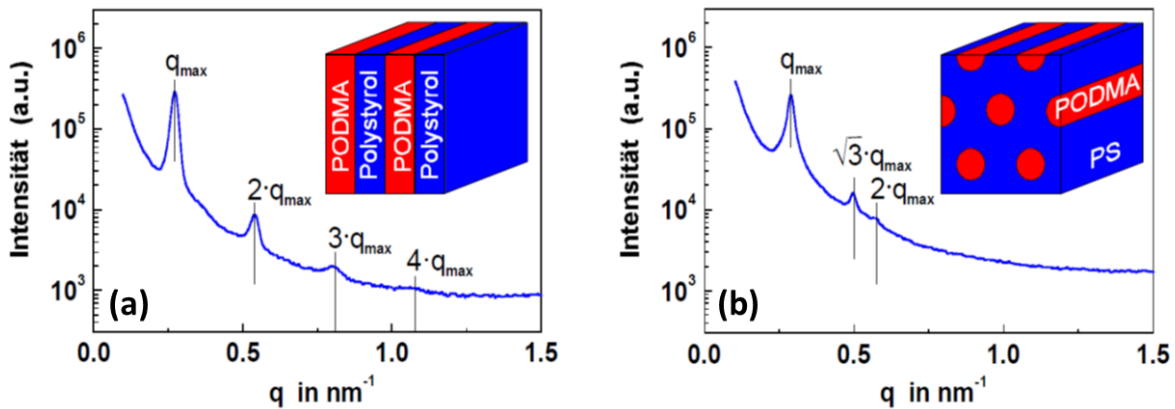


**Figure 10:** SAXS pattern of microphase-separated poly(styrene-*block*-octadecylmethacrylate) block copolymers [P(S-*b*-ODMA)] with (a) lamellar and (b) cylindrical morphology. Adapted from: Hempel, E., Budde, H., Horing, S., Beiner, M. *Lecture Notes Physics*, **2007**; 714, 201–228.

In principle, further information can be drawn from the intensity of individual scattering peaks in  $I(q)$ , i.e. their peak height. This is due to the fact that  $I(q)$  is related to a product of lattice factor  $L(q)$  and form factor  $F(q)$ . While the lattice factor is determined by the overall arrangement of the unit cells on a lattice (i.e. the dimensions of the unit cell), the form factor describes the content of the unit cell. The lattice factor is responsible for the position of the scattering peaks as discussed before, but the form factor strongly influences the peak heights.

SAXS measurements in this work were carried out at room temperature using a pinhole instrument designed by JJ X-rays on a Rigaku rotating anode as radiation source ( $\text{CuK}\alpha$ ,  $\lambda = 0.1542 \text{ nm}$ ) with Osmic multilayer optics, and a Bruker Hi-Star 2D detector. The scattering angle of the instrument was calibrated using silver behenate as reference material. The accessible  $q$ -range was  $0.065 \text{ \AA}^{-1} \leq q \leq 0.5 \text{ \AA}^{-1}$ . The sample-to-detector distance was about 1580 mm. The measurements were performed on non-crosslinked samples (without crosslinking additives). Thin films were prepared by pressing small polymer pieces in a frame of  $10 \times 30 \times 2 \text{ mm}^3$  with hydraulic pressure of 4 bar, at  $160^\circ\text{C}$  for 5 min.

### **6.3 Atomic Force Microscopy (AFM)**

The morphology of all PB-SBR diblock copolymers in the crosslinked state was characterized by AFM experiments. The measurements were carried out using a Nanowizard II (JPK-Instruments, Germany) scanning probe microscope with super sharp silicon tips having tip radii of about 2 nm. Phase images were measured in the tapping mode at room temperature. Ultrathin sections (100 nm) of the crosslinked molded sheets were trimmed with a cryo-ultramicrotome (PT-PC Powertome with CR-X cryo unit, RMC products) at a temperature of  $-120^\circ\text{C}$  using diamond knives. AFM measurements were carried out on freshly cut samples in order minimize the amount of additives migrating from the bulk to the surface.

### **6.4 Dynamic mechanical analysis (DMA)**

Dynamic mechanical analysis is a widely used technique to study the viscoelastic behavior of polymeric materials as a function of temperature, frequency, time, strain amplitude or a

combination of these parameters. A sinusoidal stress  $\sigma(t)$  or a strain  $\varepsilon(t)$  with small amplitudes is applied to the sample and the response is determined by measuring the complimentary quantity, i.e.  $\varepsilon(t)$  or  $\sigma(t)$ , respectively. Amplitude ratio and phase shift between  $\sigma(t)$  and  $\varepsilon(t)$  give the information about the material's viscoelastic response. Depending on the sample viscoelastic behavior the phase shift can vary within the interval 0 and 90°. For pure elastic materials,  $\sigma(t)$  and  $\varepsilon(t)$  are in-phase (0°), on the other hand for pure viscous samples  $\sigma(t)$  and  $\varepsilon(t)$  are 90° out-of-phase. Polymeric materials display a phase shift between that of pure elastic and viscous materials. **Figure 11** shows schematically the different phase shift scenarios depending on the material viscoelastic behavior. The equations below can mathematically describe the parameters,  $\sigma(t)$  and  $\varepsilon(t)$ , for the case that a sinusoidal strain  $\varepsilon(t)$  perturbation is applied to a sample, showing a stress  $\sigma(t)$  response with the same angular frequency  $\omega$  and a phase shift  $\delta$  between  $\sigma(t)$  and  $\varepsilon(t)$  <sup>112</sup>

$$\varepsilon(t) = \varepsilon_o \sin(\omega t) \quad (15)$$

$$\sigma(t) = \sigma_o \sin(\omega t + \delta) \quad (16)$$

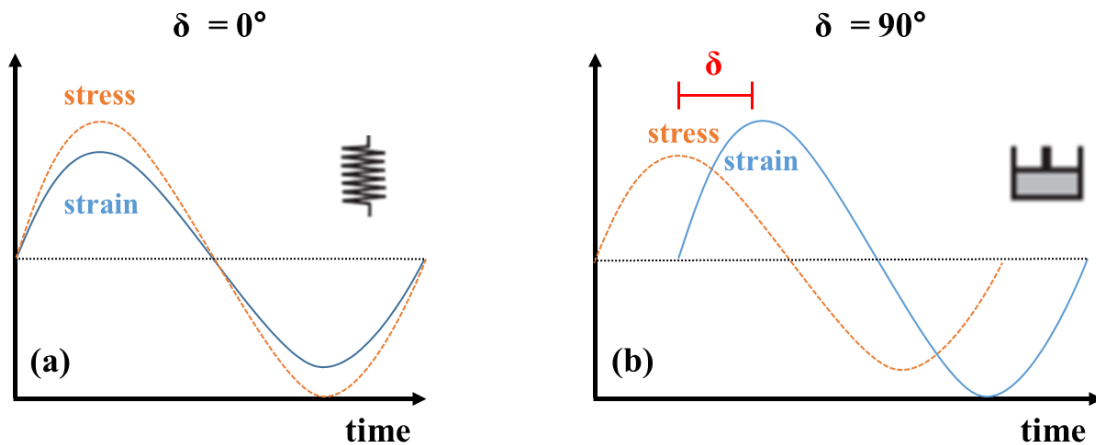


**Figure 11:** An applied sinusoidal strain (blue full line) having a sinusoidal stress response (orange dashed line) for perfectly (a) elastic and (b) viscous system.

The expansion of the stress equation response leads to the following

$$\sigma(t) = \sigma_o \sin(\omega t) \cos \delta + \sigma_o \cos(\omega t) \sin \delta \quad (17)$$

By dividing the **Eq.17** by the strain (**Eq. 15**) one can represent the stress response in terms of the “in-phase”, ( $G'$ ), and “out-phase, ( $G''$ ), shear moduli

$$\sigma(t) = \varepsilon_o G' \sin \omega t + \varepsilon_o G'' \cos \omega t \quad (18)$$

where  $G' = \frac{\sigma_o}{\varepsilon_o} \cos \delta$  and  $G'' = \frac{\sigma_o}{\varepsilon_o} \sin \delta$  are the storage and loss modulus, respectively. The storage modulus (in-phase part),  $G'$ , is a measure of the energy stored and recovered per cycle when a specimen is submitted to a periodic strain perturbation. Whereas, the loss modulus (out-of-phase part),  $G''$ , represents the energy dissipated or lost as heat per cycle when a of sinusoidal strain perturbation is applied in a sample.

Commonly, storage ( $G'$ ) and loss ( $G''$ ) moduli are combined and represented by the dynamic shear modulus,  $G^*$ , where  $G'$  and  $G''$  are the real and imaginary part, respectively.

$$G^* = G' + iG'' \quad (19)$$

The ratio  $G''/G'$  is named loss tangent or damping factor,  $\delta$  and often used in technical application since it is a (sample) geometry-independent quantity giving first information about the loss behavior.

The relaxation behavior of all vulcanized samples was investigated by DMA in a wide frequency-temperature range. The experiments were performed with an ARES rheometer (TA Instruments) in shear mode. A control strain of 0.1% was applied at low temperatures but increased to 0.3% at temperatures approximately 30 K above  $T_{g,PB}$  of the PB block. Rectangular samples with a size of  $30 \times 8 \times 2 \text{ mm}^3$  were used. Temperature sweeps were measured at four frequencies ( $\omega = 0.1, 1, 10, 100 \text{ rad/s}$ ) in the temperature range from -120 to  $T_{\alpha}^{SBR} + 30\text{K}$  with an increment of 3 K and a soak time of 100 s. In addition, isothermal frequency sweeps were measured in the range from 0.1 to 100 rad/s with five points per decade at temperatures in the range from -120°C to  $T_{\alpha}^{SBR} + 30\text{K}$  to construct master curves. The soak time in this case was 300 s at each temperature and the temperature increment was 2.5 K. All shear measurements were carried out under nitrogen gas atmosphere.

## Chapter 7

### Results

#### 7.1 Non-crosslinked PB-SBR diblock copolymer samples

##### 7.1.1 Structural analysis by small angle X-ray scattering

**Symmetric and asymmetric PB-SBR diblock copolymers with low *1,2-vinyl* contents in both blocks (Series I and Series II)** have been investigated in the non-crosslinked state by SAXS in order to learn more about microphase-separation and morphology. The SAXS patterns measured at room temperature in the scattering vector range  $0.065 \text{ \AA}^{-1} \leq q \leq 0.5 \text{ \AA}^{-1}$  are shown for all samples of these series in **Figure 12**.

The scattering patterns for most of the symmetric PB-SBR diblock copolymers (**Series I**) indicate a well-ordered lamellar morphology formed due to microphase-separation of the (PB) and (SBR) blocks (**Figure 12** (a)). The periodicities taken from Bragg's law (**Eq.14**) are listed in **Table 3**. Commonly  $d$  values in the range  $65 \pm 15 \text{ nm}$  are observed, based on the position of the first Bragg peak  $q_1$ . Note that the higher order peak at  $3q_1$  is usually well pronounced while the peak at  $2q_1$  is suppressed, which is a common feature of systems with volume fractions of both phases very close to 50% due to the influence of the form factor on the peak intensity.<sup>113</sup> The only exception, in **Series I**, is the diblock copolymer sample containing only 21 mol% styrene in the SBR block. In this case, mainly one peak is observed while higher order peaks are extremely weak or absent. This may indicate that this sample is close to the disordered state at room temperature. This seems to be reasonable for low styrene concentrations in the SBR block where a tendency towards miscibility is to be expected. Note that a certain increase of the peak width is already indicated in case of the sample containing 27 mol% S in the SBR block (in particular for the third order peak). This might be a first hint for reduced long range order (smaller coherence length) and weak segregation.

The SAXS patterns for non-crosslinked samples of the asymmetric diblock copolymers of **Series II** are presented in **Figure 12** (b). Although a strong diffraction peak at low  $q$  values is present for all samples, morphology information is in most of the cases not really available since higher order peaks are either smeared or absent. Hence, conclusions towards the morphology of the asymmetric diblock copolymers of **Series II** cannot be drawn despite of the sample with  $\Phi_{\text{SBR}} \sim 50$  vol% having obviously a lamellar structure. However, it will be shown in a later **section 7.2.1** that AFM images of the corresponding crosslinked samples prepared at  $150^\circ\text{C}$  show for various samples ( $31 \text{ vol}\% \leq \Phi_{\text{SBR}} \leq 62 \text{ vol}\%$ ) a well-defined microphase separated structure. Hence, the absence of higher order peaks in the SAXS pattern for non-crosslinked samples of **Series II** is probably caused by limited long range order. Expected positions for the higher orders in the SAXS patterns for the different volume fractions are incorporated in **Figure 12** (b). Periodicities for non-crosslinked samples are determined based on the position of the first scattering peak and Bragg's law (**Table 3**).

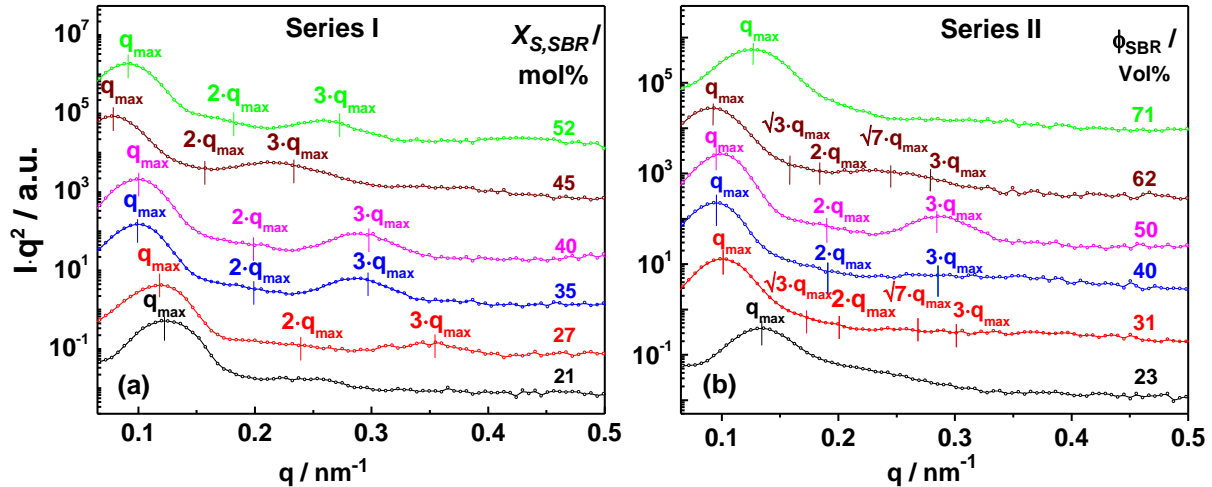


**Figure 12:** Lorentz-corrected SAXS patterns measured at room temperature for the non-crosslinked (a) symmetric (**Series I**) and (b) asymmetric (**Series II**) PB-SBR diblock copolymers with fixed  $1,2$  vinyl contents. The patterns are vertically shifted to the sake of clarity.

**Symmetric PB-SBR diblock copolymers with systematically varied  $1,2$ -vinyl contents either in the PB or SBR block (Series III and Series IV) in the non-crosslinked state are investigated analogously by SAXS in order to study miscibility behavior and structure. The scattering curves of the individual PB-SBR diblock copolymers are shown in **Figure 13**. All PB-SBR samples show**

at least one relatively narrow scattering peak ( $q_1$ ) in the 2D-SAXS patterns, hence indicating the presence of microphase separation. Besides, a higher order peak at  $3q_1$  together with a weak shoulder at  $2q_1$  were also observed for PB<sup>8</sup>-S<sup>35</sup>B<sup>65</sup>R<sup>14</sup> (**Series III**) and for all PB-SBR samples of **Series IV**. This indicates the existence of a long range ordered lamellar structure due to microphase separation of PB and SBR blocks in these samples. The scattering peak at  $2q_1$  is suppressed for most of the PB-SBR diblocks, which is expected for samples with volume fractions  $\Phi_{\text{SBR}}$  very close to 0.5 due to form factor related effects.<sup>113</sup> Although all samples of **Series III**, except PB<sub>8</sub>-S<sup>35</sup>B<sup>65</sup>R<sub>14</sub>, show a lack of higher order peaks, one can speculate that phase separation (probably weak segregation) is still present for some of them. According to their respective AFM images measured in the crosslinked state, PB<sub>8</sub>-S<sup>41</sup>B<sup>59</sup>R<sub>29</sub> and PB<sub>8</sub>-S<sup>44</sup>B<sup>56</sup>R<sub>43</sub> diblock copolymers phase separate into a lamellar structure even at 150°C (see **Section 7.1.2**). On the other hand, for the cross-linked diblock copolymers with higher *1,2-vinyl* contents in the SBR block, PB<sub>8</sub>-S<sup>40</sup>B<sup>60</sup>R<sub>46</sub> and PB<sub>8</sub>-S<sup>34</sup>B<sup>66</sup>R<sub>59</sub>, clear evidence of long range order is missing in the AFM images, although a separation between SBR and PB block seems to be still present. Probably, this can be understood as an indication for a state where concentration fluctuations are fixed by crosslinking at 150°C in a disordered system, which is slightly above the order-disorder-transition (ODT). Accordingly, the situation for the two non-crosslinked PB<sub>8</sub>-S<sup>40</sup>B<sup>60</sup>R<sub>46</sub> and PB<sub>8</sub>-S<sup>34</sup>B<sup>66</sup>R<sub>59</sub> samples at 25°C should also be relatively close to an ODT. Based on their SAXS data (**Figure 12(a)**) it is not possible to decide finally whether the relatively broad peak at  $q_1$  is indicating that these are weakly segregated diblock copolymer systems in the microphase-separated state or systems being in the disordered state with strong concentration fluctuations. In the latter case, the peak at  $q_1$  would be a so-called first sharp diffraction peak which is commonly observed slightly above the ODT.<sup>114</sup> Despite of this open point, the overall trend observed in **Series III** is reasonable since miscibility between PB and SBR blocks is expected to be enhanced by increasing *1,2-vinyl* content in the SBR block, according to literature data for respective thermodynamic interaction parameters (for details see **Section 8.1**).

By applying Bragg's law (Eq.(8)), it was possible to calculate the periodicity of the PB-SBR diblock copolymers shown in **Figure 12(a)**. Commonly  $d$  values in the range of  $47.6 \pm 9$  nm and  $65.7 \pm 3$  nm are observed for PB-SBR copolymers of **Series III** and **Series IV**, respectively (**Table 3**). The sample PB<sub>8</sub>-S<sup>35</sup>B<sup>65</sup>R<sub>14</sub> (**Series III**) has a larger periodicity compared to PB<sub>8</sub>-S<sup>41</sup>B<sup>59</sup>R<sub>29</sub> and PB<sub>8</sub>-S<sup>44</sup>B<sup>56</sup>R<sub>43</sub> samples of the same series due to its higher total molecular weight.

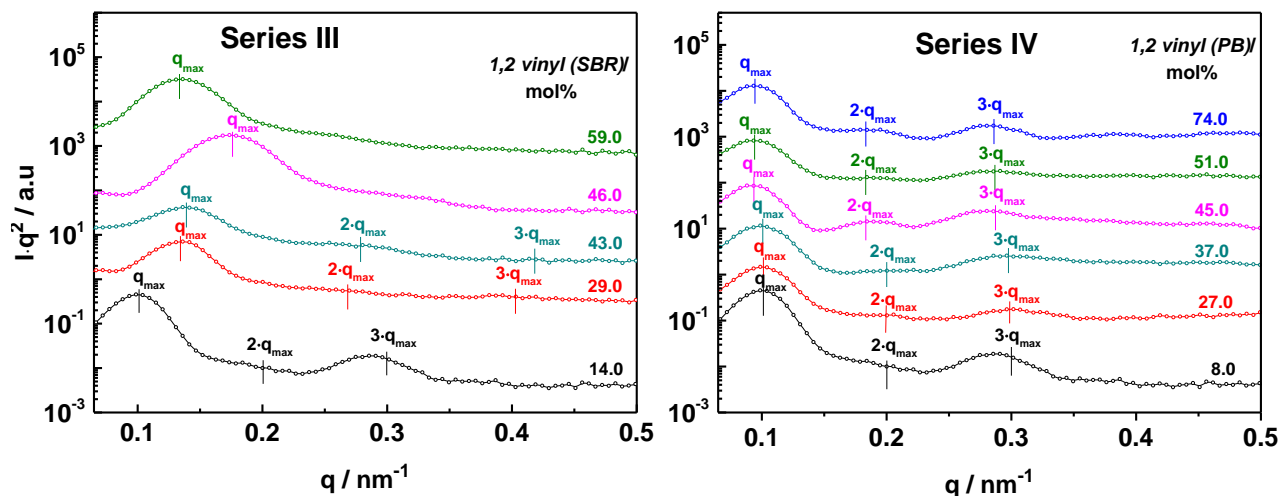


**Figure 13:** Lorentz-corrected SAXS patterns measured at room temperature for the non-crosslinked symmetric PB-SBR diblock copolymers with different *1,2-vinyl* content varying from 14 to 59 mol% in the SBR block (**Series III**) and varying from 8 to 74 mol% in the PB block (**Series IV**). The patterns are vertically shifted to the sake of clarity.

## 7.1.2 Information about the softening behavior from Differential Scanning Calorimetry

Symmetric and asymmetric PB-SBR diblock copolymers with low *1,2-vinyl* contents in both blocks (**Series I** and **Series II**) have been studied by differential scanning calorimetry (DSC) in order to understand and quantify the softening behavior of these amorphous, usually bi-phasic samples in the non-crosslinked state. Heating scans measured with a rate of +20 K/min are shown in **Figure 14** for non-crosslinked symmetric (**Series I**) and asymmetric (**Series II**) PB-SBR diblock copolymers as well as the PB and  $\text{S}^{30}\text{B}^{70}\text{R}$  samples as reference systems. All diblock copolymer samples, except  $\text{PB}_{80}\text{-S}^{30}\text{B}^{70}\text{R}_{20}$ , show two well separated glass transitions at low and high temperature, which correspond to the PB and SBR phase, respectively. The corresponding glass transition temperatures,  $T_{g,\text{PB}}$  and  $T_{g,\text{SBR}}$ , are given in **Table 5**. Most of the PB-SBR diblock copolymers (apart from  $\text{PB}_{80}\text{-S}^{30}\text{B}^{70}\text{R}_{20}$  and  $\text{PB}_{50}\text{-S}^{21}\text{B}^{79}\text{R}_{50}$ ) show a PB phase glass transition at  $T_{g,\text{PB}} = -92.8 \pm 0.6^\circ\text{C}$  which is quite comparable to  $T_{g,\text{PB}} = -93.4^\circ\text{C}$  observed for the corresponding PB homopolymer. The existence of two well-separated glass transitions and the coincidence of the

$T_{g,PB}$  values of the non-crosslinked PB-SBR samples with the PB homopolymer glass temperature can be interpreted as an additional evidence for microphase separation of PB and SBR blocks in accordance with that what has been concluded from SAXS. Only the PB-SBR samples with the lowest styrene content (21 mol% in the SBR) in **Series I** and with the smallest volume fraction  $\Phi_{SBR} = 0.20$  in **Series II** show a significantly different softening behavior. A slightly higher  $T_{g,PB}$  of  $-91.4^{\circ}\text{C}$  is observed for sample  $\text{PB}_{50}\text{-S}^{21}\text{B}^{79}\text{R}_{50}$ , and only a single glass transition at  $-90.7^{\circ}\text{C}$  is seen in case of the sample  $\text{PB}_{80}\text{-S}^{30}\text{B}^{70}\text{R}_{20}$ . These are clear hints for partially or completely miscible states indicating a trend towards one single phase.

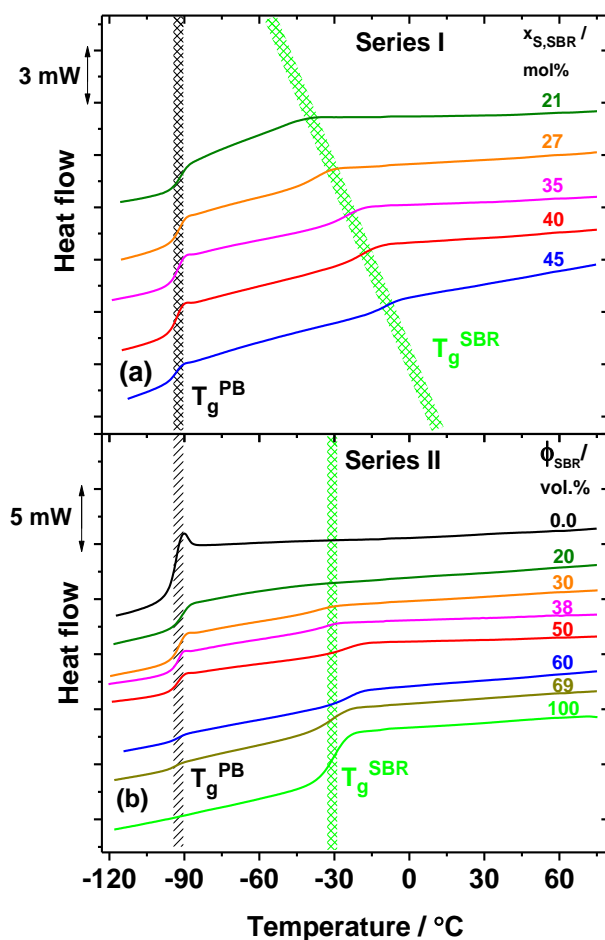


**Figure 14:** DSC heating scans measured with a heating rate of  $|dT/dt| = +20\text{K/min}$  for non-crosslinked diblock copolymer samples of (a) **Series I** with variable styrene content in the SBR block and (b) **Series II** with different volume fraction of the SBR block as well as  $\text{S}^{30}\text{B}^{70}\text{R}$  and **PB** reference systems for comparison. The heat flow curves are vertically shifted for the sake of clarity.

**Table 5:** Glass temperatures and heat capacity steps of non-crosslinked symmetric (**Series I**) and asymmetric (**Series II**) PB-SBR diblock copolymers as well as the corresponding **S<sup>30</sup>B<sup>70</sup>R** and **PB** reference systems measured with a heating rate  $|dT|/|dt|$  of 20 K/min.

Series I					Series II				
Sample	$T_{g,PB}$ , °C	$T_{g,SBR}$ , °C	$\Delta C_{p,PB}$ , J·g <sup>-1</sup> K <sup>-1</sup>	$\Delta C_{p,SBR}$ , J·g <sup>-1</sup> K <sup>-1</sup>	Sample	$T_{g,PB}$ , °C	$T_{g,SBR}$ , °C	$\Delta C_{p,PB}$ , J·g <sup>-1</sup> K <sup>-1</sup>	$\Delta C_{p,SBR}$ , J·g <sup>-1</sup> K <sup>-1</sup>
PB <sub>50</sub> - S <sup>21</sup> B <sup>79</sup> R <sub>50</sub>	-91.4	-49.8	0.190	n.a. <sup>a</sup>	PB <sub>80</sub> - S <sup>30</sup> B <sup>70</sup> R <sub>20</sub>	(-90.7) <sup>b</sup>	n.a. <sup>b</sup>	(0.431) <sup>b</sup>	n.a. <sup>b</sup>
PB <sub>50</sub> - S <sup>27</sup> B <sup>73</sup> R <sub>50</sub>	-92.1	-37.1	0.242	0.141	PB <sub>70</sub> - S <sup>30</sup> B <sup>70</sup> R <sub>30</sub>	-92.1	-35.8	0.285	0.053
PB <sub>50</sub> - S <sup>35</sup> B <sup>65</sup> R <sub>50</sub>	-92.4	-25.8	0.247	0.133	PB <sub>62</sub> - S <sup>30</sup> B <sup>70</sup> R <sub>38</sub>	-92.7	-33.5	0.275	0.080
PB <sub>50</sub> - S <sup>40</sup> B <sup>60</sup> R <sub>50</sub>	-93.1	-18.8	0.240	0.094	PB <sub>50</sub> - S <sup>35</sup> B <sup>65</sup> R <sub>50</sub>	-93.1	-25.8	0.247	0.133
PB <sub>50</sub> - S <sup>45</sup> B <sup>55</sup> R <sub>50</sub>	-93.4	-9.2	0.230	0.167	PB <sub>40</sub> - S <sup>35</sup> B <sup>65</sup> R <sub>60</sub>	-92.4	-23.8	0.122	0.256
PB <sub>50</sub> - S <sup>52</sup> B <sup>48</sup> R <sub>50</sub>	-93.8	-2.7	0.247	0.129	PB <sub>31</sub> - S <sup>35</sup> B <sup>65</sup> R <sub>69</sub>	-92.7	-28.1	0.068	0.254
S <sup>30</sup> B <sup>70</sup> R	-	-87.9	-	0.485	PB	-93.4	-	0.583	-

<sup>a</sup> The SBR glass transition of PB<sub>50</sub>-S<sup>21</sup>B<sup>79</sup>R<sub>50</sub> is too weak to calculate a  $\Delta C_p$  value. <sup>b</sup> The sample PB<sub>80</sub>-S<sup>30</sup>B<sup>70</sup>R<sub>20</sub> showed basically only one broad glass transition at -90.7°C which is slightly shifted to higher temperature compared to  $T_{g,PB}$  of **PB** homopolymer of similar microstructure.

The glass temperature of the SBR phase  $T_{g,SBR}$  for symmetric PB-SBR diblock copolymers with different styrene contents in the SBR block (**Series I, Figure 14(a)**) shifts systematically to higher temperatures as the styrene content increases like in random SBR copolymers. In case of the asymmetric PB-SBR diblock copolymers (**Series II, Figure 14(b)**) with nearly identical styrene content in the SBR block ( $x_{S,SBR} = 32 \pm 4$  mol%),  $T_{g,SBR}$  varies only within a small temperature interval. The observed scatter in  $T_{g,SBR}$  is mainly due to a small variation of the styrene concentration in the SBR block (**Table 3**).

The  $\Delta c_{p,PB}$  and  $\Delta c_{p,SBR}$  values obtained by two individual tangent constructions for the PB and SBR glass transitions are presented in **Table 4** and in **Figure 15** for all well microphase-separated diblock copolymers. A detailed analysis shows that the  $\Delta c_p$  values of the PB and SBR components as well as their sum  $\Delta c_{p,PB} + \Delta c_{p,SBR}$  do not change significantly with composition for diblock copolymers of **Series I** (**Figure 15** (a)). However, the situation in **Series II** was quite different. Here, the  $\Delta c_p$  values of the PB and SBR components correlate clearly with the volume or weight fractions ( $\Phi_{SBR}$  or  $w_{SBR}$ ) of both blocks while the sum  $\Delta c_{p,PB} + \Delta c_{p,SBR}$  is only weakly affected. This can be understood based on group contribution-like models<sup>115,116</sup> predicting that the total  $\Delta c_p$  of the diblock copolymers of **Series II** should depend on the total PB and SBR weight fractions,  $w_{PB}$  and  $w_{SBR}$ , according to

$$\begin{aligned} \Delta c_{p,total} &= w_{PB} \cdot \Delta c_{p,PB}^{ref} + w_{SBR} \cdot \Delta c_{p,S^{30}B^{70}R}^{ref} \\ &= (\phi_{PB} \cdot \rho_{PB} / \langle \rho \rangle) \cdot \Delta c_{p,PB}^{ref} + (\phi_{SBR} \cdot \rho_{SBR} / \langle \rho \rangle) \cdot \Delta c_{p,S^{30}B^{70}R}^{ref} \end{aligned} \quad (14)$$

where  $\langle \rho \rangle$  is the average density of the PB-SBR diblock copolymer and the heat capacity step heights  $\Delta c_p^{ref}$  are those for the reference materials given in J/gK. Since  $\Delta c_{p,PB}^{ref} = 0.583$  J/gK is only slightly bigger than  $\Delta c_{p,S^{30}B^{70}R}^{ref} = 0.485$  J/gK, the  $\Delta c_{p,total}$  values change only moderately with block copolymer composition in case of **Series II**. Interestingly, the experimental values of  $\Delta c_{p,PB} + \Delta c_{p,SBR}$  remain commonly about 35% smaller than  $\Delta c_{p,total}$ . Moreover, according to **Figure 15b** a linear extrapolation of  $\Delta c_{p,PB}$  and  $\Delta c_{p,SBR}$  approaches zero before the weight fraction of PB or SBR in the microphase-separated diblock copolymers goes to zero. This happens at about 20 to 25 wt% for PB and SBR phases, respectively.

All these findings may indicate that there are contributions between the glass transitions of both pure phases related to the existence of interfacial material, which are not considered if a standard tangent construction is used to evaluate the glass transition of the ‘pure’ PB and SBR phases. The contributions of interfacial material to  $\Delta c_p$  should exist in between  $T_{g,PB}$  and  $T_{g,SBR}$  and should be even more pronounced in weakly segregated diblock copolymers. The weak changes in  $\Delta c_{p,PB} + \Delta c_{p,SBR}$  for diblock copolymers of **Series I** can also be understood based on group contribution like models considering the relatively small variation of the total styrene content in these diblock copolymers. Assuming that  $\Delta c_{p,SBR}^{ref}$  of SBR is basically proportional to its styrene content one

would expect small changes between 0.462 J/gK and 0.388 J/gK for the SBR phase for the strongly segregated samples with styrene contents of  $x_{S,SBR} = 27$  mol% ( $w_S = 42.05$  wt%) and  $x_{S,SBR} = 52$  mol% ( $w_S = 67.72$  wt%) in the SBR block, respectively. Since PB has a larger  $\Delta c_{p,PB}^{ref} = 0.583$  J/gK and all samples of **Series I** contain the same volume fractions of SBR and PB,  $\Phi_{SBR} \sim \Phi_{PB} \sim 50$  vol.%, the change of  $\Delta c_{p,total}$  for the entire diblock copolymer according to **Eq.(14)** should be relatively small. In accordance with this prediction the changes in  $\Delta c_{p,PB} + \Delta c_{p,SBR}$  for the strongly segregated samples of **Series I** are found to be weak as shown in **Figure 15** (a). A common aspect of **Series I** and **Series II** is, however, that also  $\Delta c_{p,PB} + \Delta c_{p,SBR}$  of **Series I** is much smaller than  $\Delta c_{p,total}$  indicating the existence of a large amount of interfacial material. Elsewhere, the group contribution-like concept has also been used for diblock copolymers in order to predict the heat capacity of the individual phases.<sup>117</sup>

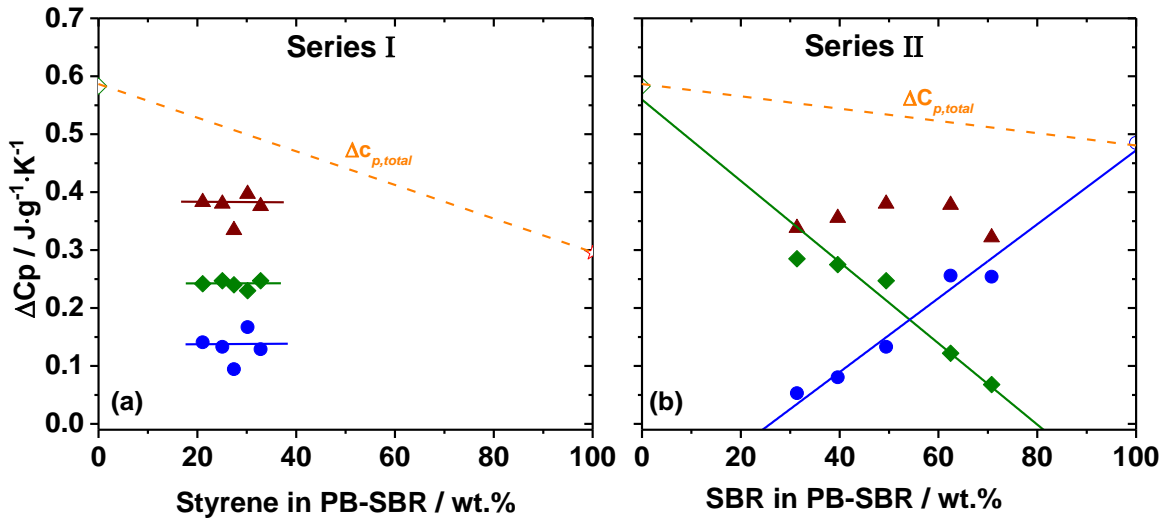


**Figure 15:** Step height  $\Delta c_p$  of the PB (diamonds) and SBR (circle) glass transition as well as the sum of both individual  $\Delta c_p$  values (triangles) for strongly segregated non-crosslinked PB-SBR diblock copolymers as function of (a) total styrene content in the PB-SBR block for **Series I** and (b) weight fraction of SBR block in the total PB-SBR diblock copolymer for **Series II**. The  $\Delta c_p$  values of PB and  $S^{30}B^{70}R$  reference systems are given for comparison in part (b). The dotted line is an interpolation based on the group contribution concept. The solid lines are linear fits to the data for strongly segregated diblock copolymer data.

**Symmetric PB-SBR diblock copolymers with systematically varied *1,2-vinyl* content in the PB block (Series IV)** are investigated in the same context by DSC. In contrast to the previously shown data, where heat flow data from DSC have been analyzed, absolute heat capacity data are reported here for **Series IV** giving additional information regarding the thermodynamic situation. Heat capacity data from a DSC heating scan measured with a rate of +10 K/min for non-crosslinked symmetric PB-SBR diblock copolymers of **Series IV** with systematically varied *1,2-vinyl* content in the PB block are presented in **Figure 16**. All samples display two well separated glass transitions at low and high temperature which correspond to the PB and SBR phase, respectively. This softening behavior can be understood as further evidence for the existence of well separated PB and SBR phases in the non-crosslinked state as also indicated by SAXS data for **Series IV (Section 7.1.1)**. According to an extrapolation made for  $T_{g,PB}$  and  $T_{g,SBR}$  as a function of *1,2-vinyl* and styrene content, respectively, it was found that in case of the PB<sup>74</sup>-S<sup>27</sup>B<sup>73</sup>R<sup>16</sup> sample  $T_{g,PB}$  is higher than  $T_{g,SBR}$  (**section 8.1**) due to the significant high *1,2-vinyl* content in the PB block. The glass temperature of the PB phase,  $T_{g,PB}$ , is systematically shifted to higher temperatures as *1,2-vinyl* content increases (**Table 6**), as expected based on related studies on PB homopolymers.<sup>107,108</sup> The trend in  $T_{g,PB}$  depending on the PB microstructure will be considered in some more detail in **Section 8.1**. For samples with higher *1,2-vinyl* contents in the PB block,  $T_{g,PB}$  is quite close to  $T_{g,SBR}$ . For the sample PB<sup>74</sup>-S<sup>27</sup>B<sup>73</sup>R<sup>16</sup> both glass transitions,  $T_{g,PB}$  and  $T_{g,SBR}$ , almost coincide. Note that this behavior of  $T_{g,PB}$  has in a first approximation nothing to do with miscibility-related effects since all samples are microphase-separated showing a well-defined lamellar structure (**Section 7.1.1**). The observed scatter in  $T_{g,SBR}$  (**Table 6**) is mainly due to a certain variation of the styrene concentration in the SBR block in the range  $x_{S,SBR} = 31 \pm 4$  mol% (**Table 3**). The resulting changes in  $T_{g,SBR}$  depending on  $x_{S,SBR}$  will be also shortly considered in **Section 8.1**.

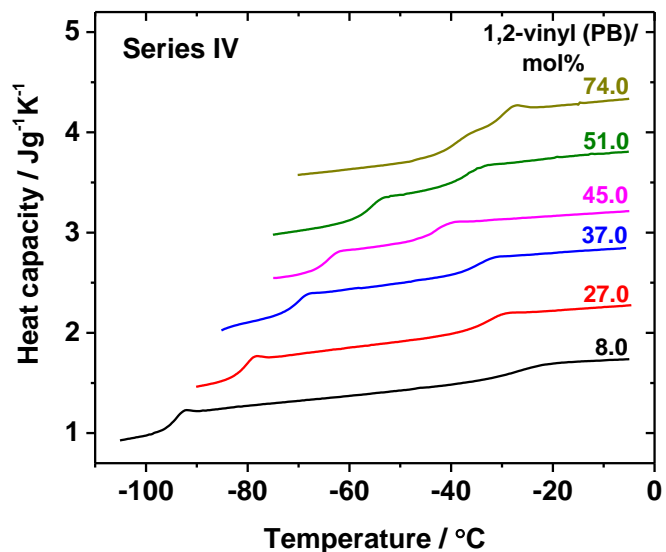


**Figure 16:** DSC heat capacity were measured with a heating rate of +10 K/min for non-crosslinked symmetric PB-SBR diblock copolymers with systematically varied *1,2-vinyl* content in the PB block (**Series IV**). The heat capacity curves are vertically shifted by 0.5 J/g<sup>-1</sup>K<sup>-1</sup> for the sake of clarity.

The heat capacity steps of the individual phases,  $\Delta c_{p,PB}$  and  $\Delta c_{p,SBR}$ , as obtained from two individual tangent constructions are given in **Table 6**. Obviously, there is a relatively weak scatter in both quantities depending on the *1,2-vinyl* content in the PB block (**Table 6** and **Figure 17**). Their sum ( $\Delta c_{p,PB} + \Delta c_{p,SBR}$ ) is also not significantly dependent on this parameter. Values of about  $0.32 \pm 0.02$  J/g<sup>-1</sup>·K<sup>-1</sup> are commonly observed for all samples in **Series IV**. Considering (i) group contribution-like concepts, (ii) strong segregation of PB and SBR phases and (iii) a weak dependence of  $\Delta c_{p,PB}$  on the microstructure, it is expected that the  $\Delta c_p$  values of the PB and SBR components as well as their sum  $\Delta c_{p,PB} + \Delta c_{p,SBR}$  do not change significantly with composition (*1,2-vinyl* content in the PB block). Most interestingly, and in line with that what has been found above for **Series I** and **Series II**, is that the experimental values of  $\Delta c_{p,PB} + \Delta c_{p,SBR}$  for **Series IV** are also about 40% smaller than those calculated based on group contribution-like concepts (**Figure 17**). This result is a clear indication for contributions to  $c_p(T)$  related to interfacial material which are not considered if two standard tangent constructions are used to evaluate the glass transitions of the „pure“ PB and SBR phases. Interfacial material should contribute to  $c_p(T)$  in the region between the glass transitions

of both pure phases. A detailed consideration, incorporating the estimation of interfacial width in the investigated block copolymers (**Section 8.1**) and the possible influence of Cooperative Rearranging Regions (CRRs) on the softening behavior will be presented in **Section 8.2**.

**Table 6:** Glass temperatures and heat capacity steps corresponding to the individual PB and SBR phase of non-crosslinked symmetric PB-SBR diblock copolymers (**Series IV**) measured with a heating rate  $|dT|/|dt|$  of 10 K/min.

Samples	$T_{g,PB}$ , °C	$T_{g,SBR}$ , °C	$\Delta C_{p,PB}$ , $J \cdot g^{-1}K^{-1}$	$\Delta C_{p,SBR}$ , $J \cdot g^{-1}K^{-1}$	$\Delta C_{p,PB} + \Delta C_{p,SBR}$ , $J \cdot g^{-1}K^{-1}$
PB <sup>8</sup> - S <sup>35</sup> B <sup>65</sup> R <sup>14</sup>	-95.9	-27.5	0.19	0.14	0.33
PB <sup>27</sup> - S <sup>31</sup> B <sup>66</sup> R <sup>18</sup>	-82.1	-34.7	0.18	0.16	0.34
PB <sup>37</sup> - S <sup>35</sup> B <sup>65</sup> R <sup>17</sup>	-70.9	-35.2	0.16	0.13	0.29
PB <sup>45</sup> - S <sup>36</sup> B <sup>64</sup> R <sup>16</sup>	-64.8	-43.5	0.16	0.15	0.31
PB <sup>51</sup> - S <sup>31</sup> B <sup>69</sup> R <sup>17</sup>	-57.2	-37.4	0.20	0.15	0.35
PB <sup>74</sup> - S <sup>27</sup> B <sup>73</sup> R <sup>16</sup>	-31.7	-41.4	0.18	0.13	0.31

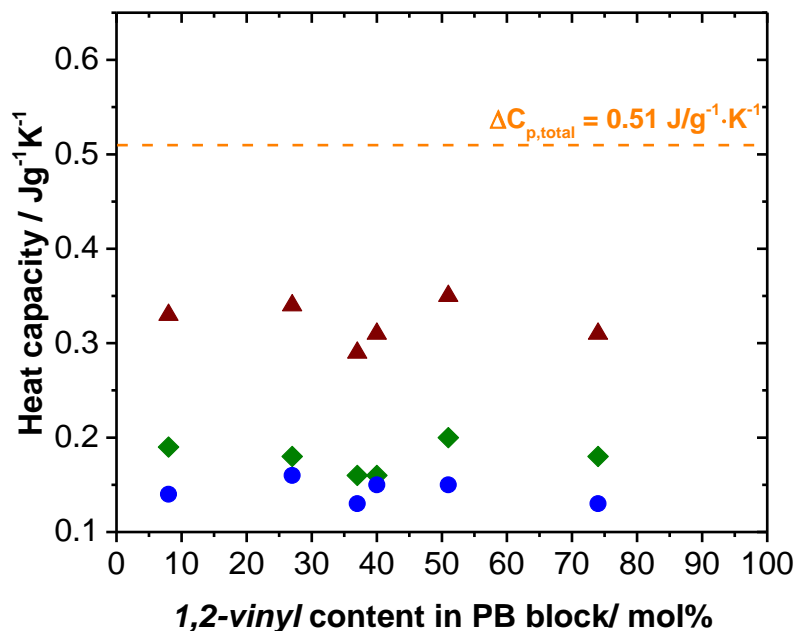


**Figure 17:** Step height  $\Delta C_p$  of the PB (diamonds) and SBR (circle) glass transition as well as the sum of both individual  $\Delta C_p$  values (triangles) for strongly segregated non-crosslinked PB-SBR diblock copolymers as function of *1,2-vinyl* content in the PB block for **Series IV**. The dotted line is an extrapolation from the group contribution concept considering the average total styrene content in the PB-SBR diblock copolymer of 25 wt%.

## 7.2 PB-SBR diblock copolymers in the cross-linked state

### 7.2.1 Structural information from Atomic Force Microscopy

**Symmetric and asymmetric PB-SBR diblock copolymers with low *1,2-vinyl* contents in both blocks (Series I and Series II)** in the vulcanized state are investigated by AFM in order to clarify their morphology. Phase contrast images of crosslinked symmetric diblock copolymers (**Series I**) show that all samples with styrene contents in the SBR block larger than 27 mol% are microphase separated (**Figure 18**). This is an expected finding for symmetric diblock copolymers with incompatible components. Interestingly, long range order and morphology are practically

unaffected by the relatively harsh vulcanization procedure. The observed morphologies and periodicities  $D$  are comparable to those observed for the corresponding diblock copolymers in the non-crosslinked state, as indicated by small angle x-ray scattering experiments (**Section 7.1.1**). AFM images for samples with lower styrene contents in the SBR block (21 and 27 mol% S) show a completely different behavior. A lamellar morphology is definitively absent in this case. This can be clearly seen in the zoomed insets on their respective AFM images. The zooms indicate that both diblock copolymers are in the disordered state due to increased compatibility of PB and SBR blocks. Thus, one can conclude that a transition from a well-ordered microphase-separated state to disordered state occurs in this sample series, under the given preparation conditions, somewhere between 35 and 27 mol% S in the SBR block. Note that larger amounts of additives migrating from the bulk and crystallizing on the surface are present in both disordered samples. Zoomed images made in regions where these migrated additives are practically absent (insets in **Figure 18**) indicate that the two components, PB and SBR, are not homogeneously mixed in these obviously disordered samples. PB and SBR enriched domains still exist. This behavior might be the consequence of concentration fluctuations, which are preserved above order-disorder-transition and fixed during the vulcanization step at 150°C. Such a state seems to be, somehow, expected considering the SAXS data for the corresponding samples in the non-crosslinked state at 25°C (**Section 7.1.1**).

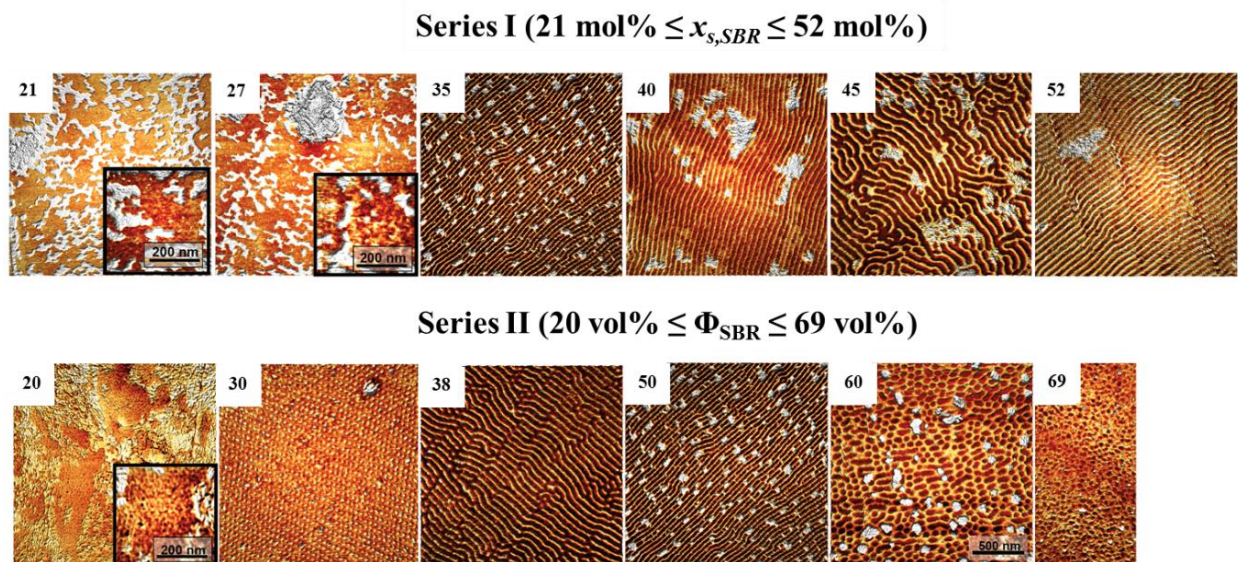


**Figure 18:** AFM phase contrast images for crosslinked symmetric PB-SBR diblock copolymers (**Series I**) with styrene contents in the SBR block varying from 21 to 52 mol% (upper row) and asymmetric block copolymer samples (**Series II**) with SBR volume fractions in the range  $20 \text{ vol}\% \leq \Phi_{SBR} \leq 69 \text{ vol}\%$  (lower row). The scale bar with a length 500 nm is applicable for all images. For the zoomed images the scale bar has a length of 200 nm.

AFM images of asymmetric PB-SBR diblock copolymers (**Series II**) with volume fractions in the range  $30 \text{ vol}\% \leq \Phi_{SBR} \leq 60 \text{ vol}\%$  show well microphase-separated states with different morphologies (**Figure 18**, lower row). Hexagonally packed SBR cylinders embedded in a PB matrix ( $\Phi_{SBR} = 30 \text{ vol}\%$ ), lamellar morphologies ( $\Phi_{SBR} = 38$  and  $50 \text{ vol}\%$ ), or PB domains dispersed in the SBR phase ( $\Phi_{SBR} = 60 \text{ vol}\%$ ) are observed depending on the volume fraction. Note that in the latter case neither a lamellar nor a cylindrical morphology is seen although microphase separation obviously occurs. One can speculate that a non-equilibrium morphology is formed and fixed during processing at high temperatures (mixing at 70 to 110°C and crosslinking at 150°C). This might be due to a temperature-dependent transition from lamellae to cylinders during heating combined with kinetic hindrance of block copolymers with limited mobility under the used preparation conditions. AFM images for the crosslinked diblock copolymer with  $\Phi_{SBR} = 20 \text{ vol}\%$  indicate that this sample is in the disordered state. Long range order and clear indications for microphase-separated domains are missing. Similar features occur for the diblock copolymer with  $\Phi_{SBR} = 69 \text{ vol}\%$ . However, in this case a certain concentration gradient seems to be present although clear evidence for long range order is missing. This may be related again to concentration

fluctuation in the disordered state frozen during the crosslinking step. Morphology studies on the diblock copolymer with  $\Phi_{\text{SBR}} = 20$  vol% are again impaired by the presence of additives on its surface.

**Symmetric PB-SBR diblock copolymers with systematically varied 1,2-vinyl contents either in the PB or SBR block (Series III and Series IV)** in the vulcanized state are also studied by AFM. Corresponding phase contrast images of crosslinked symmetric diblock copolymers with different 1,2-vinyl contents  $c_{1,2\text{-vinyl}}$  in the SBR block (**Series III**) are shown in the upper part of **Figure 19**. A well-defined lamellar morphology is observed for samples with  $c_{1,2\text{-vinyl}}$  in the SBR block smaller than 43 mol%, as expected for microphase-separated symmetric ( $\Phi_{\text{SBR}} \sim 50$  vol.%) diblock copolymers. The AFM images for the two samples with higher 1,2-vinyl (SBR) contents, 46 and 59 mol% (PB<sub>8</sub>-S<sup>40</sup>B<sup>60</sup>R<sub>46</sub> and PB<sub>8</sub>-S<sup>34</sup>B<sup>66</sup>R<sub>59</sub>), indicate that both samples are disordered. Remaining indications for the existence of PB and SBR enriched domains are restricted to very small length scales, eventually corresponding to fluctuating patterns with small characteristic length scales formed above the order-disorder transition and fixed by cross-linking. This observation, for samples cross-linked at 150°C, seems to be compatible with the absence of higher orders and a broad scattering peak observed in their respective SAXS patterns for non-crosslinked samples (**Section 7.1.1**) measured at 25°C.

AFM pictures of crosslinked symmetric diblock copolymers with different 1,2-vinyl content in the PB block (**Series IV**) are shown in **Figure 19** (lower part). All PB-SBR copolymer samples are microphase-separated showing a well-defined long range ordered lamellar morphology. These results are in agreement with findings from small angle X-ray scattering (SAXS) data performed on their corresponding samples (**Section 6.1.1**) in the non-crosslinked state at 25°C. For those PB-SBR diblock copolymers in the strongly segregated state, morphology was not affected by applying high shear forces along the mixing process and high temperatures up to 150 °C during vulcanization.

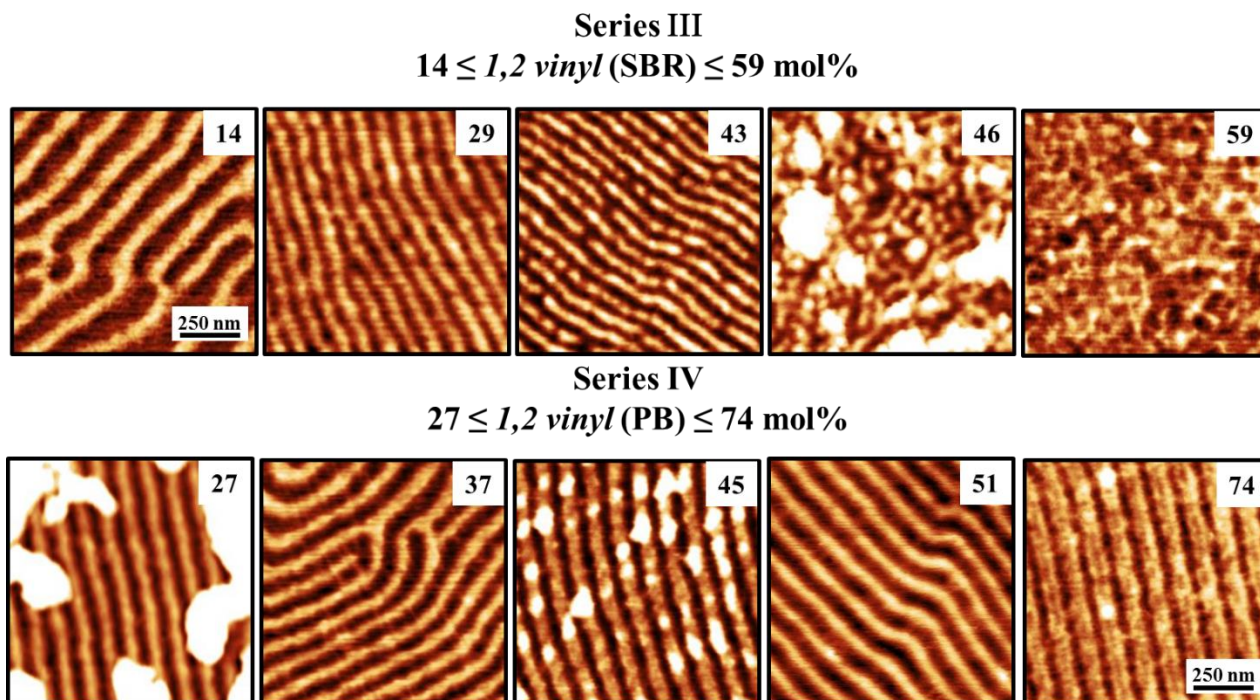


**Figure 19:** AFM phase contrast images showing  $2 \times 2 \mu\text{m}^2$  scans for crosslinked symmetric PB-SBR diblock copolymers with different *1,2-vinyl* content in the SBR block (**Series III**) varying from 14 to 59 mol% (upper row) and in the PB block (**Series IV**) varying from 27 to 74 mol% (lower row). The scale bar with a length 250 nm is applicable for all images.

Finally, it should be noted here that SAXS experiments on crosslinked diblock copolymer samples do not give useful information since the presence of additives like zinc oxide (ZnO) causes strong additional scattering contributions making it impossible to extract information about the diblock copolymer morphology. **Figure 20** shows a comparison of the SAXS pattern for the  $\text{PB}_{50}\text{-S}^{35}\text{B}^{65}\text{R}_{50}$  samples in the non-crosslinked (additive-free) and crosslinked state as a representative example. A decay-like behavior without obvious scattering peaks is observed for the crosslinked sample. This is due to scattering contributions of well dispersed particles masking those of the periodic diblock copolymer matrix. This phenomenon has been also reported for crosslinked SBR rubbers containing dispersed ZnO particles.<sup>118</sup> As shown on AFM images in **Figure 18** the absence of diffraction peaks in the SAXS pattern for the crosslinked samples is definitively not caused by a missing long-range order after the mixing and vulcanization processes. Accordingly, by plotting a Kratky plot such as  $(I(q) \cdot q^3 \text{ vs. } q)$  it was possible to observe a weak shoulder for crosslinked samples at the same  $q_1$  of its corresponding non-crosslinked sample. This is shown in the insert of

**Figure 20** and clearly indicates that domain size was maintained for samples in the strongly segregated state after processing.

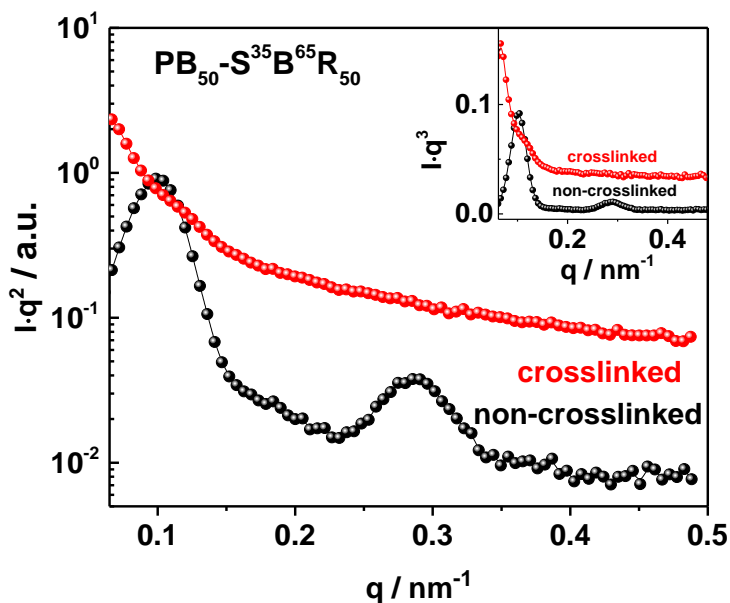


**Figure 20:** Lorentz-corrected SAXS patterns measured at room temperature for sample  $\text{PB}_{50}\text{-S}^{35}\text{B}^{65}\text{R}_{50}$  in the non-crosslinked (red) and crosslinked (black) states. The inset shows a plot  $Iq^3$  vs.  $q$  where the presence of a scattering peak near  $0.1 \text{ \AA}^{-1}$  is indicated.

## 7.2.2 Relaxation dynamics from dynamic shear measurements

The relaxation behavior of **symmetric and asymmetric PB-SBR diblock copolymers with low 1,2-vinyl contents in both blocks (Series I and Series II)** are systematically investigated by dynamic shear measurements. Temperature-dependent data for shear storage  $G'(T)$  and loss  $G''(T)$  moduli measured at a fixed frequency ( $\omega = 10 \text{ rad/s}$ ) for crosslinked samples of **Series I, Series II** and the reference systems (PB and  $\text{S}^{30}\text{B}^{70}\text{R}$ ) are presented in **Figure 21**. Symmetric diblock copolymers (**Series I**) with  $x_{\text{S,SBR}} \geq 35 \text{ mol\%}$  show two independent relaxation processes at low and high temperatures corresponding to the dynamic glass transitions of both phases,  $\alpha_{\text{PB}}$  and  $\alpha_{\text{SBR}}$ , respectively (**Figure 21a**). This can be understood as further evidence for a segregation of both phases, PB and SBR, for high styrene contents in the SBR block. Expectedly, the  $\alpha_{\text{SBR}}$  relaxation process shifts systematically to higher temperatures with increasing styrene content as known for

random SBR copolymers and it was also observed in  $T_{g,SBR}$  values taken from DSC measurements for their corresponding non-crosslinked PB-SBR samples (**Section 7.1.2**). Only the symmetric samples with the lowest styrene contents in the SBR block, PB<sub>50</sub>-S<sup>21</sup>B<sup>79</sup>R<sub>50</sub> and PB<sub>50</sub>-S<sup>27</sup>B<sup>73</sup>R<sub>50</sub>, depict a different behavior. The only relaxation process observed for the PB<sub>50</sub>-S<sup>21</sup>B<sup>79</sup>R<sub>50</sub> sample is slightly shifted towards higher temperatures compared to the  $\alpha_{PB}$  processes for strongly segregated samples. A separate  $\alpha_{SBR}$  process at higher temperatures is missing in this case. This can be interpreted as an indication for a high degree of miscibility of PB and SBR blocks, i.e. the existence of one single phase in accordance with structural information from AFM (**Figure 18**). In case of PB<sub>50</sub>-S<sup>27</sup>B<sup>73</sup>R<sub>50</sub>, the major  $\alpha$  relaxation peak in  $G''(T)$  is shifted to higher temperature compared to the  $\alpha_{PB}$  peaks for strongly segregated diblock copolymers with higher styrene contents. Besides, a weak shoulder is observed at higher temperatures (near -45°C) indicating probably the existence of SBR enriched domains. One may understand this relaxation behavior as a consequence of a structure with PB enriched domains containing a small fraction of styrene units combined with a lot of interfacial material with higher concentration of styrene. Consequently, there are pronounced styrene concentration gradients in the sample as indicated also in the AFM image by revealing a lack of defined phase boundary between PB and SBR phase. This should lead to a broader distribution of  $\alpha$  relaxation times with two maxima corresponding to PB and SBR enriched domains where the latter should have a higher  $T_g$  compared to  $T_{g,PB}$  corresponding to longer  $\alpha$  relaxation times under isothermal conditions. Further details will be considered in **section 8.2**.

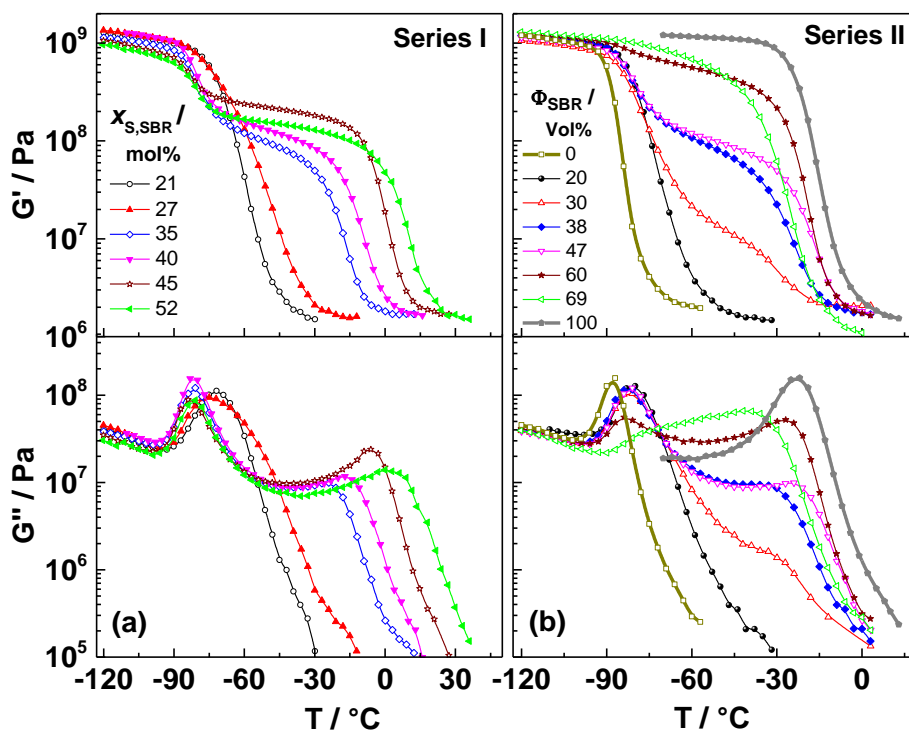


**Figure 21:** Temperature-dependence of the shear storage ( $G'$ ) and loss ( $G''$ ) modulus for crosslinked samples of (a) **Series I** with variable styrene content in the SBR block and (b) **Series II** with different volume fraction of the SBR block including  $S^{30}B^{70}R$  and PB as reference systems.

Shear measurements for diblock copolymers of **Series II** with volume fractions in the range  $30 \text{ vol.}\% \leq \Phi_{\text{SBR}} \leq 60 \text{ vol.}\%$  (**Figure 21b**) show two well-separated main relaxation processes at about  $-80^\circ\text{C}$  ( $\alpha_{\text{PB}}$ ) and at about  $-25^\circ\text{C}$  ( $\alpha_{\text{SBR}}$ ). This is the typical relaxation behavior of diblock copolymers in the strong segregation limit. The intensity of both relaxation processes,  $\alpha_{\text{PB}}$  and  $\alpha_{\text{SBR}}$ , varies systematically with  $\Phi_{\text{SBR}}$  although the intensity is not expected to be directly proportional to the volume fraction. Note that a certain scatter in the  $T_{\alpha, \text{SBR}}^{10 \text{ rad/s}}$  values (**Table 7**) corresponding to the maximum position of  $\alpha_{\text{SBR}}$  peak in  $G''(T)$  is mostly due to a slight variation of styrene content during synthesis (**Table 3**). Quite different behavior is observed for the diblock copolymers of **Series II** with pronounced asymmetries ( $\text{PB}_{31}\text{-S}^{35}\text{B}^{65}\text{R}_{69}$  and  $\text{PB}_{80}\text{-S}^{30}\text{B}^{70}\text{R}_{20}$ ). The  $\text{PB}_{31}\text{-S}^{35}\text{B}^{65}\text{R}_{69}$  sample depicts a broad bimodal relaxation process with two maxima in  $G''(T)$  located at temperatures between those of the  $\alpha_{\text{PB}}$  and  $\alpha_{\text{SBR}}$  processes in strongly segregated members of this series. This indicates the absence of pure PB and SBR domains and instead

indicates the existence of a large amount of interfacial material. The relaxation behavior of the PB<sub>80</sub>-S<sup>30</sup>B<sup>70</sup>R<sub>20</sub> sample is reminiscent of a miscible diblock copolymer. The peak maximum of the main  $\alpha$  relaxation process in  $G''(T)$  is slightly shifted towards higher temperatures compared to that of the  $\alpha_{PB}$  process in case of strongly segregated systems. However, weak contributions of SBR rich domains, which are just too low to be detectable as a separated peak or shoulder, can hardly be excluded.

Finally, we should note that the relaxation temperatures  $T_{\alpha, PB}^{10 \text{ rad/s}}$  of all strongly segregated and crosslinked PB-SBR diblock copolymers are about 7K higher than the corresponding value of the crosslinked PB reference (**Figure 21**). Possibly, this indicates a higher crosslinking density of the PB phase in PB-SBR diblock copolymers since it is well known that  $T_{g, PB}$  of pure PB homopolymers increases with crosslinking density.<sup>119</sup> The fact that the DSC glass temperatures  $T_{g, PB}$  of the PB phase in non-crosslinked PB-SBR copolymers are similar to that of the PB homopolymer (**Table 7**) may support this hypothesis.

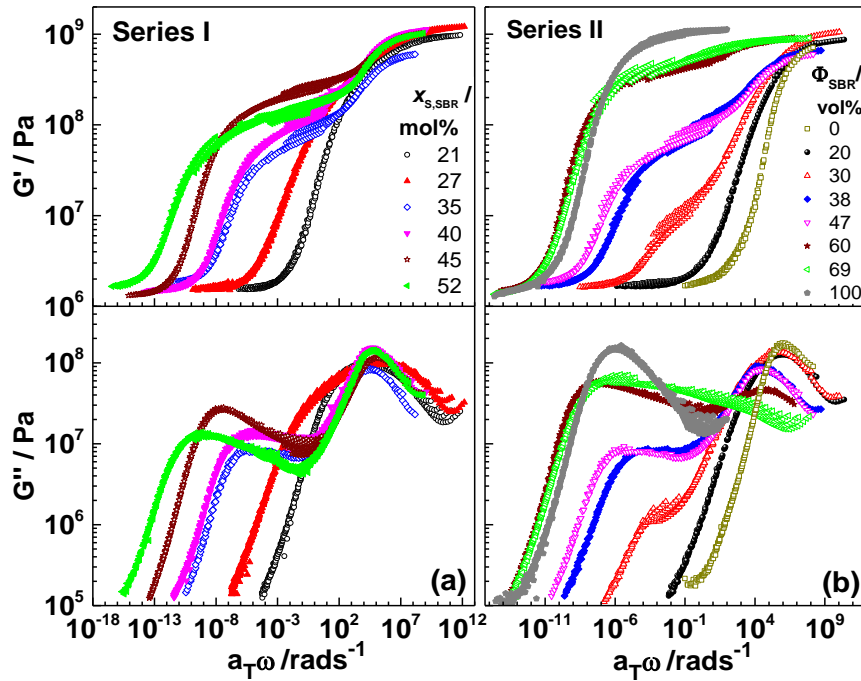


**Figure 22:** Master curves of the shear storage ( $G'$ ) and loss ( $G''$ ) modulus for crosslinked samples of (a) **Series I** with variable styrene content  $x_{S,SBR}$  and (b) **Series II** with different volume fraction  $\Phi_{SBR}$ . Data for S<sup>30</sup>B<sup>70</sup>R and PB samples are shown for comparison. All master curves are constructed using  $-60^\circ\text{C}$  as reference temperature.

In order to understand further details of the relaxation behavior, isothermal shear experiments in the frequency range 0.1-100 rad/s are carried out in a broad temperature interval including both  $\alpha$  relaxation processes. **Figure 22** shows the resulting master curves constructed by shifting the isotherms horizontally along the log frequency axis assuming that the shape of the relaxation spectrum is temperature-independent as predicted by the time temperature superposition principle (TTS). The reference temperature is in all cases  $-60^{\circ}\text{C}$ . This shifting procedure neglects differences in the temperature dependence of the relaxation processes  $\alpha_{\text{PB}}$  and  $\alpha_{\text{SBR}}$  dominating in different temperature ranges but gives a first overview of the relaxation behavior of the investigated systems. The scatter in the data between both dynamic glass transitions is basically due to the fact that the temperature dependence of  $\alpha_{\text{PB}}$  and  $\alpha_{\text{SBR}}$  is significantly different. Thus, the isotherms do not superimpose well. However, the master curves confirm the main trends in the relaxation behavior discussed above based on the isochrones. In **Series I** the shift of  $\alpha_{\text{SBR}}$  relaxation towards lower frequencies with increasing styrene content in the SBR block is clearly seen (**Figure 22 a**) although details should be influenced by the violation of the TTS as discussed below. The relaxation strength of the  $\alpha_{\text{SBR}}$  processes is very similar for all strongly segregated systems ( $x_{\text{S,SBR}} \geq 35$  mol%). In case of **Series II**, the most important changes in the relaxation behavior with block copolymer composition are also confirmed by the master curves (**Figure 22 b**). It is clearly seen that the relaxation strength of the  $\alpha_{\text{SBR}}$  process ( $\Delta G'_{\text{SBR}}$ ) decreases systematically with decreasing volume fraction  $\Phi_{\text{SBR}}$ . The position of both relaxation processes,  $\alpha_{\text{PB}}$  and  $\alpha_{\text{SBR}}$ , is weakly influenced for well microphase-separated blocks ( $38 \text{ vol}\% \leq \Phi_{\text{SBR}} \leq 60 \text{ vol}\%$ ). The strong shift of the  $\alpha_{\text{SBR}}$  process for  $\Phi_{\text{SBR}} = 30 \text{ vol}\%$  relative to the others is at least partly artificial and a consequence of the violations of the TTS as confirmed by a more detailed evaluation below. A single relaxation process located close to  $\alpha_{\text{PB}}$  is observed, as expected, for the disordered sample  $\text{PB}_{80}\text{-S}^{30}\text{B}^{70}\text{R}_{20}$ . A bimodal peak in  $G''(\text{T})$  with strong relaxation modes at intermediate frequencies is found for  $\text{PB}_{31}\text{-S}^{35}\text{B}^{65}\text{R}_{69}$  supporting the absence of pure PB and SBR phases.

In a final step, the information about the temperature dependence of the average relaxation times ( $\tau_{\alpha} = \omega_{\alpha}^{-1}$ ) of both segmental relaxation processes,  $\alpha_{\text{PB}}$  and  $\alpha_{\text{SBR}}$ , is extracted from shear data for strongly segregated diblock copolymers measured in a broad frequency-temperature range. The shifting behavior of both  $\alpha$  relaxation processes was evaluated independently assuming that the segmental dynamics of both phases, PB and SB, are independent. Individual shift factors  $a_{\text{T,PB}}$  and  $a_{\text{T,SBR}}$  are determined by decomposing the isotherms in parts belonging to  $\alpha_{\text{PB}}$  and  $\alpha_{\text{SBR}}$ ,

respectively. These pre-evaluated isotherms are used to construct two independent master curves giving individual shift factors  $a_{T,PB}$  and  $a_{T,SBR}$  related to the temperature dependence of the average relaxation frequencies  $\omega_{\alpha,PB}$  and  $\omega_{\alpha,SBR}$ , respectively. Another approach to learn more about the temperature dependence of  $\omega_{\alpha,PB}$  and  $\omega_{\alpha,SBR}$  is to determine the relaxation temperatures,  $T_{\alpha,PB}^{\omega}$  and  $T_{\alpha,SBR}^{\omega}$ , corresponding to the maxima of the  $\alpha_{PB}$  and  $\alpha_{SBR}$  relaxation peaks in  $G''(T)$  isochrones measured at different frequencies in the range  $0.1 \text{ rad/s} \leq \omega \leq 100 \text{ rad/s}$  (see isochrones for 10 rad/s in **Figure 21**). Arrhenius plots combining such relaxation temperatures,  $T_{\alpha,PB}^{\omega}$  and  $T_{\alpha,SBR}^{\omega}$ , with shift factors,  $a_{T,PB}$  and  $a_{T,SBR}$ , obtained from a horizontal shift of decomposed isotherms are shown in **Figure 23**. One can clearly see that the temperature dependencies of  $\omega_{\alpha,PB}$  and  $\omega_{\alpha,SBR}$  are quite different for **Series I** as well as **Series II**.

In order to quantify the temperature dependence of the cooperative  $\alpha$  dynamics in pure PB and SBR domains the individual shift factors  $(a_T)_{PB}$  and  $(a_T)_{SBR}$  are fitted using the Vogel-Fulcher-Tammann (VFT) equation (**Equation 6**). It describes quite well the segmental  $\alpha$  dynamics in many glass forming materials over a wide temperature range. The VFT parameters for the investigated samples are listed in **Table 7**. Note that, in principle, only the value of  $a_{T,0}$  is dependent on the reference temperature chosen for the master curve construction while the other parameters should be unaffected.

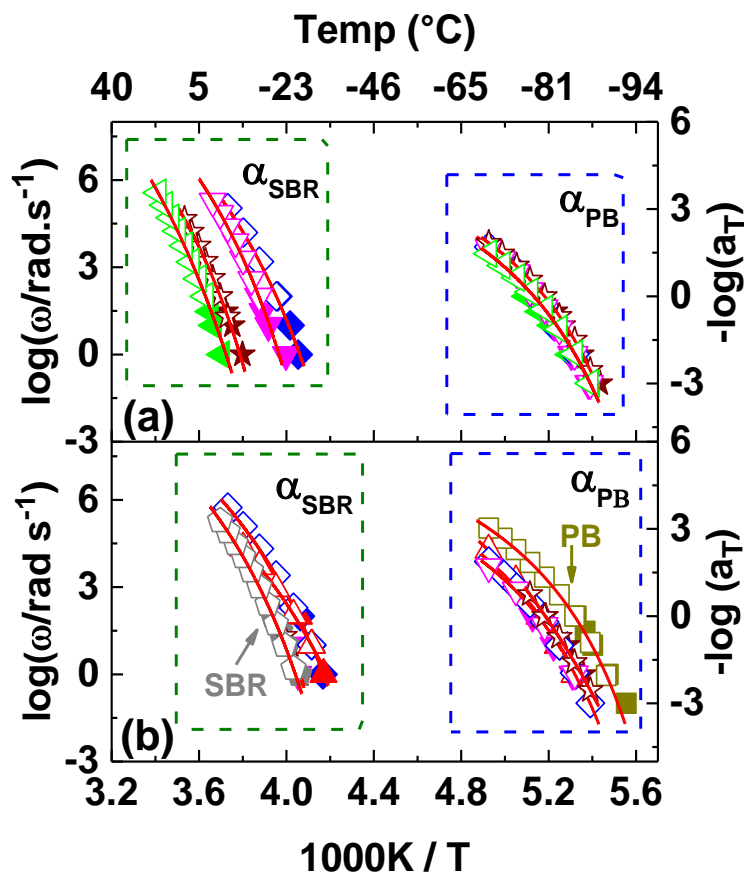


**Figure 23:** Arrhenius diagram showing shift factors  $a_T$  (open symbols) and relaxation temperatures  $T_{\alpha^0}$  taken from  $G''(T)$  isochrones (full symbols) for the relaxation processes,  $\alpha_{PB}$  and  $\alpha_{SBR}$ , of crosslinked diblock copolymers of (a) **Series I** with variable styrene content  $x_{S,SBR}$  and (b) **Series II** with different volume fraction  $\Phi_{SBR}$ . Data for  $S^{30}B^{70}R$  and PB reference systems are shown for comparison. The symbols and colors correspond to those used in **Figures 21** and **22**. The reference temperature was adapted in such a way that the  $a_T$  values coincide with  $T_{\alpha^0}$ . The solid lines are VFT fit curves for the shift factors.

Considering the temperature-dependent data for the  $\alpha_{PB}$  relaxations for all strongly segregated samples it can be directly seen in **Figure 23** that the traces (more or less) coincide. This holds for **Series I** as well as **Series II**. Thus, one can conclude that the softening behavior of the PB domains in well microphase-separated diblock copolymers is basically domain shape and domain size independent. Note that the obtained  $\omega_{\alpha_{PB}}$  traces are also in reasonable agreement with those for the corresponding PB homopolymer with similar microstructure, although a certain vertical shift is obvious in the Arrhenius plot. The temperature dependencies are clearly identical although the

average relaxation frequencies are significantly different. This finding corresponds to the already mentioned fact that the  $T_{\alpha, \text{PB}}^{10 \text{ rad/s}}$  values for crosslinked diblock copolymers are commonly a bit higher compared to the value for the crosslinked PB homopolymer.

One can also see in **Figure 23** that the relaxation temperatures  $T_{\alpha, \text{SBR}}^{10 \text{ rad/s}}$  in **Series I** systematically increase with increasing styrene content as long as the samples are well microphase-separated. A systematic shift of the individual  $\alpha_{\text{SBR}}$  traces to higher temperatures appears in the Arrhenius diagram as the styrene content increases. This is expected based on the findings for random SBR copolymers. This effect is accompanied by a certain change in the overall temperature dependence of the relaxation frequencies. For instance, different  $T_{\alpha, \text{SBR}}^{10 \text{ rad/s}}$  values,  $\alpha_{\text{SBR}}$  traces as well as VFT fitting parameters (**Table 7**) are found for the SBR phase of strongly segregated PB-SBR samples of **Series I**. The  $\alpha_{\text{SBR}}$  traces in the Arrhenius plot for asymmetric samples (**Series II**) in the range  $30 \text{ vol}\% \leq \Phi_{\text{SBR}} \leq 60 \text{ vol}\%$  are nearly identical (although weak differences due to variation of styrene content in the SBR block are indicated). The data for the  $\alpha_{\text{SBR}}$  process in these diblock copolymers with practically identical styrene content in the SBR block ( $28 \text{ mol}\% \leq x_{\text{S, SBR}} \leq 36 \text{ mol}\%$ ) are also comparable with the results for the S<sup>30</sup>B<sup>70</sup>R copolymer used as reference

**Table 7:** VFT fit parameters for crosslinked diblock copolymers in the microphase-separated state and for PB and S<sup>30</sup>B<sup>70</sup>R reference systems.

Label	PB phase					SBR phase				
	T <sub>g</sub> <sup>a</sup> ,	T <sub>α</sub> <sup>10 rad/s</sup> ,	log(a <sub>T,0</sub> )	B,	T <sub>∞</sub> ,	T <sub>g</sub> <sup>a</sup> ,	T <sub>α</sub> <sup>10 rad/s</sup> ,	log(a <sub>T,0</sub> )	B,	T <sub>∞</sub> ,
	°C	°C		K	°C	°C	°C		K	°C
<b>Series I</b>										
PB <sub>53</sub> -	-92.4	-81.5	9.1	200	-107	-25.8	-25.0	15.5	701	-72
S <sup>35</sup> B <sup>65</sup> R <sub>47</sub>										
PB <sub>54</sub> -	-93.1	-81.7	10.8	315	-114	-18.8	-17.7	15.9	660	-63
S <sup>40</sup> B <sup>60</sup> R <sub>46</sub>										
PB <sub>54</sub> -	-93.4	-83.0	9.0	195	-108	-9.2	-6.5	14.9	620	-51
S <sup>45</sup> B <sup>55</sup> R <sub>46</sub>										
PB <sub>54</sub> -	-93.8	-81.3	9.1	220	-107	-2.7	-0.3	19.0	1120	-63
S <sup>52</sup> B <sup>48</sup> R <sub>46</sub>										
<b>Series II</b>										
PB <sub>70</sub> -	-92.1	-82.3	11.6	298	-111	-35.8	-30.1	13.2	640	-83
S <sup>30</sup> B <sup>70</sup> R <sub>30</sub>										
PB <sub>62</sub> -	-92.7	-82.6	10.5	266	-111	-33.5	-33.0	14.7	650	-77
S <sup>30</sup> B <sup>70</sup> R <sub>38</sub>										
PB <sub>53</sub> -	-93.1	-81.5	9.1	200	-107	-25.8	-25.0	15.5	701	-72
S <sup>35</sup> B <sup>65</sup> R <sub>47</sub>										
PB <sub>40</sub> -	-92.4	-83.8	17.0	760	-131	-23.8	-27.4	14.2	573	-67
S <sup>35</sup> B <sup>65</sup> R <sub>60</sub>										

<sup>a</sup> taken from DSC scans on non-crosslinked samples (**Section 7.1.2**)

Temperature-dependent dynamic shear measurements on **symmetric PB-SBR diblock copolymers with systematically varied 1,2-vinyl contents either in the PB or the SBR block (Series III and Series IV)** in the vulcanized state are also performed. Data for shear storage G'(T) and loss G''(T) moduli measured at a fixed angular frequency ( $\omega = 10$  rad/s) are shown in **Figure 24** for crosslinked samples of **Series III** and **Series IV**. Samples with 1,2-vinyl content in the SBR block lower than 46 mol% (**Series III**) show two independent relaxation processes at low and high temperatures corresponding to the dynamic glass transition of PB and SBR phases,  $\alpha_{PB}$  and  $\alpha_{SBR}$ , respectively (**Figure 24 a**). The relaxation temperature  $T_{\alpha,PB}^{10rad/s}$  of about  $-78.06 \pm 3.4^\circ\text{C}$  of the

PB phase of these samples is comparable to that which is found for the strongly segregated samples of **Series I** and **II**. This observation supports the existence of phase separation of both blocks, PB and SBR, indicated already by AFM images (**Figure 19**). However, despite of this similarity there is also a systematic variation in the shear loss modulus curves  $G''(T)$  in these samples. The  $G''(T)$  values between  $\alpha_{PB}$  and  $\alpha_{SBR}$  processes seemingly increase by increasing  $c_{1,2\text{ vinyl}}$  content in the SBR block indicating the existence of various relaxation modes with intermediate  $T_g$  values and intermediate  $\alpha$  relaxation times. This might be related to a decrease of  $\chi N$  (cf. **Section 8.1**) and an accompanied increase in the fraction of interfacial material. Although, a long range ordered lamellar structure is missing in the AFM image of the disordered sample PB<sub>8</sub>-S<sup>40</sup>B<sup>60</sup>R<sub>46</sub>, PB and SBR enriched phases seem to be still present. This hypothesis can be proven by the existence of two  $\alpha$  relaxation processes located between those of strongly microphase-separated samples. This corresponds to that what has been concluded from the AFM images in **Section 7.2.1**, i.e. that two different phases still occur due to concentration fluctuations fixed during the crosslinking at 150°C. This effect is even more clear for the sample PB<sup>8</sup>-S<sup>34</sup>B<sup>66</sup>R<sup>59</sup> having the highest  $c_{1,2\text{ vinyl}}$  content in the SBR block. It is seen in the shear curves for this sample that there are two strong  $G''(T)$  peaks that are overlapping. This indicates that the material is not homogenous and two “phases” do still exist. However, these phases are not any longer pure but have two different average concentrations (contain either a lot or only a few styrene units). Additional relaxation modes in  $G''(T)$  are covering practically the entire range between  $T_{\alpha,PB}^{10\text{rad/s}}$  and  $T_{\alpha,SBR}^{10\text{rad/s}}$  for strongly segregated systems. This indicates, however, that additional interfacial material is present. Note that one could expect a certain increase of the dynamic relaxation temperature of the SBR phase,  $T_{\alpha,SBR}^{10\text{rad/s}}$ , as  $1,2\text{-vinyl}$  (SBR) contents increases. This hypothesis is made based on results of relaxation temperature dependence of  $1,2\text{-vinyl}$  contents reported for PB homopolymers.<sup>120,121</sup> However, this trend is not really observed for this series of PB-SBR samples with variable  $c_{1,2\text{ vinyl}}$  in the SBR block probably since there is a competing effect of miscibility between PB and SBR blocks at the same time. Besides, the slight variation of styrene content in the SBR block due to synthesis uncertainties could also affect  $T_{\alpha,SBR}^{10\text{rad/s}}$ .

In general, one can understand the relaxation behavior of **Series III** as a consequence of an enhancement in miscibility by increasing  $1,2\text{-vinyl}$  content in the SBR block going towards one single phase. This behavior is in line with the AFM images shown in **Figure 19**. It became also clear from features seen in the relaxation dynamics that the two components (PB and SBR blocks)

are not homogeneously mixed even in cases where the samples are “disordered” from the thermodynamic models point of view. The phase separation behavior of diblock copolymers are well describe by some thermodynamic models. This result also shows that the  $\alpha$  relaxation behavior of diblock copolymers is not coupled to the existence of long range order but more sensitively depending on the concentration profile in the sample.

The relaxation behavior of crosslinked samples belonging to **Series IV**, which is composed of PB-SBR diblock copolymers with variable *1,2-vinyl* contents in the PB block, shows typical features which are commonly found for samples in the microphase-separated state. There are two independent  $\alpha$  relaxation processes,  $\alpha_{PB}$  and  $\alpha_{SBR}$ , corresponding to the segmental dynamics in the PB and SBR phases, respectively. By increasing *1,2-vinyl* contents in the PB block, the relaxation temperature  $T_{\alpha, PB}^{10\text{rad/s}}$  is systematically increased, as expected based on literature results for PB homopolymers with varied microstructure.<sup>120,121</sup> For the PB<sup>74</sup>-S<sup>27</sup>B<sup>73</sup>R<sup>16</sup> sample, with the highest *1,2-vinyl* content in the PB block, both  $\alpha$  relaxation processes,  $\alpha_{PB}$  and  $\alpha_{SBR}$ , do superimpose although the AFM images (**Figure 19**) of this sample clearly demonstrate a well pronounced long range ordered lamellar structure. Obviously, phase separation is still present and the segmental dynamics of both phases, PB and SBR, are only by coincidence relatively similar. This is also supported by DSC heat capacity curves (**Figure 16**) showing two glass transitions. To what extend the interaction parameter  $\chi$  as well as the amount of interfacial material is enhanced by changing *1,2-vinyl* contents in the PB block, as predicted by recent studies on PB-SBR blends,<sup>3</sup> cannot be judged based only on the presented shear modulus data. This question will be considered in more details based on thermodynamic models predicting interfacial width in **Sections 8.1** and a further analysis of heat capacity data in **Section 8.2**.

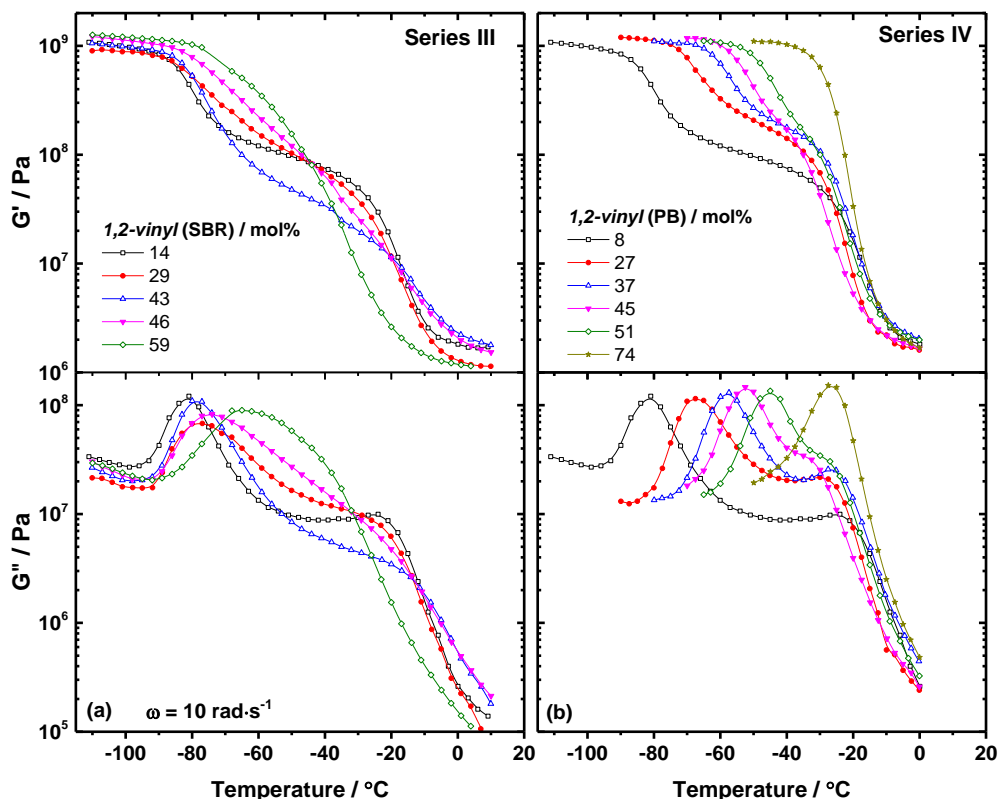


**Figure 24:** Temperature-dependence of the shear storage ( $G'$ ) and loss ( $G''$ ) moduli for symmetric crosslinked PB-SBR diblock copolymer samples with variable *1,2-vinyl* content (a) in the SBR block (**Series III**) and (b) in the PB block (**Series IV**). Isochrones were measured at an angular frequency of  $10 \text{ rad}\cdot\text{s}^{-1}$ .

### 7.3 Mechanical performance of silica-filled $\text{PB}_{50}\text{-S}^{45}\text{B}^{55}\text{R}_{50}$ diblock copolymer composites

Temperature-dependent data for shear storage  $G'(T)$  and loss  $G''(T)$  moduli as well as for the loss tangent  $\tan\delta$  of  $\text{PB}_{50}\text{-S}^{45}\text{B}^{55}\text{R}_{50}$  composites filled with 0-80 phr silica nanoparticles are shown in **Figure 25**. All composite samples are vulcanized with 1.5 phr sulfur and measured at a fixed angular frequency ( $\omega = 10 \text{ rad/s}$ ). Two independent relaxation processes,  $\alpha_{\text{PB}}$  and  $\alpha_{\text{SBR}}$ , corresponding to the dynamic glass transitions in PB and SBR phases are found for all composites. This is indicated by two steps in  $G'(T)$  and the corresponding peaks in  $G''(T)$  and  $\tan\delta(T)$ . The dynamic glass transition temperatures of the PB and SBR phases,  $T_{\alpha,\text{PB}}^{10\text{rad/s}}$  and  $T_{\alpha,\text{SBR}}^{10\text{rad/s}}$ , were

obtained from the maxima in  $G''(T)$ . Values of  $T_{\alpha, \text{PB}}^{10 \text{ rad/s}} = -83.5 \pm 0.4^\circ\text{C}$  and  $T_{\alpha, \text{SBR}}^{10 \text{ rad/s}} = -6.2 \pm 1.4^\circ\text{C}$  are found for the  $\text{PB}_{50}\text{-S}^{45}\text{B}^{55}\text{R}_{50}$  composites, which are comparable to relaxation temperatures of the unfilled  $\text{PB}_{50}\text{-S}^{45}\text{B}^{55}\text{R}_{50}$  sample in the crosslinked state. This result shows that the relaxation behavior of the individual phases is not significantly affected by the incorporation of silica. Expectedly, there is a clear reinforcement effect in the rubber plateau range like in classical elastomer nanoparticle composites as indicated by a systematic increase of the storage  $G'(T)$  modulus. A more specific finding for the investigated diblock copolymer based composites is that  $G'(T)$  and loss  $G''(T)$  modulus in the range between the  $\alpha_{\text{PB}}$  and  $\alpha_{\text{SBR}}$  processes also increase. This can be interpreted as an effect due to the reinforcement in the PB phase and/or increasing content of interfacial material having intermediate  $T_g$ 's. Similar behavior can be also seen in elastomeric blends containing nanofillers.<sup>10</sup> Like in practically all other composites investigated in the literature, the height of the  $\tan\delta$  peaks corresponding to  $\alpha_{\text{PB}}$  and  $\alpha_{\text{SBR}}$  is systematically reduced with increasing filler content. These findings can be understood by replacing elastomer by filler but has probably also to do with immobilized elastomer segments located on the filler surface.<sup>6,103</sup> There is absolutely no indication in the shear modulus data for composites in **Figure 24** that microphase separation and concentration profile in the  $\text{PB}_{50}\text{-S}^{45}\text{B}^{55}\text{R}_{50}$  matrix are significantly affected by the incorporation of reinforcing silica fillers with loadings up to 80 phr. This observation is also in line with what is seen in the corresponding AFM images of the  $\text{PB}_{50}\text{-S}^{45}\text{B}^{55}\text{R}_{50}$  composites filled with 20, 40 and 60 phr silica as shown in **Figure 26**.

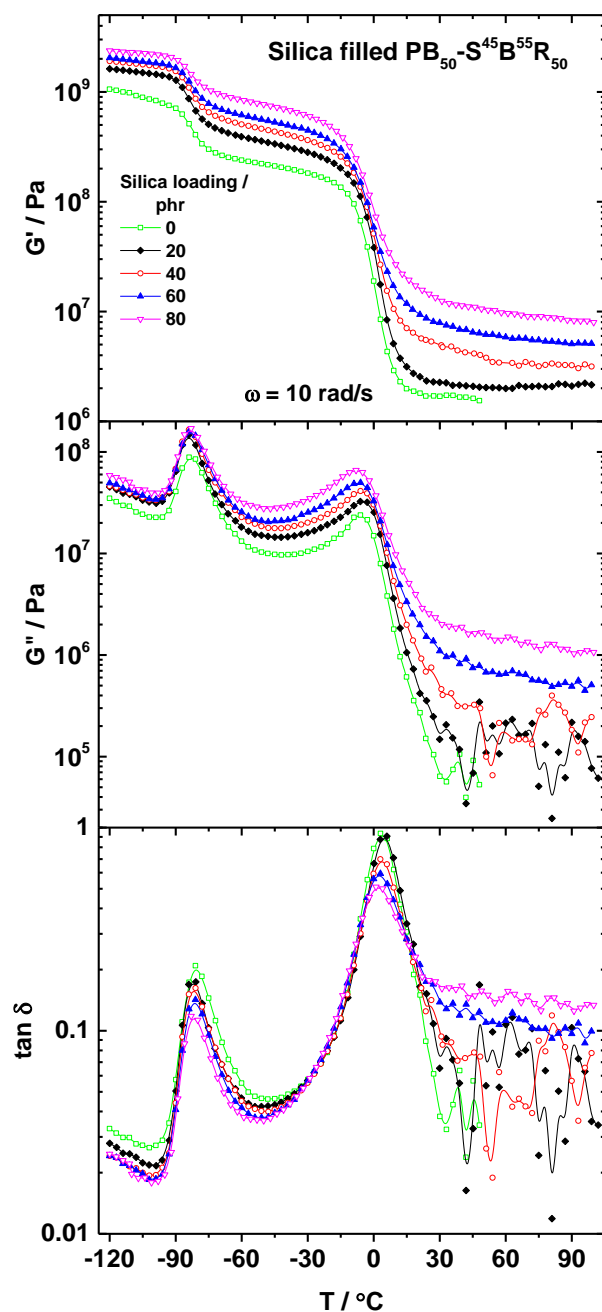


**Figure 25:** Temperature-dependence of the shear storage ( $G'$ ) and loss ( $G''$ ) moduli as well as of  $\tan\delta$  of  $\text{PB}_{50}\text{-S}^{45}\text{B}^{55}\text{R}_{50}$  composites filled with variable silica loading ranging from 0 to 80 phr. Isochrones were measured at an angular frequency of  $10 \text{ rad}\cdot\text{s}^{-1}$ .

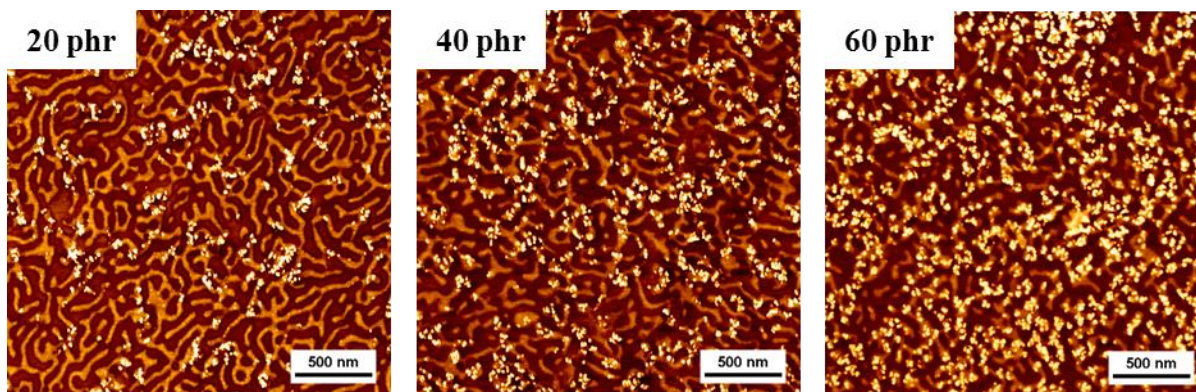


**Figure 26:** AFM phase contrast images showing  $2 \times 2 \mu\text{m}^2$  scans for  $\text{PB}_{50}\text{-S}^{45}\text{B}^{55}\text{R}_{50}$  composites filled with 20, 40 and 60 phr silica nanoparticles. The scale bar with a length 500 nm is applicable for both images.

AFM phase contrast images for the different silica filled PB-SBR composites in **Figure 26** show a nice phase separation of PB-SBR phases but no well pronounced long range order compared to the AFM images of the non-filled  $\text{PB}_{50}\text{-S}^{45}\text{B}^{55}\text{R}_{50}$  sample (**Figure 18**, upper part) illustrating a long range ordered lamellar morphology. Hence, one can conclude that upon silica incorporation long range order is lost, although domain size seems to be weakly affected. This might be due to stronger shear forces and higher temperatures during processing of composites. Interestingly, the silica particles are mainly located in the SBR phase for silica loadings of 20, 40 and 60 phr. This is indicating a high silica phase selectivity in the  $\text{PB}_{50}\text{-S}^{45}\text{B}^{55}\text{R}_{50}$  matrix, which might be due to attractive interaction between silica/SBR compared to silica/PB. Note that, to the best of our knowledge, a similar degree of phase selectivity has never been observed in silica filled SBR/PB blends.<sup>122,123</sup>

In a further set of experiments, isothermal shear experiments in the frequency range 0.1-100 rad/s are carried out in a broad temperature interval including both  $\alpha$  relaxation processes. Isotherms for shear storage  $G'(\omega)$  and loss  $G''(\omega)$  moduli as well as for  $\tan\delta(\omega)$  are measured for  $\text{PB}_{50}\text{-S}^{45}\text{B}^{55}\text{R}_{50}$  composites filled with different silica loadings (0-80 phr) and used to construct master curves as shown in **Figure 27**. These master curves are obtained by shifting the isotherms horizontally along the log frequency axis assuming that the time temperature superposition principle (TTS) is applicable in the whole temperature range which is not completely true in case of block copolymer based systems (cf. **Section 7.2.2**). The reference temperature is in all cases  $-60^\circ\text{C}$ . The master curves show identical trends as those found in the isochronal sweeps: in particular the two main

relaxation processes,  $\alpha_{PB}$  and  $\alpha_{SBR}$ , which appear basically at the same frequency position independent of the filler content. Tiny shifts of the  $G''(a_T\omega)$  peak position in the master curves depending on silica content are probably more related to uncertainties of the shift procedure than due to true changes in the relaxation dynamics of the polymer matrix. However, there are also changes, which are indeed caused by the filler incorporation. Besides the well-known increase of  $G'(a_T\omega)$  in the rubber plateau range due to reinforcement, there is also in all other frequency regions an increase in  $G'$  with increasing filler content. Obviously, the silica filler leads effectively in all frequency ranges to an increase of  $G'(a_T\omega)$  and can reinforce the material even in the fully glassy state to a certain extent. A possibly related effect is seen in the loss modulus  $G''(a_T\omega)$ , which is systematically increasing in the entire frequency range. On the other hand, by increasing silica content the relative quantity  $\tan\delta(a_T\omega)$  shows lower values in the range of the relaxation peaks ( $\alpha_{PB}$  and  $\alpha_{SBR}$ ). An increase of  $\tan\delta$  is observed in the rubber plateau range, at low frequencies  $a_T\omega$ , as filler content increases. Further, systematic changes in the rubber plateau range are observed which are comparable to those recently reported for classical rubber composites (SBR-silica<sup>6</sup>, NR-carbon black<sup>124</sup>). It is found that there is an increase in the slope  $d\log G'/d\log\omega$  in the rubber plateau with increasing filler contents. While this slope is nearly 0, as expected, in unfilled systems, a clear increase of the storage modulus with frequency ( $d\log G'/d\log\omega \gg 0$ ) is found in the rubber plateau of composites with high filler contents (**Figure 27**). This change in  $G'(a_T\omega)$  with filler content is accompanied by a systematic increase in  $G''(a_T\omega)$  as is expected as long as the Kramers-Kronig relations are applicable. These features have been attributed to the presence of an immobilized, glassy polymer layer with a thickness of 1-2 nm located at the filler surface, which softens at temperature significantly above  $T_g$  of the bulk rubber.<sup>6</sup>

In particular, the trends of the dissipation-related quantities  $G''$  and  $\tan\delta$  will be discussed in more detail in **Section 8.3** since these quantities are extremely relevant for tire tread applications. The loss tangent values  $\tan\delta(0^\circ\text{C}, 10\text{Hz})$  and  $\tan\delta(60^\circ\text{C}, 10\text{Hz})$  are commonly used in the tire industry as laboratory indicators for wet grip and rolling resistance, respectively. Accordingly, one can try to estimate based on the changes found in these quantities for block copolymer based composites trends to be expected in the performance of related tire treads.

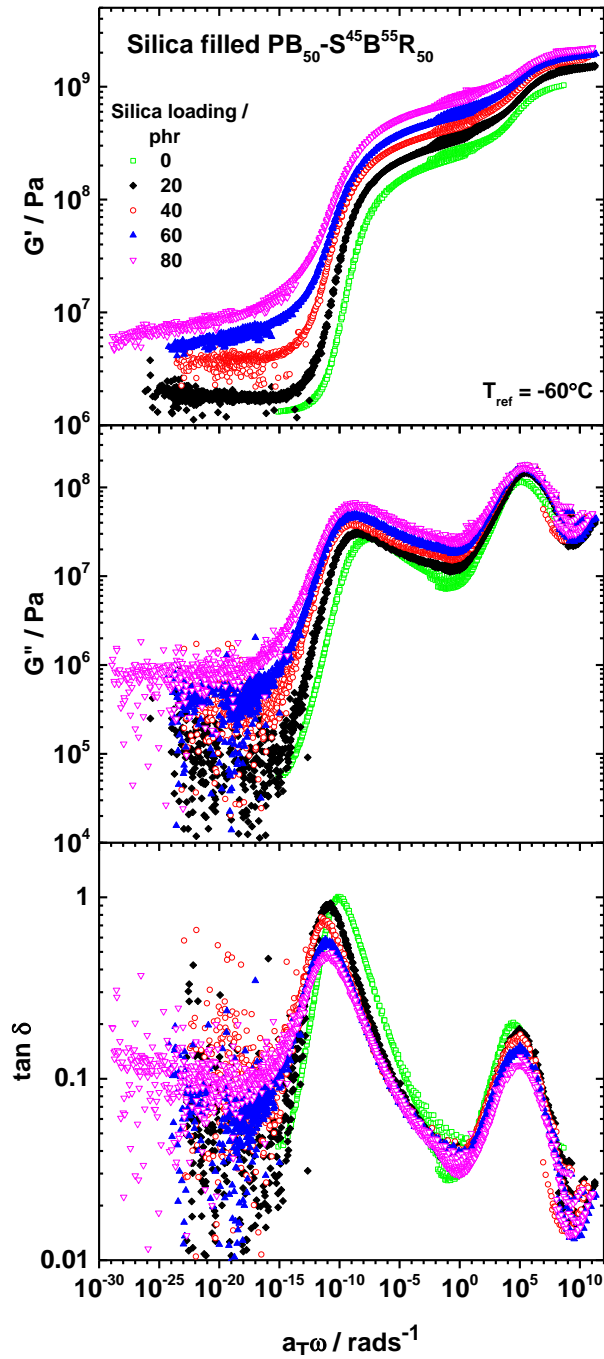


**Figure 27:** Master curves of the shear storage ( $G'$ ) and loss ( $G''$ ) modulus as well as  $\tan \delta$  for PB<sub>50</sub>-S<sup>45</sup>B<sup>55</sup>R<sub>50</sub> composites filled with variable silica contents ranging from 0 to 80 phr. The original isotherms are only horizontally shifted. All master curves are constructed using -60°C as reference temperature.

## Chapter 8

### Discussion

#### 8.1 Order-disorder-transition and interfacial width from thermodynamic models

**Thermodynamic model predicting phase behavior of PB-SBR diblock copolymers.** It has been demonstrated in this work based on the results for different series of diblock copolymers that the miscibility and segregation strength of PB-SBR diblock copolymers can be systematically influenced by microstructural parameters such as styrene content in the SBR block  $x_{S,SBR}$  (**Series I**) and/or *1,2-vinyl* content  $c_{1,2\ vinyl}$  in SBR (**Series III**) or PB (**Series IV**) blocks. This can be directly seen in the X-ray diffraction pattern (**Section 6.1.1**), AFM images (**section 7.2.1**) as well as indirectly concluded from related features in DSC scans (**Section 6.1.2**) and the relaxation behavior in shear data (**Section 7.2.2**). A very important finding is that the phase behavior and/or morphology of diblock copolymers are commonly not changed by harsh rubber processing procedures, which are quite similar to those used in tire production. One can conclude that the diblock copolymer state, for non-filled systems, is not significantly altered by shear forces applied during mixing processes and morphology is fixed during vulcanization at 150°C. Hence, it is interesting and highly application relevant to predict, based on thermodynamic models Flory-Huggins interaction parameter  $\chi$  and order-disorder-transition (ODT) in PB-SBR diblock copolymers depending on composition and temperature, which determine their structural state. Equilibrium predictions for non-crosslinked diblock copolymers can be made based on conventional thermodynamic approaches.<sup>52</sup> Leibler's weak segregation theory predicts that the ODT occurs for symmetric diblock copolymers at a critical value of the order parameter  $(\chi N)_c = 10.5$ .<sup>16</sup> An effective interaction parameter  $\chi_{eff}$  has to be introduced in order to describe the equilibrium phase behavior of PB-SBR diblock copolymers with variable styrene contents in the SBR block.<sup>3,29,31</sup> A thermodynamic model taking into account the individual pair interactions between styrene (S), *1,2-vinyl* (V) and *1,4-cis/trans* (B) units has been reported by Sakurai et al

based on experimental data for SBR/PB blends. According to their phase separation studies on blends an effective interaction parameter,  $\chi_{eff}$ , can be used to describe the phase behavior, where  $\varphi_{S,SBR}$  is the styrene volume fraction in the SBR component <sup>3</sup>

$$\chi_{eff} = k \cdot \varphi_{S,SBR} \cdot \chi_{VS} + (\varphi_{S,SBR} - k) \cdot \varphi_{S,SBR} \cdot \chi_{BS} - k \cdot (\varphi_{S,SBR} - k) \cdot \chi_{VB} \quad (20)$$

The parameter  $k$  is defined as  $k = \varphi_{V,PB} - \varphi_{V,SBR} (1 - \varphi_{S,SBR})$  with  $\varphi_{V,PB}$  and  $\varphi_{V,SBR}$  being the volume fractions of *1,2-vinyl* in PB and SBR component, respectively. Values for the specific interaction parameters between different co-units are reported ( $\chi_{VS} = 56.5 \cdot 10^{-3} + 5.62/T$ ;  $\chi_{BS} = 8.43 \cdot 10^{-3} + 10.2/T$ ;  $\chi_{VB} = 2.69 \cdot 10^{-3} + 1.87/T$ ). These values indicate that the *1,2-vinyl*/styrene repulsion is the strongest interaction.

Based on **Eq.(20)** as well as on  $\chi_{VS}$ ,  $\chi_{BS}$  and  $\chi_{VB}$ , the segregation strengths  $\chi_{eff}N$  of the symmetric diblock copolymer samples of **Series I** has been calculated at 25°C and 150°C (**Figure 28 a**). As expected there is a strong increase of the segregation strength  $\chi_{eff}N$  by increasing styrene volume fraction in the SBR block  $\varphi_{S,SBR}$ . An interpolation of the calculated  $\chi_{eff}N$  data at 150°C predicts an ODT ( $\chi_{eff}N = 10.5$ ) at about  $\varphi_{S,SBR} = 0.31$  corresponding to  $x_{S,SBR} \sim 21$  mol%. This prediction is in a reasonable agreement with AFM results for **Series I (Figure 18)** where clear indications of disorder and a trend towards miscibility are seen for the samples PB<sub>50</sub>-S<sup>21</sup>B<sup>79</sup>R<sub>50</sub> ( $x_{S,SBR} = 21$  mol%) and PB<sub>50</sub>-S<sup>27</sup>B<sup>73</sup>R<sub>50</sub> ( $x_{S,SBR} = 27$  mol%). Based on these model predictions, the sample B<sub>50</sub>-S<sup>27</sup>B<sup>73</sup>R<sub>50</sub> ( $\chi_{eff}N = 15.6$ ) should be close to the order-disorder transition during the vulcanization process at 150°C while the sample PB<sub>50</sub>-S<sup>21</sup>B<sup>79</sup>R<sub>50</sub> ( $\chi_{eff}N = 9.8$ ) should be disordered under identical conditions. This shows that the model used to calculate the effective interaction parameter  $\chi_{eff}$  (Eq.(14)) is describing well the phase separation behavior for symmetric diblock copolymers with a random SBR block. Note that we assume here that the microphase-separated state occurring at 150°C is fixed without further changes during the vulcanization process. This is understandable if we consider that the crosslinking reaction is much faster than reorganization processes in a block copolymer at temperatures below the  $T_{ODT}$ .

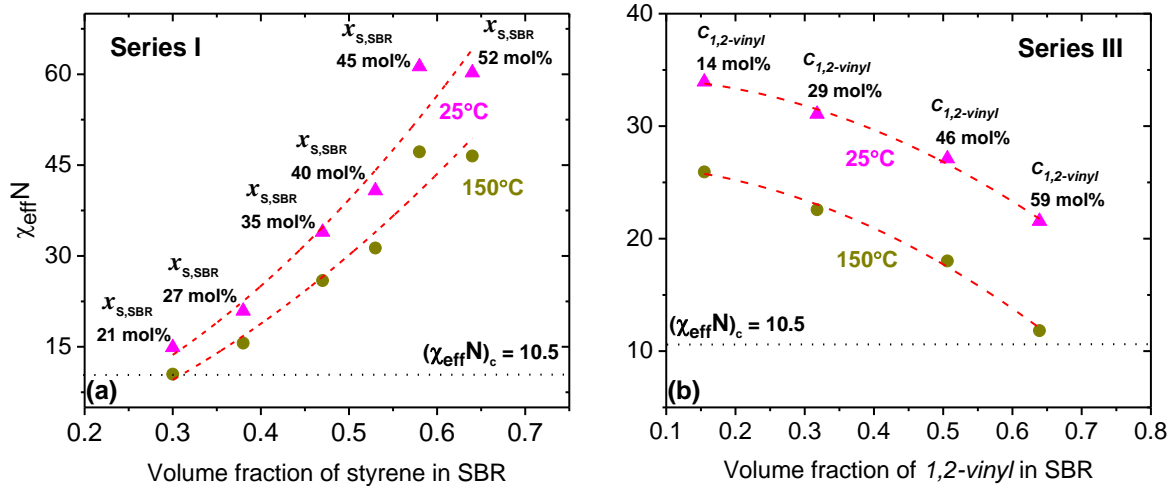


**Figure 28:** Segregation strength  $\chi_{eff}N$  for PB-SBR diblock copolymers as a function of the volume fraction of (a) styrene (**Series I**) and (b) *1,2-vinyl* (**Series III**) contents in the SBR block. The total chain length  $N$  was determined based on the total molecular weight values and the effective interaction parameter  $\chi_{eff}$  was calculated at 25°C (triangles) and 150°C (circles) using **Eq. (20)**. The dashed lines are an interpolation of the data. The dotted line represents the ODT at  $\chi_{eff}N = 10.5$ .

An alternative way of accessing different segregation strengths between SBR and PB blocks is by varying the *1,2-vinyl* content in the SBR block. Thus, phase separation behavior of symmetric PB-SBR diblock copolymers with variable *1,2-vinyl* in the SBR block has been investigated for **Series III**. AFM data for vulcanized samples (**Figure 19**, upper row) clearly demonstrate that all investigated symmetric PB-SBR diblock copolymers with *1,2-vinyl* contents in the SBR block  $\leq 43$  mol% remain in the microphase separated state, with lamellar morphology, even after being subjected to high shear forces and elevated temperatures during processing and vulcanization.

The segregation strength values  $\chi_{eff}N$  of the individual diblock copolymers of **Series III** have been calculated at room temperature (25°C) and at the vulcanization temperature (150°C) using the total molecular weights (related to the total chain length  $N$ ) and the actual values for the microstructure parameters  $C_{1,2-vinyl}$  and  $x_{S,SBR}$  values (**Table 3**). **Figure 28b** illustrates the segregation strength dependence on temperature as well as on *1,2-vinyl* content in the SBR block. It clearly shows that  $\chi_{eff}N$  values decrease as *1,2-vinyl* content in the SBR increases (**Series III**). The dotted line is an interpolation of the data using a polynomial fit. Considering these calculated  $\chi_{eff}N$  data, microphase

separation should occur ( $\chi_{eff}N > 10.5$ ) for *1,2-vinyl* content lower than 59 mol% (SBR block) at 150°C, being the vulcanization temperature at which the structural state is fixed. Although, according to this model PB<sub>8</sub>-S<sup>40</sup>B<sup>60</sup>R<sub>46</sub> with  $c_{1,2-vinyl} = 46$  mol% should be microphase separated ( $\chi_{eff}N = 18.02$ ), the AFM image in **Figure 19** shows typical features of a disordered diblock copolymer system slightly above the  $T_{ODT}$ . In the case of the PB<sub>8</sub>-S<sup>34</sup>B<sup>66</sup>R<sub>59</sub> diblock copolymer having the highest *1,2-vinyl* content in the SBR block, ( $c_{1,2-vinyl} = 59$  mol%),  $\chi_{eff}N = 11.83$ ), is certainly very close to the critical value defining the order-disorder transition (10.5) during the vulcanization process at 150°C. Accordingly it is not so unexpected that the experiments show a typical state expected slightly above the ODT while **Eq.(20)** predicts a weakly segregated state. Whether these deviations from the model predictions are due to not well-defined processing parameters ( $T$ ), uncertainties regarding the microstructure ( $N, \Phi_{SBR}, x_{S,SBR}, c_{1,2-vinyl}$ ) or small deviations regarding the interaction parameters ( $\chi_{BS}, \chi_{VS}, \chi_{VB}$ ) from the literature remains open. In any case, the variation in any of these parameters would result in a certain scatter in the value of  $\chi_{eff}N$ , which could explain the observed deviations.

Another possible way to improve segregation strength between the SBR and PB block is by increasing the *1,2-vinyl* content in the PB block (**Series IV**). This effect is due to the strong repulsive forces between the *1,2-vinyl* and styrene units, as previously discussed for samples of **Series III**. The segregation strength values  $\chi_{eff}N$  of the individual diblock copolymers of **Series IV** have been calculated at room temperature (25°C) and at the vulcanization temperature (150°C) using the total molecular weights (related to the total chain length  $N$ ) and the actual values for the microstructure parameters  $c_{1,2-vinyl}$  and  $x_{S,SBR}$  values (**Table 3**). **Figure 29** illustrates the order parameter ( $\chi_{eff}N$ ), at 25 and 150 °C, depending on  $c_{1,2-vinyl}$  in the PB block for samples of **Series IV**. According to  $\chi_{eff}N$  values, calculated based on **Eq.(20)**, all samples are predicted to be microphase separated ( $\chi_{eff}N > 10.5$ ) as well as being significantly above the ODT. These findings are in line with the AFM images shown in **Figure 19**, in which a well-ordered lamellar morphology is observed for all crosslinked PB-SBR diblock copolymers.

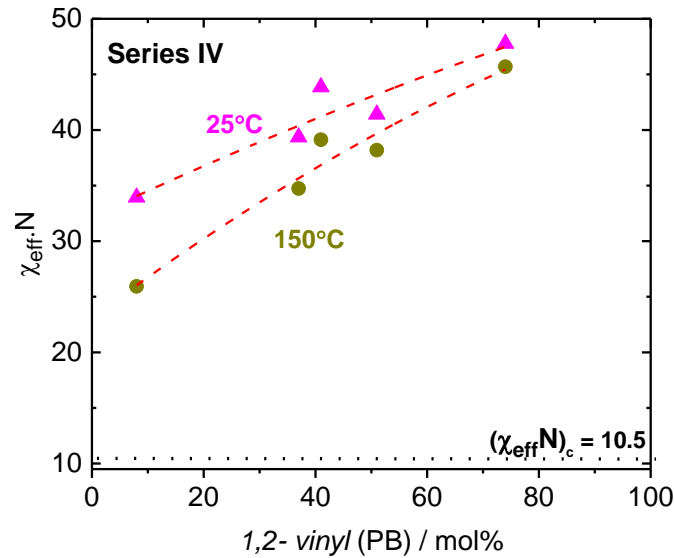


**Figure 29:** Segregation strength  $\chi_{eff}N$  for PB-SBR diblock copolymers as a function of the volume fraction of *1,2-vinyl* contents in the PB block (**Series IV**). The total chain length  $N$  was determined based on the total molecular weight values and the effective interaction parameter  $\chi_{eff}$  was calculated at 25°C (triangles) and 150°C (circles) using **Eq. (20)**. The dashed lines are an interpolation of the data using a quadratic fit. The dotted line represents the ODT at  $\chi_{eff}N = 10.5$ .

In summary, one can conclude that the applied thermodynamic model (**Eq.(20)**) makes reasonable predictions regarding the phase separation behavior of symmetric PB-SBR diblock copolymers with variable styrene contents  $x_{S,SBR}$  as well as *1,2-vinyl* contents  $c_{1,2\ vinyl}$  in the SBR or PB block. The relevant temperature determining the structural situation, in case of crosslinked diblock copolymers, is obviously the vulcanization temperature (150°C in this work). These insights will allow making suitable estimates for the thermodynamic state achieved depending on diblock copolymer microstructure and crosslinking temperature in case new diblock copolymer systems and composites have to be designed based on the requirements of special applications.

**Interfacial width calculations for PB-SBR diblock copolymers.** It is commonly known that the changes in the segregation strength  $\chi N$  are accompanied by changes in the interfacial width  $d_{IF}$ , i.e. the size of spatial regions where segments of both blocks are mixed close to the interface between both microphases.<sup>101</sup> For strongly segregated systems ( $\chi N \gg 10.5$ ) this region is very narrow, while a significant amount of interfacial material has to be expected for weakly segregated

systems ( $\chi N > 10.5$ ). Although this difference is not influencing the pronounced long range order in microphase-separated block copolymers, it has a significant influence on the relaxation behavior since the segmental  $\alpha$  dynamics which are cooperative in nature will be seriously affected.<sup>125</sup> This interrelation will be further discussed in **Section 8.2**. For that reason, it is very interesting and important to have quantitative information about the interfacial width  $d_{IF}$  in PB-SBR diblock copolymers. Experimentally, it is very difficult to get structural information about interphases with nanoscopic dimensions. However, reasonable estimates can be taken from corresponding models. Semenov has derived a thermodynamic model,<sup>126</sup> allowing to calculate the interfacial width  $d_{IF}$  of strongly segregated symmetric diblock copolymers as a function of the interaction parameter  $\chi$ . This model was originally developed for PS-PMMA diblock copolymers in the strong segregation limit ( $\chi N \gg 10.5$ ).<sup>126</sup> For the symmetric PB-SBR diblock copolymers of **Series IV**, being in the strongly segregated state, the effective interaction parameter  $\chi_{eff}$  has to be used as it was introduced above (**Figure 29**). With this modification one gets an equation for calculating the interfacial width

$$d_{IF} = [d_0(1 + 1.34/(\chi_{eff}N)^{\frac{1}{3}} + \frac{\nu d_0}{2a^2} \ln(d/d_0))]^{0.5} \quad (21)$$

where  $d_0 = 2a\chi_{eff}^{-0.5}$  and  $a = (l_{PB-SBR} \cdot b_{PB-SBR}/6)^{0.5}$  has to be calculated from  $\chi_{eff}$ ,  $l_{PB-SBR}$  and  $b_{PB-SBR}$  being effective interaction parameter, the average statistical Kuhn length and the average bond length of the individual PB-SBR copolymers, respectively. The average volume per link  $\nu = \bar{m}_0/\bar{\rho} N_{AV}$  is depending on  $\bar{m}_0$ , the mean molecular weight of a link,  $\bar{\rho}$  the PB-SBR average density and  $N_{AV}$  the Avogadro number.  $d$  is the domain size.

This model is applicable for all symmetric PB-SBR samples of **Series IV** having commonly relatively large  $\chi_{eff}N$  values significantly greater than 10.5 (cf. **Figure 29**). Values for the interfacial width  $d_{IF}$  can be calculated based on  $\chi_{eff}N$  data (**Figure 29**), ( $D = 2d$ ) values from SAXS (**Table 3**), and statistical Kuhn length  $l_{PB-SBR}$  and bond length  $b_{PB-SBR}$  of the individual PB-SBR copolymers calculated as from the mean average from literature values. The values for  $l_{PB}$  were obtained from an interpolation of Kuhn lengths for PB homopolymers with different microstructures,<sup>127</sup> The average statistical Kuhn length of the SBR component  $l_{SBR}$  was averaged according to the molar contents of styrene and butadiene, as well as their respective Kuhn lengths.<sup>94,127,128</sup> The dependence of the interfacial width  $d_{IF}$  on  $\chi_{eff}$  for samples of **Series IV**

calculated at 25 and 150°C is presented in **Figure 30**. Expectedly,  $d_{IF}$  decreases significantly as  $\chi_{eff}$  increases for both temperatures. The  $d_{IF}$  values at higher temperatures are commonly greater than those at lower temperatures. This result is a direct consequence of the  $\chi_{eff}$  dependence on temperature:  $\chi_{eff}$  increases with temperature. Note that small temperature-dependent changes in  $D$  are neglected in the calculation of  $d_{IF}$  at 150°C. The average interfacial width calculated at 25°C and 150°C are  $6.46 \pm 0.69$  and  $6.93 \pm 1.04$  nm, i.e the average interfacial width is nearly constant even if the temperature is increased by 125K. Interestingly, both isotherms coincide indicating that temperature and composition can be used alternatively to control interfacial width. This is interesting information for judging the  $\alpha$  relaxation behavior and defining routes to design new materials based on self-assembled block copolymers.

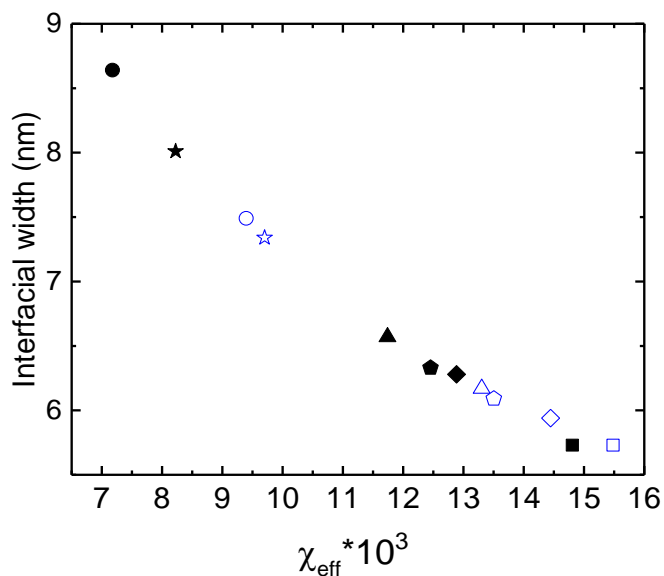


**Figure 30:** Interfacial width  $d_{IF}$  as function of the effective interaction parameter calculated at 25 (open symbols) and 150°C (full symbols) for the individual PB-SBR diblock copolymers of **Series IV**. The *1,2-vinyl* contents in the PB block are 8 mol% (circle), 27 mol% (star), 37 mol% (triangle), 45 mol% (pentagon), 51 mol% (diamond) and 71 mol% (cube).

In conclusion, it is possible to calculate interfacial width for symmetric PB-SBR diblock copolymers by the thermodynamic model proposed by Semenov. The obtained interfacial fractions,  $\phi_{IF} = \left(\frac{2d_{IF}}{D}\right) \cdot 100$ , are about 19.65 to 21.07 vol% and they seem to be reasonable considering that what has been reported in the literature.<sup>129, 130</sup> Further correlations between

structure and dynamics will be considered and quantitative comparisons will be made in the next section of this discussion chapter.

## 8.2 Correlations between block copolymer microstructure, self-assembled morphology and segmental $\alpha$ dynamics

**Dependence of segmental  $\alpha$  dynamics on microstructure in strongly segregated systems.** Styrene content in SBR copolymers is known to influence systematically the glass transition temperature and the  $\alpha$  relaxation dynamics.<sup>131</sup> Accordingly, the styrene concentration should have a similar effect on the glass temperature  $T_{g,SBR}$  of the SBR phase in strongly segregated PB-SBR diblock copolymers. Hence, the dependence of the thermal (non-crosslinked samples) and dynamic (crosslinked samples) glass transition temperatures of the SBR block,  $T_{g,SBR}$  and  $T_{\alpha,SBR}^{10 \text{ rad/s}}$ , on its styrene content  $x_{S,SBR}$  is plotted in **Figure 31 (a)** for strongly segregated, symmetric diblock copolymers of **Series I**. Both data sets were fitted to the phenomenological Gordon-Taylor equation describing the softening behavior of random copolymers depending on composition<sup>132</sup>

$$T_{g,SBR} = (T_{g,PS} \cdot w_{S,SBR} + A \cdot T_{g,PB} \cdot (1 - w_{S,SBR})) / (w_{S,SBR} + A \cdot (1 - w_{S,SBR})) \quad (22)$$

where  $w_{S,SBR}$  is the weight fraction of styrene in the SBR (block) and  $T_{g,PB}$  ( $T_{\alpha,PB}^{10 \text{ rad/s}}$ ) and  $T_{g,PS}$  ( $T_{\alpha,PS}^{10 \text{ rad/s}}$ ) are the thermal (or dynamical) glass transition temperatures of polybutadiene and polystyrene, respectively.  $A$  is a system-dependent fitting parameter. It is becoming clear that both values,  $T_{g,SBR}$  for non-crosslinked samples as well as  $T_{\alpha,SBR}^{10 \text{ rad/s}}$  for crosslinked samples, increase systematically by increasing styrene content, as expected. Fits to  $T_{g,SBR}$  and  $T_{\alpha,SBR}^{10 \text{ rad/s}}$  data for the well microphase-separated members of **Series I** with the Gordon-Taylor equation give  $A$  parameters of 2.16 and 2.33, respectively (**Figure 31a**). This confirms that the trends in the softening behavior of the SBR phase, for well microphase-separated PB-SBR diblock copolymers, correspond to those which are known for random SBR copolymers with fixed *1,2 vinyl* content. The softening behavior of the SBR phase seems to be also weakly affected by the applied mixing and vulcanization processes. **Figure 31 (a)** also illustrates that  $T_{g,SBR}$  (non-crosslinked) and  $T_{\alpha,SBR}^{10 \text{ rad/s}}$  (crosslinked) of strongly microphase separated samples of **Series III** are quite

comparable. Moreover, one can also observe that the scatter of  $T_{g,SBR}$  (non-crosslinked) and  $T_{\alpha,SBR}^{10\text{ rad/s}}$  (crosslinked), for samples of **Series II**, is mainly due to the variation of styrene content in the SBR block. These latter statements are also applicable for samples of **Series IV**. A zoomed plot shown in **Figure 31 (a)**, with styrene content range from 40 to 70 wt%, clearly confirms the trends mentioned above. Note that there seems to be a certain discrepancy between  $T_{g,SBR}$  (non-crosslinked) and their corresponding  $T_{\alpha,SBR}^{10\text{ rad/s}}$  (crosslinked) values in case of **Series IV** although the overall dependence on the weight fraction  $w_{S,SBR}$  is preserved. This indicates probably a certain influence of crosslinking on the SBR glass temperature.

A similar correlation between glass temperature  $T_{g,PB}$  and microstructure is known for PB homopolymers depending on the *1,2-vinyl* content.<sup>107,108</sup> Hence, the influence of the *1,2-vinyl* content on the glass temperature and on the  $\alpha$  relaxation dynamics of the PB phase was investigated for **Series IV**, in which *c*<sub>1,2-vinyl</sub> was systematically varied in the PB block. As expected, both values,  $T_{g,PB}$  for non-crosslinked samples as well as  $T_{\alpha,PB}^{10\text{ rad/s}}$  for crosslinked samples, increase systematically with increasing *1,2-vinyl* content in the PB block (**Figure 31b**) similar to the glass transition dependence on microstructure for PB homopolymers.<sup>107,108</sup> A Gordon-Taylor fit to  $T_{g,PB}$  for non-crosslinked samples gives  $A=1.6155$ . However, the  $T_{\alpha,PB}^{10\text{ rad/s}}$  values for crosslinked samples are about 13K higher than for the corresponding  $T_{g,PB}$  values. This effect is (at least partly) due to crosslinking that reduces the average chain mobility, and therefore increases the glass temperature. Similar relaxation behavior effects has been reported for PB homopolymers with different crosslink density.<sup>119</sup>

Finally, one can conclude that the dependencies of  $T_g$  on microstructural parameters like styrene content, in case of SBR copolymers, or *1,2-vinyl* content, in case of PB homopolymers, are also hold for the corresponding phases of strongly segregated PB-SBR diblock copolymers. Hence, strategies which are used to tune  $T_g$  of SBR or PB can be systematically applied in diblock copolymers. Another finding is that there are hints for a certain influence of the crosslink density on the glass temperature in microphase-separated PB-SBR diblock copolymers as accordingly reported for differently crosslinked PB homopolymers.

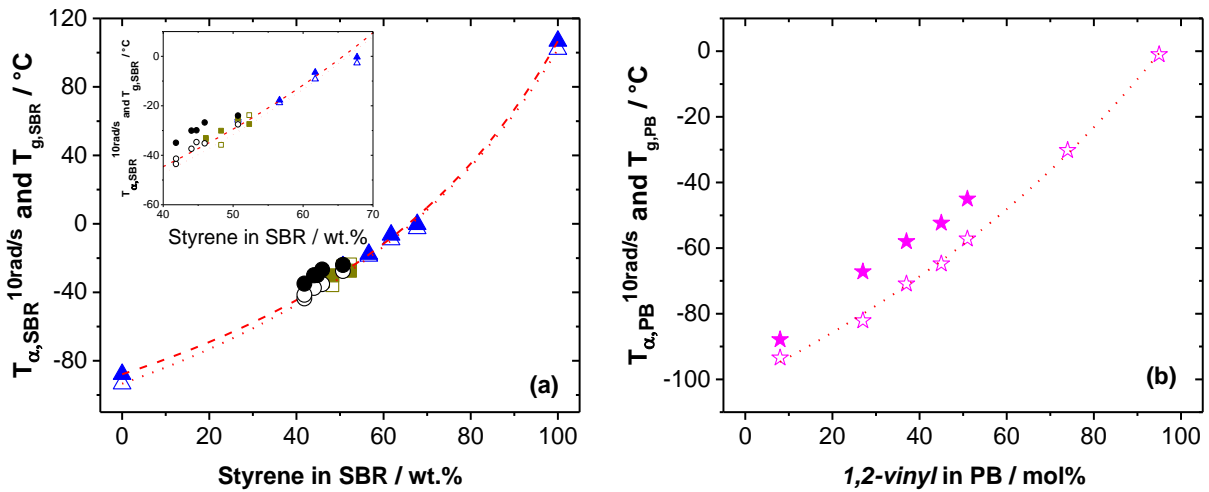


**Figure 31:** (a)  $T_{g,SBR}$  of non-crosslinked samples (open symbol) and  $T_{\alpha,SBR}^{10 \text{ rad/s}}$  of crosslinked samples (full symbols) depending on the weight styrene content  $w_{S,SBR}$  in the SBR block for well microphase separated samples of **Series I** (triangle), **Series II** (squares) and **Series IV** (circles). The dashed, and dotted lines are independent Gordon-Taylor fits for the  $T_{g,SBR}$  and  $T_{\alpha,SBR}^{10 \text{ rad/s}}$  data of **Series I**. (b)  $T_{g,PB}$  of non-crosslinked samples (open symbol) and  $T_{\alpha,PB}^{10 \text{ rad/s}}$  of crosslinked samples (full symbols) depending on the *1,2-vinyl* content in the PB block for samples of **Series IV**. The dashed line represents a Gordon-Taylor fits to  $T_{g,PB}$ .

### Influence of the self-assembled block copolymer structure on the segmental $\alpha$ dynamics.

Considering DSC scans and relaxation behavior from shear measurements for diblock copolymers in the (i) strongly segregated, (ii) the weakly segregated state and (iii) the disordered state it is obvious that their softening behavior is quite different.

For strongly segregated diblock copolymers two narrow bulk-like glass transitions representing both phases are found (cf.  $PB_{50}\text{-}S^{52}B^{48}R_{50}$  and  $PB^{74}\text{-}S^{27}B^{73}R^{16}$  in **Figure 21** and **24**) containing basically only two pure phases and a negligible amount of interfacial material. This relaxation behavior corresponds to that of well phase-separated polymer blends<sup>10</sup> where interfacial material is also negligible. Note that there is no obvious influence of domain size on the cooperative  $\alpha$  dynamics as long as the domains have dimensions of about 20-30 nm like in the investigated samples. Although there is a certain  $T_g$  difference compared to bulk samples with similar microstructure and crosslink density it is not obvious that there are significant effects due to geometrical confinement. The observed  $T_g$  differences are more likely due to a certain scatter in

*1,2-vinyl* and styrene contents as well as differences in crosslink density. This finding is not really new but important in light of the ongoing controversial debate about changes in the  $\alpha$  relaxation dynamics and  $T_g$  in ultrathin films.<sup>28,133,134</sup> This observation supports the observation that the  $\alpha$  dynamics commonly change only in extremely small domains of a few nanometers in size.<sup>21, 108, 135,136,137</sup>

In weakly segregated diblock copolymers with a large fraction of interfacial material, two broad dynamic glass transitions and additional relaxation modes between the bulk values of the dynamic glass transition temperatures ( $T_\alpha^{10 \text{ rad/s}}$ ) are usually found (cf. PB<sub>21</sub>-S<sup>35</sup>B<sup>65</sup>R<sub>69</sub> and PB<sup>8</sup>-S<sup>40</sup>B<sup>60</sup>R<sub>46</sub> **Figure 21** and **24**). Accordingly, there are also significant contributions to  $c_P(T)$  between both  $T_g$ 's in such cases (**Figure 14**). This can be understood as consequence of a lot of material in interphases containing segments of both blocks and having a composition of a mixed phase. Further, there might also be concentration gradients within these interphases. These features result in interfacial material with intermediate  $T_g$ , i.e. a certain fraction of the material in weakly segregated block copolymers undergoes its thermal/dynamic glass transitions at temperatures between those of the pure phases. An extreme example where this behavior can be nicely seen are the so-call gradient block copolymers with continuous concentration gradients along the chain.<sup>99</sup>

These materials consist basically only of interfacial material and show even in the well segregated state a softening behavior where the glass transition is smeared practically over the entire range between the bulk  $T_g$ 's of both components.

Block copolymers in the disordered state do not show a priori a relaxation behavior similar to that of random copolymers like SBR where only one narrow  $\alpha$  relaxation peak is seen (**Figure 21**). In most of the cases you still see indications of two relaxation processes between those of the pure components (cf. PB<sub>50</sub>-S<sup>27</sup>B<sup>63</sup>R<sub>50</sub> in **Figure 21**) or a relatively broad softening interval at intermediate temperatures (cf. PB<sub>50</sub>-S<sup>21</sup>B<sup>69</sup>R<sub>50</sub> in **Figure 21**). This can be explained by the fact that disordered block copolymers are often not homogeneously mixed down to the subsystem sizes having dimensions of a few nanometers as is realized in random copolymers where the subunits are randomly arranged along the chain and in the volume. There are remaining concentration fluctuations in the disordered state slightly above the ODT<sup>15</sup> (fixed at the vulcanization temperature for the crosslinked samples) which cause differences in the segmental  $\alpha$  dynamics. Depending on the concentration of a particular subunit, in a particular nano-sized subsystem (e.g. a CRR being the representative subsystem determining the cooperative  $\alpha$  dynamics according to

related glass transition models),<sup>91</sup> the softening behavior will be intermediate of that between of both pure phases but also different from that of a homogenous mixture, as realized in random copolymers. Finally, this means that block copolymers in the disordered state are often far away from homogeneously mixed from the viewpoint of the  $\alpha$  relaxation dynamics causing the dynamic glass transition. The absence of long range order in the “disordered” state of block copolymers is often not accompanied by one single (random copolymer-like)  $\alpha$  relaxation since disordered block copolymers are not homogeneously mixed in a certain temperature range above the order-disorder transition. In this work such structural states have been fixed by cross-linking. Hence, it was possible to investigate their relaxation behavior in a wide temperature range without significant structural changes.

A fundamental question in this context is:<sup>138</sup> In sub-volumes of which size the mixture of sub-units must be “homogeneous” in order to cause one single, random copolymer-like  $\alpha$  relaxation? For localized mechanisms like  $\beta$  relaxation processes the answer might be that the environment of each individual subunit determines its local dynamics. Hence, the fraction of interfacial material should correspond to that fraction of the block copolymer which shows a dynamic that behaves differently from that of the pure phases. In case of the  $\alpha$  dynamics the answer to this question is not trivial since the  $\alpha$  dynamics is assumed to be cooperative in nature, i.e. it incorporates many subunits which have not to belong to one chain but have to be neighbored in space. There are ongoing controversial debates about the number of subunits (particles  $N_\alpha$ ) involved in a cooperative  $\alpha$  motion and about the related size of cooperatively rearranging regions (CRRs) of volume  $V_\alpha = \xi_\alpha^3$  containing  $N_\alpha$  subunits and being the representative subsystem for the cooperative  $\alpha$  dynamics.<sup>24,25,37</sup> Values for  $\xi_\alpha$  in the range 1-3 nm are often discussed.<sup>139</sup> Note that CRRs are no structural features but that one talks in this case about dynamic heterogeneities, i.e. fluctuative spatiotemporal density patterns with a characteristic length scale  $\xi_\alpha$ .<sup>91</sup>

Data for the heat capacity  $c_p(T)$  for block copolymers which varied systematically the segregation strength are nice model systems in this context since the contribution of each subunit to  $c_p(T)$  should contribute in an additive manner to the total  $c_p$ . This is also the very basis of so-called group contribution concepts<sup>115,116</sup> making suitable predictions for the  $c_p$  values of complex systems depending on composition.<sup>141, 140</sup> Applied to the case of block copolymers with different segregation strength this should allow to judge whether the fraction of interfacial materials is

sufficient to explain the fraction of material showing a softening behavior (glass transition) different from that of the pure phases or whether there are indications that a significantly larger fraction of material is influenced by the interface due to the fact that the CRR size  $\xi_\alpha$  has to be considered in addition. There is hope that this can be judged in case of block copolymers since both  $\xi_\alpha$  and the interfacial width  $d_{IF}$  have both comparable values of few nanometers. Moreover, the amount of interfacial material in the block copolymers is in general large since the domain sizes are only a few times larger than the interfacial width.

**Interrelation between static and dynamic length scales.** The influence of static quantities like domain size (periodicity  $D$ ) and interfacial width  $d_{IF}$  as well as the concentration profile at the interface of diblock copolymers on the relaxation behavior can be nicely investigated in the PB-SBR diblock copolymers showing a large variety of segregation strengths. In this part of the discussion, the static interfacial fraction,  $\phi_{IF,STAT} = \left(\frac{2d_{IF}}{D}\right) \cdot 100$ , as obtained from small angle X-ray scattering data and thermodynamic models (**Section 8.1**) will be compared with the information about the fraction of materials behaving dynamically differently, taken from DSC scans and group contribution-like approach as

$$\phi_{IF,DYN} = [\Delta c_{p,total} - (\Delta c_{p,SBR} + \Delta c_{p,PB}) / \Delta c_{p,total}] \cdot 100 \quad (23)$$

where  $\Delta c_{p,total}$  is the specific heat capacity calculated from group contribution-like concepts considering an average total styrene content of 25 wt% in the PB-SBR diblock copolymer (cf. **Figure 15**) while  $\Delta c_{p,SBR}$  &  $\Delta c_{p,PB}$  are experimental data (**Table 6**). This approach assumes in a first approximation that  $\Delta c_{p,total}$  is linearly dependent on the total styrene content in the PB-SBR diblock copolymer. Data for the PB-SBR diblock copolymers of **Series IV** with systematically varied values of the order parameter  $\chi_{eff}N$  and the static interfacial width  $d_{I,STAT}$  will be considered. **Figure 32** shows a plot of the static and dynamic interfacial fraction,  $\phi_{IF,STAT}$  and  $\phi_{IF,DYN}$ , as a function of the *1,2-vinyl* content in the PB block for all samples of **Series IV**. The  $\phi_{IF,STAT}$  values are calculated based on  $d_{IF,STAT}$  data measured at 150°C where the diblock copolymer structure is fixed by crosslinking. It can be clearly seen that  $\phi_{IF,STAT}$  is significantly lower than  $\phi_{IF,DYN}$ . This means that the fraction of material which is affected regarding its softening behavior is much larger

compared to the fraction of interfacial material from the structural point of view. The difference is large and strongly indicating that there is an additional effect, which is relevant in this case. An approach how this discrepancy can be explained based on an intrinsic interference of structural with dynamic lengths scales related to the cooperative nature of the dynamic glass transition, i.e. the CRR size  $\xi_\alpha$ , is discussed in the next part.

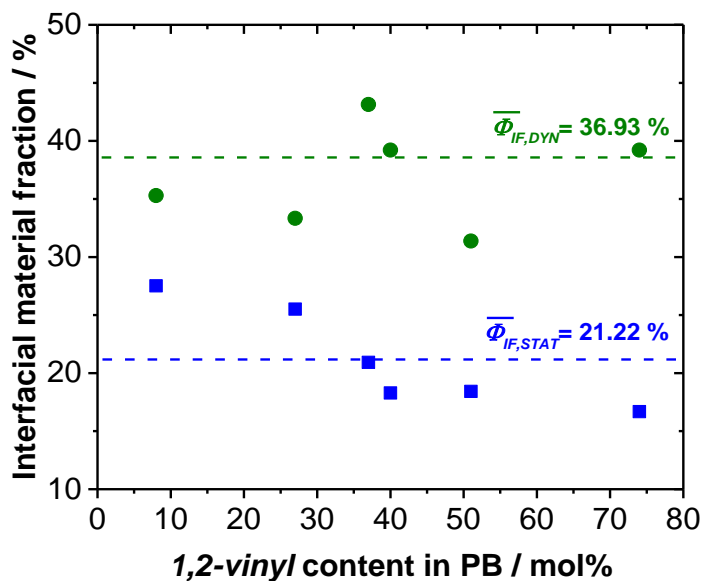


**Figure 32:** Static (cube) and dynamic (circles) interfacial fractions,  $\phi_{IF,STAT}$  and  $\phi_{IF,DYN}$ , as a function of the *1,2-vinyl* content in the PB block for all samples of **Series IV**. The dashed lines represent the average interfacial fraction,  $\overline{\phi_{IF,STAT}}$  and  $\overline{\phi_{IF,DYN}}$ .

Obviously, the structural interfacial fraction  $\phi_{IF,STAT}$  alone cannot explain the large fraction of material in relatively strongly segregated PB-SBR diblock copolymers showing a non-bulk like softening behavior in DSC scans. Therefore, a simple 1-D model simulation will be presented in order to provide a possible explanation for the observed discrepancy between  $\phi_{IF,STAT}$  and  $\phi_{IF,DYN}$ . This model is based on the CRR concept for the glass transition, assuming typical  $\xi_\alpha$  values at  $T_g$  of about 2-3 nm.<sup>141</sup> A 1-D model simulation has been made, in order to explain differences in the DSC softening and  $\alpha$  relaxation behavior of strongly and weakly segregated diblock copolymers. A common lamellar structure with a periodicity of  $D=66$  nm is measured and three different interfacial scenarios are considered. The sketch in **Figure 33** illustrates these three

interfacial scenarios: **(1)** interfacial width equal to zero; **(2)** interface with a width of 6 nm and a uniform (random) concentration profile and; **(3)** interface with a width of 6 nm but having a gradient concentration profile. This interfacial width value is a realistic average value for the strongly segregated PB-SBR diblock copolymers under investigation, as it has been shown for samples of **Series IV (Figure 30)**. Moreover,  $\xi_\alpha$  was chosen to be 3 nm for SBR and PB, as it is a typical CRR size predicted by the fluctuation approach to the glass transition.<sup>141</sup>

A 1-D lattice simulation is performed in order to come to a realistic distribution of the chemical composition of CRRs under the pre-defined conditions. Underlying assumption that the subunits being present in a CRR of size  $\xi_\alpha^3$  determines its individual glass temperature  $T_g$  (and  $\alpha$  dynamics). For diblock copolymers with lamellar morphology the simulation can be reduced to a 1-D lattice. For reasons of simplicity two diblocks containing subunits A or B are considered here (**Figure 33**). Depending on the spatial position and on the concentration profile at the interface, the CRR subunits can have different chemical compositions varying from “only subunits of type A”, “various mixtures of subunits of types A&B” or “only subunits of type B”. The histogram shown in **Figure 33** (lower part) illustrates the probability density of having CRRs of size of 3nm with different chemical compositions depending on the considered interfacial scenario **(1)-(3)**. This simple model can explain the finding in **Figure 32** in which the  $\phi_{IF,DYN}$ , fraction of material behaving dynamically, different from “pure A” or “pure B” phases is much larger than the  $\phi_{IF,STAT}$ , static interfacial fraction, which is relevant from the structural point of view. The most straightforward example is scenario **(1)** in **Figure 33**, with  $d_{IF} = 0$ . Even in this case there are CRRs with compositions between “pure A” or “pure B” resulting in sub-volumes having intermediate  $T_g$  values. In accordance with the idea of this simulation the material fraction,  $\phi_{IF,DYN}$ , with different dynamics is related to the existence of CRRs with a size  $\xi_\alpha \sim 3nm$ . Consequently, one also observes  $\alpha$  relaxation modes between those of “pure A” or “pure B” phases. The same effect occurs for cases **(2)** and **(3)** where the fraction of material with a softening behavior different from that of the pure phases ( $T_g$  values between  $T_{g,A}$  and  $T_{g,B}$ ) is increased by the existence of these CRRs. Actually, this is a good qualitative description of the experimental finding  $\phi_{IF,STAT} < \phi_{IF,DYN}$ , (**Figure 32**). In principle, this approach allows even to estimate the length  $\xi_\alpha$ . Although the uncertainties are significant one can conclude that several nanometers are at least a realistic value.

Taking into consideration that the heat capacity is an additive quantity, it is possible to calculate the  $c_p(T)$  curves based on the histograms in **Figure 33** for diblock copolymers having the three investigated interfacial scenarios (1)-(3). **Figure 34** shows the results of such a simplified  $c_p(T)$  simulation assuming

- (I) that each CRR contributes equally to  $c_p(T)$ ,
- (II) that each CRR has one distinct  $T_g$  and
- (III) that  $T_g$  of CRRs containing different subunits varies linearly with composition between those of the pure phases,  $T_{g,A}$  and  $T_{g,B}$ .

It can be seen that even for  $d_{IF} = 0$  (no interface) the softening at intermediate  $T_g$ 's occurs due the existence of CRRs with finite size of 3 nm. These contributions at intermediate  $T_g$ 's are strongly amplified if interfacial material exists ( $d_{IF} = 6$  nm) like in real block copolymers with finite segregation strength ( $\chi N < \infty$ ). Depending on the chemical composition profile at the interface, the contributions to  $c_p(T)$  at intermediate temperatures in **Figure 34a** are either linear (interfacial scenario (3)) or non-linear (interfacial scenario (2)). Expectedly, in both these cases the contributions occurring at  $T_{g,A}$  and  $T_{g,B}$ ,  $\Delta c_{p,A}$  and  $\Delta c_{p,B}$ , are reduced compared to idealized interfacial scenario (1).

An important general finding is that the contributions between  $T_{g,A}$  and  $T_{g,B}$  do significantly increase independent of the chosen interfacial scenario (1)-(3) if a CRR with finite size (e.g.  $\xi_\alpha = 3$  nm) is introduced. These contributions at intermediate  $T_g$  are missing if each A or B subunit contributes equally to  $c_p$  at a  $T_g$  depending only on its local environment ( $\xi_\alpha = 0$ ). This effect can be directly seen comparing the  $c_p(T)$  simulations in **Figure 34b**, where heat capacity curves for  $\xi_\alpha = 0$  are plotted, with those in **Figure 34a** considering  $\xi_\alpha = 3$  nm.

The simulations in the last paragraph can qualitatively explain the main finding in **Figure 31**,  $\phi_{IF,STAT} < \phi_{IF,DYN}$ , by considering the existence of CRRs with typical dimensions of a few nanometers. In particular, it provides a physical reason for observation that the static interfacial fraction  $\phi_{IF,STAT} = 21.22$  % calculated based on structural parameters for **Series IV** is much too small to explain the large fraction of material in these microphase-separated diblock copolymers showing a softening behavior different from that of its pure phases. An average of about 37% for  $\phi_{IF,DYN}$  was obtained for non-crosslinked samples of **Series IV** based on their DSC heating scans

(Figure 14) and the group contribution-like models for calculating  $\Delta c_{p,\text{total}}$ . Comparing the predictions of the oversimplified model in Figure 32 with experimentally observed values for  $\phi_{IF,DYN}$  one gets at least a reasonable coincidence. The material fraction that is not behaving like both pure phases, taken from the ratio of CRR number having chemical compositions of “A&B” compared to the total number of CRR subsystems, is  $\phi_{IF,THEO} = 27\%$  (Figures 33 and 34). Note that this oversimplified heat capacity model considers only average values ( $d_{IF} = 6\text{nm}$ ,  $D = 66\text{nm}$  and  $\xi_\alpha = 3\text{nm}$ ) which slightly differ from true values for the samples used for comparison. Considering this and the fact that additional assumptions are made, the degree of coincidence between  $\phi_{IF,DYN}$  and  $\phi_{IF,THEO}$  seems to be indeed reasonable. Moreover, one should keep in mind that uncertainties can also appear due to limitation in assessing the actual interfacial width  $d_{IF}$ .

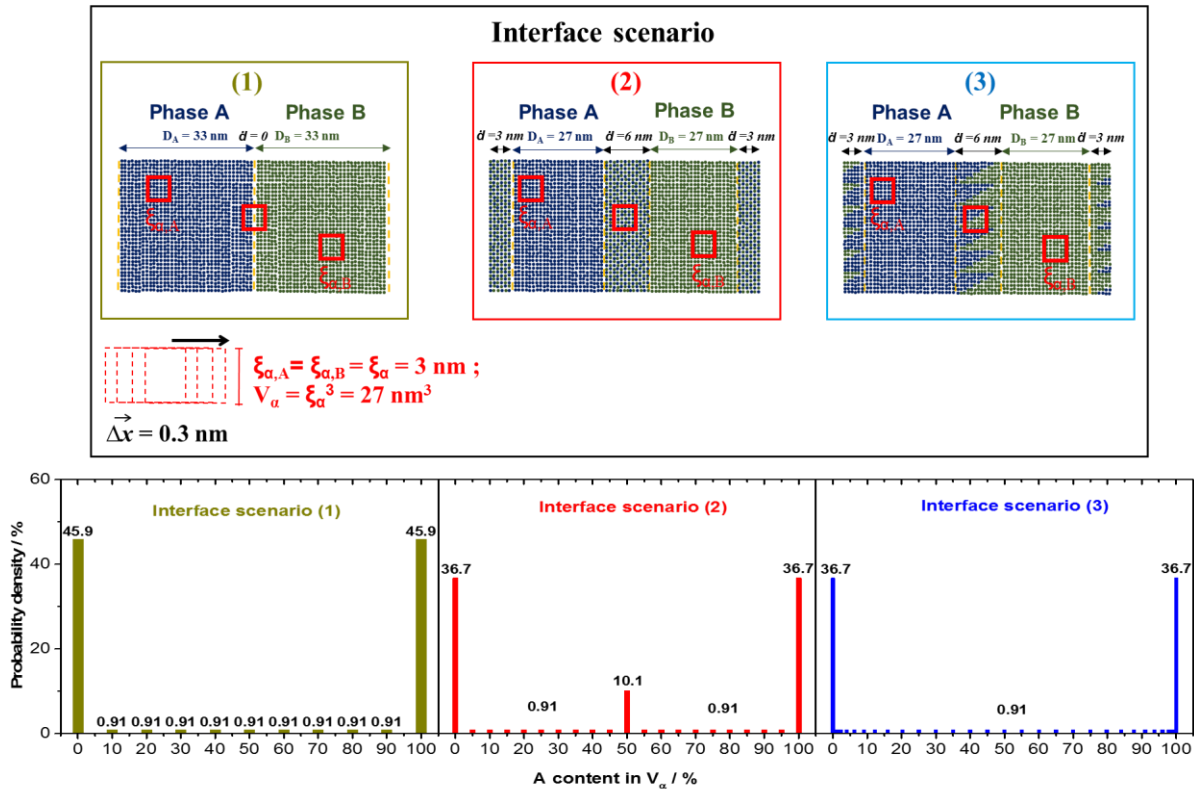


**Figure 33:** Sketch of an 1-D simulation model aimed to describe the glass transition of microphase-separated lamellar diblock copolymers containing phase A (blue), phase B (green) and partly an interphase. Different interface scenarios are considered: (1) no interfacial material  $d_{IF} = 0$ , (2) interphase having a width of  $d_{IF} = 6\text{nm}$  and a homogenous composition (50% A : 50% B) and (3) interphase having a width of  $d_{IF} = 6\text{nm}$  with linear gradient concentration profile. The

CRRs are represented by subsystems of size of  $V_\alpha = \xi_\alpha^3$  according to the cooperatively rearranging regions (CRR) concept. The periodicity  $D$  is chosen to be 66 nm, the used CRR size is  $\xi_\alpha = 3$  nm for both subunits A and B. In the lower part there are histograms showing the probability density to find CRRs with different chemical composition for the three individual interfacial scenarios.

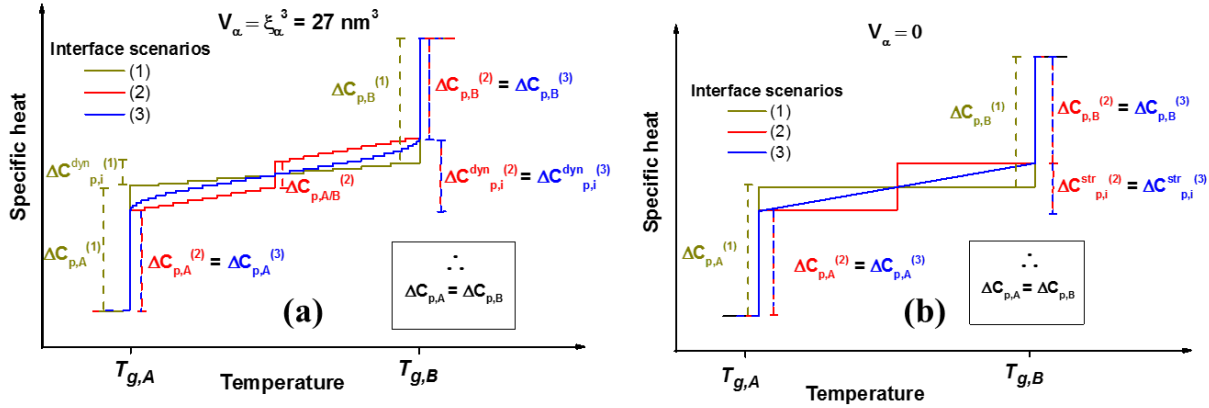


**Figure 34:** (a) Heat capacity curves calculated based on the histograms from the 1-D simulation model in **Figure 33**. Lamellar diblock copolymers composed of two different subunits and  $\xi_\alpha = 3$  nm are considered. The interfacial scenarios (1)-(3) like introduced in **Figure 33** are used. (b) The same interfacial scenarios are used but  $\xi_\alpha = 0$  is considered (related to non-cooperative motions).

In summary, we understand the experimental findings in heat capacity data from DSC for strongly and weakly separated PB-SBR diblock copolymers as a certain evidence for the existence of CRRs with a characteristic length scale  $\xi_\alpha$  in the range of about 3 nm. Without considering such a characteristic length scale  $\xi_\alpha$  controlling the glass transition, it is hard to explain the differences in the segmental  $\alpha$  dynamic between the investigated diblock copolymers depending on the amount of interfacial material. The insights reported in the section should be useful guidelines applicable in future approaches towards fine-tuning relaxation and dissipation behavior of complex composite materials like those used for tire treads.

### 8.3 Relaxation behavior of silica-filled diblock copolymer composites

Wet grip and rolling resistance of tires are known to depend to a large extent on the dissipation behavior of the composite materials used in the tire tread. Conventional lab indicators for the wet grip and rolling resistance are values of the loss tangent  $\tan\delta$  values at 10Hz and 0°C and 60°C, respectively. **Figure 35** shows the temperature dependence of  $\tan\delta$  for composites based on a conventional PB/SBR blend and PB-SBR diblock copolymer in the wet grip and rolling resistance relevant range. The dissipation behavior of commonly applied composites with elastomer blends as matrix can be mainly tuned by changing blend composition, the processing parameters as well as the filler matrix interaction. However, it is very hard to introduce dissipation in the wet grip relevant range without increasing the rolling resistance relevant dissipation. Both parameters are usually strongly coupled, so an increase in wet grip, needed for car safety, is usually accompanied by an increase in rolling resistance, leading to higher fuel consumption. Another major difficulty is that the morphology of the rubber matrix is in the case of blends mainly controlled by the processing step. Any variation in the highly complex processing procedure can influence the performance requiring a high degree of process control, which is usually hard to achieve. This shows that innovative composites based on block copolymers as rubber matrix may have certain advantages caused by their self-assembled morphology resulting in well-defined and predictable dissipation properties.

The first potential advantage of block copolymer based composites is indicated in **Figure 35**. PB-SBR diblock copolymers allow to introduce wet grip at the required temperature-frequency position by changing the SBR microstructure without changing necessarily the rolling resistance indicator significantly. The presented data for composites containing 80 phr silica also show that the relaxation contributions of the SBR phase are basically unchanged regarding their frequency-temperature position if silica filler particles are used. This finding is related to the second advantage being that the self-assembled block copolymer morphology is (at least locally) unchanged even by processing technologies, which are used commonly in the tire industry. This means that the relaxation behavior is to a large extent defined by the diblock copolymer components used and less by the processing technology. A third advantage might be related to the

finding that the silica particles are preferentially localized in the SBR phase of the block copolymer matrix (**Figure 26**). This should allow, in principle, to tune the filler network and to reduce the total filler content needed to achieve a certain reinforcement. If this approach is successful, one could probably also reduce the rolling resistance since the dissipation in the relevant range is usually proportional to the filler content (**Figure 25**).<sup>6,107</sup> The discussion above nicely demonstrates that self-assembled block copolymers are a powerful approach to control the dissipation of the elastomer matrix in rubber composites. From this point of view block copolymers are potentially advantageous compared to classical elastomer blends as matrix systems for tire tread applications.

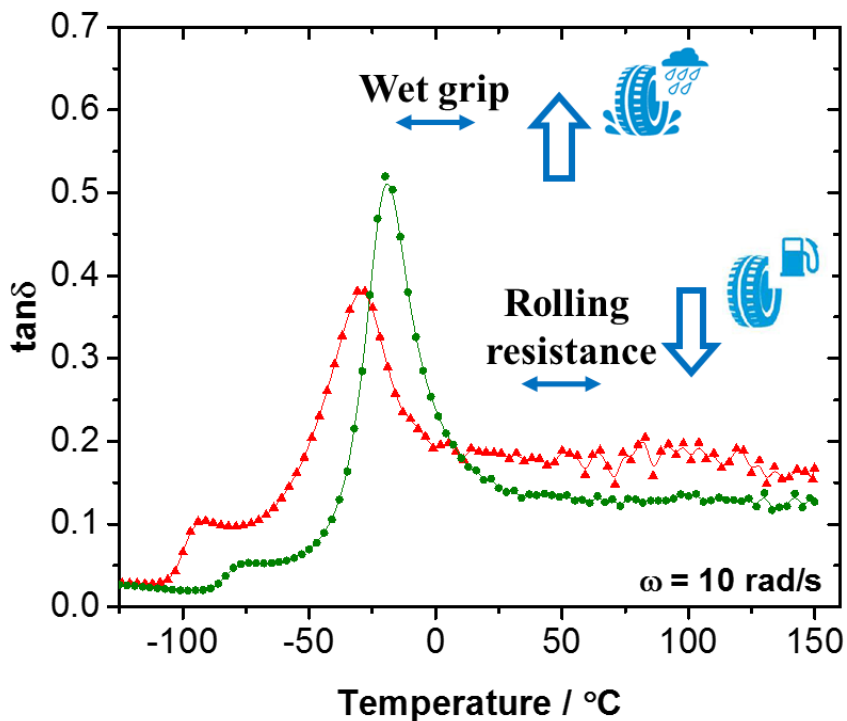


**Figure 35:** Loss tangent  $\tan\delta$  vs. temperature for aPB/ScBR blend (triangle) and a PB-SBR diblock copolymer (circle) both filled with 80 phr silica. The wet grip and rolling resistance compound indicators are quantified as  $\tan\delta$  values measured at 10 rad/s in the temperature intervals from -10 to 10°C and from 40 to 60°C, respectively.

## Chapter 9

### Conclusions

Central aim of this work was to study the influence of local chemical composition and interfacial material as well as structural parameters like domain size and domain shape on the cooperative  $\alpha$  dynamics based on four series of PB-SBR diblock copolymers with different composition. A novel anionic polymerization route has been developed in order to obtain PB-SBR diblock copolymers having low *1,2-vinyl* contents in the SBR block and low styrene blockiness. The synthesis of the SBR block was carried out at 70°C with n-BuLi/TMEDA (1:0.4) and the sequential addition of butadiene monomer by means of a metering pump. The synthesis is starting with the PB block in the presence of n-BuLi while the SBR block is grown assisted by n-BuLi/TMEDA (1:1) with sequential addition of butadiene monomer. Using this strategy the microstructures of the butadiene sequences in PB and SBR blocks can be controlled and the blockiness in the SBR block is commonly below the NMR detection limit (styrene sequences longer than six units). The PB-SBR diblock copolymers have an average molecular weight of  $\underline{M}_n \sim 200$  kg/mol and a narrow molecular weight distribution ( $M_w/M_n < 1.10$ ). All diblock copolymer samples are vulcanized afterwards using a standard procedure commonly applied in the tire industry.

The microstructural parameters and the structural properties of the four diblock copolymer series can be summarized as follows:

- **Series I:** the styrene content in the SBR block is varied in the range 21 - 52 mol% for a given volume fraction of  $\Phi_{\text{SBR}} \approx 50$  vol% and fixed *1,2-vinyl* content in the butadiene sequences. This gives a series of diblock copolymers with lamellar morphology but varied segregation strength  $\chi_{\text{eff}}N$  including two disordered samples.
- **Series II** the PB-SBR samples have variable volume fraction ( $\Phi_{\text{SBR}}$ ) ranging from 20 to 69 vol% and low *1,2-vinyl* amounts in both blocks (PB and SBR). The styrene content in the SBR varies only slightly ( $x_{\text{S,SBR}} = 32 \pm 4$  mol%). In this series different cylindrical and lamellar morphologies are observed. The most asymmetric samples are disordered.

- **Series III** is composed of symmetric ( $\Phi_{PB} \approx \Phi_{SBR} \approx 50$  vol%) PB-SBR copolymer samples with low *1,2-vinyl* content in the PB block ( $c_{1,2-vinyl,PB} \approx 8.0$  mol%), an average styrene content of  $x_{S,SBR} = 39 \pm 4$  mol% and *1,2-vinyl* content range  $14.0 \text{ mol}\% \leq c_{1,2-vinyl,SBR} \leq 59.0 \text{ mol}\%$  in the SBR block. This gives a series of samples with lamellar morphology where only the samples with highest  $c_{1,2-vinyl,SBR}$  values are disordered. The segregation strength  $\chi_{eff}N$  varies.
- **Series IV** consists of symmetric ( $\Phi_{PB} \approx \Phi_{SBR} \approx 50$  vol%) PB-SBR diblock copolymer samples with low *1,2-vinyl* content ( $c_{1,2-vinyl,SBR} \approx 16$  mol%) and average styrene concentration of  $x_{S,SBR} = 32 \pm 4$  mol% in the SBR block as well as *1,2-vinyl* contents in the range  $8.0 \text{ mol}\% \leq c_{1,2-vinyl,PB} \leq 74.0 \text{ mol}\%$  in the PB block. In this case all samples show lamellar morphology but the segregation strength  $\chi_{eff}N$  is systematically varied.

Based on these four diblock copolymer series, it could be shown that the morphology and the  $\alpha$  relaxation dynamics are only weakly affected by the crosslinking procedure used. It can be concluded that the morphology existing at the crosslinking temperature is basically fixed by the relatively fast crosslinking reaction at 150°C. This allows to study the relaxation behavior without significant changes in the structural state.

It was further possible (i) to verify thermodynamic models predicting segregation strength  $\chi_{eff}N$ , (ii) to estimate the interfacial width  $d_{IF,STAT}$ , (iii) to determine free parameters of models connecting the microstructure of the individual blocks with their glass transition temperatures and (iv) to study interrelations between structural features and the cooperative  $\alpha$  dynamics systematically. In particular, it has been shown that

- a) the thermodynamic model for the determination of  $\chi_{eff}$  for PB/SBR blends with different microstructure proposed by Sakurai et al.<sup>3</sup> can be applied to PB-SBR diblock copolymers. The composition-dependent ODT in **Series I** and **Series III** is successfully predicted with an adequate quality.
- b) the interfacial widths  $d_{IF,STAT}$  have been calculated based on the thermodynamic model introduced by Semenov.<sup>126</sup> The values for **Series IV** seem to be in reasonable agreement with trends seen in  $\alpha$  relaxation data from shear measurements and

- microstructure-dependent changes in  $c_p(T)$ , although a quantitative description of the sequential softening behavior  $c_p(T)$  based on  $d_{IF,STAT}$  was not successful
- c) the expected trends in  $T_g$  depending on styrene content in SBR and *1,2-vinyl* content in the PB block have been confirmed. The Gordon-Taylor equation is successfully applied for the interpolation of  $T_{g,SBR}$  for strongly segregated samples of **Series I, II** and **IV** and  $T_{g,PB}$  for **Series IV**.
  - d) the fraction of interfacial material  $\Phi_{IF,STAT}$  is estimated based on structural data as well as  $d_{IF}$  from thermodynamic models. A dynamic interfacial fraction  $\Phi_{IF,DYN}$  was estimated from  $\Delta c_p(T)$  at the glass transition of both individual phases, PB and SBR, compared to total  $\Delta c_p$  calculated from group-contribution like concepts. Static and dynamic interfacial material fractions,  $\Phi_{IF,STAT}$  and  $\Phi_{IF,DYN}$ , are compared. It is found for **Series IV** that  $\Phi_{IF,STAT}$  is significantly smaller than  $\Phi_{IF,DYN}$ . The observed discrepancy is explained based on a model introducing the size of cooperative rearranging regions (CRRs)  $V_\alpha = \xi_\alpha^3 \sim 27 \text{ nm}^3$  being the estimated size of this characteristic subsystem at  $T_g$ . This approach predicts that the fraction of material with intermediate  $T_g$ 's is significantly higher than  $\Phi_{IF,STAT}$  being in reasonable agreement with the values which have been found for  $\Phi_{IF,DYN}$ . This result can be understood as an experimental indication for a characteristic length of the glass transition  $\xi_\alpha$  in the range of a few nanometers at  $T_g$ .

Finally, potential advantages of block copolymer based composites are demonstrated based on one series of silica-filled PB-SBR diblock copolymers. It is shown that morphology and  $\alpha$  relaxation behavior are basically controlled by the block copolymer microstructure and only weakly affected by the filler. This allows introducing dissipative contributions in the wet grip relevant frequency-temperature range by varying the SBR block microstructure without changing the rolling resistance. Further, the influence of the processing conditions is significantly reduced. Most interesting is, however, that the silica particles are selectively located in the SBR phase of the investigated diblock copolymer. This could be used in the future to fine-tune the filler network and reduce the filler content that is commonly accompanied by a reduction of the rolling resistance. These promising results show that there are several fields where diblock copolymers could offer

technical advantages if used as matrices, for example, in tire treads. However, further investigations and developments are needed to make use of this potential in future applications.

## References

- [1] Kelly, A.; *Concise encyclopedia of composite materials*; Pergamon publisher: Cambridge, United Kingdom, 1994, pp 22.
- [2] Hofmann, W.; Verlag, C.H. *Rubber Technology handbook*; Hanser publisher: Munich, Germany, 1989, pp 62.
- [3] Sakurai, S.; Izumitani, T.; Hasegawa, H.; Hashimoto, T.; Han, C. C. Small-Angle Neutron-Scattering and Light-Scattering Study on the Miscibility of Poly(Styrene-Ran-Butadiene) Polybutadiene Blends. *Macromolecules* **1991**, *24* (17), 4844-4851.
- [4] Wang, M. Effect of filler-elastomer interaction on tire tread performance part I. *KGK-Kaut Gummi Kunst* **2007**, *60* (9), 438-443.
- [5] Wang, M. Effect of filler-elastomer interaction on tire tread performance part II. *KGK-Kaut Gummi Kunst* **2008**, *61* (1-2), 33-42.
- [6] Mujtaba, A.; Keller, M.; Ilisch, S.; Radusch, H.; Thurn-Albrecht, T.; Saalwaechter, K.; Beiner, M. Mechanical Properties and Cross-Link Density of Styrene-Butadiene Model Composites Containing Fillers with Bimodal Particle Size Distribution. *Macromolecules* **2012**, *45* (16), 6504-6515.
- [7] Persson, B. N. J. Theory of rubber friction and contact mechanics. *J. Chem. Phys* **2001**, *115* (8), 3840-3861.
- [8] Persson, B. N. J. On the theory of rubber friction. *Surf. Sci.* **1998**, *401* (3), 445-454.
- [9] Ruzette, A. V.; Leibler, L. Block copolymers in tomorrow's plastics. *Nat. Mat.* **2005**, *4* (1), 19-31.
- [10] Thielen, G. Filler impact on rubber blend miscibility. *KGK-Kaut Gummi Kunst* **2007**, *60* (7-8), 389-392.

- [11] Kawazura, T.; Kawazoe, M.; Kikuchi, Y.; Nakamura, T.; Nakamura, M.; Karato, T. (The Yokohama Rubber Co. Ltd., Japan; Nippon Zeon Co., Ltd., Japan). Block copolymer rubber composition comprising the same and pneumatic tire made therefrom. US Patent 6,355,728, March 12, 2002.
- [12] Yasumasa, T.; Mitsuhiro, S.; Fumio, T.; Akio, T.; Iwakazu, H. (Japan Synthetic Rubber Co. LTD, Japan). Styrene-butadiene block copolymer. European Patent 01349009 B1
- [13] Feng, H.; Zhang, X.; Zhao, S. Tin-coupled star-shaped block copolymer of styrene and butadiene (I) synthesis and characterization. *J. Appl. Polym. Sci.* **2008**, *110* (1), 228-236.
- [14] Leibler, L. Theory of Microphase Separation in Block Co-Polymers. *Macromolecules* **1980**, *13* (6), 1602-1617.
- [15] Bates, F. S.; Fredrickson, G. H. Block Copolymer Thermodynamics - Theory and Experiment. *Annu. Rev. Phys. Chem* **1990**, *41*, 525-557.
- [16] Hamley, I.W. *The physics of block copolymers*; Oxford University Press: Oxford, U.K., 1998.
- [17] Floudas, G.; Paraskeva, S.; Hadjichristidis, N.; Fytas, G.; Chu, B.; Semenov, A. N. Dynamics of polyisoprene in star block copolymers confined in microstructures: A dielectric spectroscopy study. *J. Chem. Phys* **1997**, *107* (14), 5502-5509.
- [18] Alig, I.; Floudas, G.; Avgeropoulos, A.; Hadjichristidis, N. Junction point fluctuations in microphase separated polystyrene-polyisoprene-polystyrene triblock copolymer melts. A dielectric and rheological investigation. *Macromolecules* **1997**, *30* (17), 5004-5011.
- [19] Alcoutlabi, M.; McKenna, G. B. Effects of confinement on material behaviour at the nanometre size scale. *J. Phys. Condens. Matter* **2005**, *17* (15), R461-R524.

- [20] Alba-Simionesco, C.; Coasne, B.; Dosseh, G.; Dudziak, G.; Gubbins, K.; Radhakrishnan, R.; Sliwinska-Bartkowiak, M. Effects of confinement on freezing and melting. *J. Phys. Condens. Matter* **2006**, *18* (6), R15-R68.
- [21] Arndt, M.; Stannarius, R.; Groothues, H.; Hempel, E.; Kremer, F. Length scale of cooperativity in the dynamic glass transition. *Phys. Rev. Lett.* **1997**, *79* (11), 2077-2080.
- [22] Kremer, F.; Huwe, A.; Arndt, M.; Behrens, P.; Schwieger, W. How many molecules form a liquid? *J. Phys. Condens. Matter* **1999**, *11* (10A), A175-A188..
- [23] Schonhals, A.; Goering, H.; Schick, C.; Frick, B.; Zorn, R. Polymers in nanoconfinement: What can be learned from relaxation and scattering experiments? *J. Non-Cryst. Solids* **2005**, *351* (33-36), 2668-2677.
- [24] Schick, C.; Donth, E. Characteristic Length of Glass-Transition - Experimental-Evidence. *Phys. Scripta* **1991**, *43* (4), 423-429.
- [25] Hempel, E.; Vieweg, S.; Huwe, A.; Otto, K.; Schick, C.; Donth, E. Characteristic length of glass transition from calorimetry in different confinements. *J Phys. IV* **2000**, *10* (P7), 79-82.
- [26] Beiner, M.; Huth, H. Nanophase separation and hindered glass transition in side-chain polymers. *Nat. Mater.* **2003**, *2* (9), 595-599.
- [27] Pankaj, S.; Beiner, M. Confined Dynamics and Crystallization in Self-Assembled Alkyl Nanodomains. *J. Phys. Chem. B* **2010**, *114* (47), 15459-15465.
- [28] Forrest, J. A.; Dalnoki-Veress, K. The glass transition in thin polymer films. *Adv. Colloid Interface Sci.* **2001**, *94* (1-3), 167-196.
- [29] Ellison, C. J.; Mundra, M. K.; Torkelson, J. M. Impacts of polystyrene molecular weight and modification to the repeat unit structure on the glass transition-nanoconfinement effect and the cooperativity length scale. *Macromolecules* **2005**, *38* (5), 1767-1778.

- [30] Swallen, S. F.; Bonvallet, P. A.; McMahon, R. J.; Ediger, M. D. Self-diffusion of tris-naphthylbenzene near the glass transition temperature. *Phys. Rev. Lett.* **2003**, *90* (1), 015901.
- [31] Sergei, A.; Tress, M.; Kremer, F. The glass transition of thin polymer films in relation to the interfacial dynamics. *J. Chem. Phys* **2009**, *131* (15), 1415-1428.
- [32] Ellison, C. J.; Torkelson, J. M. The distribution of glass-transition temperatures in nanoscopically confined glass formers. *Nat. Mater.* **2003**, *2* (10), 695-700.
- [33] Dutcher, J.; Ediger, M. Materials science - Glass surfaces not so glassy. *Science* **2008**, *319* (5863), 577-578.
- [34] Boucher, V. M.; Cangialosi, D.; Alegria, A.; Colmenero, J.; Gonzalez-Irun, J.; Liz-Marzan, L. M. Accelerated physical aging in PMMA/silica nanocomposites. *Soft Matter* **2010**, *6* (14), 3306-3317.
- [35] Papon, A.; Saalwaechter, K.; Schaefer, K.; Guy, L.; Lequeux, F.; Montes, H. Low-Field NMR Investigations of Nanocomposites: Polymer Dynamics and Network Effects. *Macromolecules* **2011**, *44* (4), 913-922.
- [36] Cangialosi, D.; Alegria, A.; Colmenero, J. Predicting the time scale of the component dynamics of miscible polymer blends: The polyisoprene/poly(vinylethylene) case. *Macromolecules* **2006**, *39*, 7149-7156.
- [37] Donth, E. J. *The Glass Transition. Relaxation Dynamics in Liquids and Disordered Materials*; Springer, Berlin, 2001.
- [38] Babur, T.; Balko, J.; Budde, H.; Beiner, M. Confined relaxation dynamics in long range ordered polyesters with comb-like architecture. *Polymer* **2014**, *55* (26), 6844-6852.
- [39] Szwarc, M. Living Polymers. *Nature* **1956**, *178* (4543), 1168-1169.
- [40] Hillmyer, M. Block copolymer synthesis. *Curr. Opin. Solid St. M* **1999**, *4* (6), 559-564.

- [41] Hsieh, H.; Quirk, R.P. Anionic Polymerization: Principles and Practical Applications
- [42] Beylen, M.V.; Morita, H.; Peculiarities of the anionic copolymerization of styrene and dienes in non-polar solvents with Li<sup>+</sup> as counter-ion m.v.b. *Macromol. Symp.* **2011**, *308*, 12–16.
- [43] Kuntz, I. Copolymerization of 1,3-Butadiene with Styrene by Butyllithium Initiation. *J. Polym. Sci. A Polym. Chem.* **1961**, *54* (160), 569-586.
- [44] Korotkov, A.A. *Angew. Chem.* **1958**, *70*, 85.
- [45] Odriscoll, K. F.; Kuntz, I. Kinetics of Anionic Copolymerization of Monomers of Similar Polarities. *J. Polym. Sci.* **1962**, *61* (171), 19-24.
- [46] Antkowiak, T. A.; Tate, D. P.; Oberster, A. E.; Halasa, A. F. Temperature and Concentration Effects on Polar-Modified Alkylolithium Polymerizations and Copolymerizations. *J. Polym. Sci. A Polym. Chem.* **1972**, *10* (5), 1319-1334.
- [47] Iovu, M. C.; Buzdugan, E.; Teodorescu, M.; Britchi, A. G.; Hubca, G.; Iovu, H. Copolymerization of styrene with butadiene using methyl tert-butyl ether as active center modifier. *Angew. Chem.* **1999**, *271*, 18-23.
- [48] Halasa, A.F.; Jasiunas, C.; Hsu, B.; Henning, S.; Seo, K.S. Synthesis of random or tapered solution styrene-butadiene copolymers in the presence of sodium dodecylbenzene sulfonate as a polar modifier. *J. Appl. Polym. Sci.* **2013**, *127* (3), 2116-2120.
- [49] Beckelmann, D.; Bandermann, F. Classification of polar additives with respect to their influence on the microstructure in anionic polymerization of isoprene with butyllithium by transition energy measurements. *J. Appl. Polym. Sci.* **1999**, *73* (8), 1533-1547.
- [50] Cheng, T. C. Anionic-Polymerization .8. Effect of Polar Modifiers on Uptake of Styrene and the Rate of Lithium Morpholinide Initiated Butadiene-Styrene Copolymerization. *Macromolecules* **1981**, *14* (3), 664-668.

- [51] Bates, F. S.; Fredrickson, G. H. Block copolymers - Designer soft materials. *Phys Today* **1999**, 52 (2), 32-38.
- [52] Bates, F. S. Polymer-Polymer Phase-Behavior. *Science* **1991**, 251 (4996), 898-905.
- [53] Matsen, M. W.; Bates, F. S. Origins of complex self-assembly in block copolymers. *Macromolecules* **1996**, 29 (23), 7641-7644.
- [54] Flory, P.J. *Principle of polymer chemistry*; Cornell Univ. Press, Ithaca: New York, 1953.
- [55] Guggenheim, E.A. *Thermodynamics*; Elsevier: New York, 1985.
- [56] Flory, P.J. Thermodynamics of High Polymer Solutions. *J. Chem. Phys.* **1942**, 10, 51.
- [57] Huggins, M. Some Properties of Solutions of Long-chain Compounds. *J. Chem. Phys.* **1942**, 46 (1), 151-158.
- [58] Huggins, M. Theory of Solutions of High Polymers. *J. Am. Chem Soc.* **1942**, 64 (7), 1712-1719.
- [59] De Gennes, P.G. *Scaling Concepts in Polymer Physics*; Cornell Univ. Press, Ithaca: New York, 1979.
- [60] Matsen, M. W.; Bates, F. S. Block copolymer microstructures in the intermediate-segregation regime. *J. Chem. Phys* **1997**, 106 (6), 2436-2448.
- [61] Fredrickson, G. H.; Helfand, E. Fluctuation Effects in the Theory of Microphase Separation in Block Copolymers. *J. Chem. Phys* **1987**, 87 (1), 697-705.
- [62] Matsen, M. W.; Schick, M. Stable and unstable phase of a diblock copolymer melt. *Phys. Rev. Lett.* **1994**, 72 (16), 2660-2663.
- [63] Mai, Y.; Eisenberg, A. Self-assembly of block copolymers. *Chem. Soc. Rev.* **2012**, 41 (18), 5969-5985.

- [64] Ogawa, T.; Sakamoto, N.; Hashimoto, T.; Han, C. D.; Baek, D. M. Effect of volume fraction on the order-disorder transition in low molecular weight polystyrene-block-polyisoprene copolymers .2. Order-disorder transition temperature determined by small-angle X-ray scattering. *Macromolecules* **1996**, *29* (6), 2113-2123.
- [65] Pochan, D. J.; Gido, S. P.; Zhou, J.; Mays, J. W.; Whitmore, M.; Ryan, A. J. Morphologies of microphase-separated conformationally asymmetric diblock copolymers. *J. Polym. Sci. Part B Polym. Phys.* **1997**, *35* (16), 2629-2643.
- [66] Matsen, M. W.; Bates, F. S. Unifying weak- and strong-segregation block copolymer theories. *Macromolecules* **1996**, *29* (4), 1091-1098.
- [67] Semenov, A. N. Contribution to the Theory of Microphase Layering in Block-Copolymer Melts. *J. Exp. Theor. Phys.* **1985**, *88* (4), 1242-1256.
- [68] Cohen, M.; Turnbull, D. Molecular Transport in Liquids and Glasses. *J. Chem. Phys* **1959**, *31* (5), 1164–1169.
- [69] Turnbull, D.; Cohen, M. Free-Volume Model of the Amorphous Phase: Glass Transition. *J. Chem. Phys* **1961**, *34* (1), 120–125.
- [70] Richert, R.; Angell, C.A. Dynamics of glass-forming liquids. V. On the link between molecular dynamics and configurational entropy. *J. Chem. Phys* **1998**, *108* (21), 9016–9026.
- [71] Berthier, L.; Biroli, G.; Bouchaud, J.-P.; Cipelletti, L.; El Masri, D.; L'Ho<sup>^</sup>te, D.; Ladieu, F.; Pierno, M. Direct Experimental Evidence of a Growing Length Scale Accompanying the Glass Transition. *Science* **2005**, *310*, 1797-1800.
- [72] Donth, E. The size of cooperatively rearranging regions at the glass transition. *J. Non-Cryst. Solids* **1982**, *53* (3), 325-330.

- [73] Götze, W.; Sjögren, L. Relaxation processes in supercooled liquids. *Rep. Prog. Phys.* **1992**, *55* (3), 241–376.
- [74] Ngai, K. L.; Tsang, K. Y. Similarity of relaxation in supercooled liquids and interacting arrays of oscillators. *Phys. Rev. Lett.* **1999**, *60* (4), 4511–4517.
- [75] Angell, C.A. Formation of Glasses from Liquids and Biopolymers. *Science* **1995**, *267* (5206), 1924-1935.
- [76] Angell, C.A; Ngai, K.L.; McKenna, G.B.; McMillan, P.F.; Martin, S.W. Relaxation in glass forming liquids and amorphous solids. *J. Chem. Phys* **2000**, *88* (6), 3113-3157.
- [77] Kohlrausch, F. Ueber das Dellmann'sche Elektrometer. *Ann der Phys.* **1847**, *11* (148), 353-405.
- [78] Richert, R. Evidence for Dynamic Heterogeneity near  $T_g$  from the Time-Resolved Inhomogeneous Broadening of Optical Line Shapes. *J. Chem. Phys B* **1977**, *101* (33), 6323–6326.
- [79] Richert, R. Molecular dynamics analyzed in terms of continuous measures of dynamic heterogeneity. *J. Non-Cryst. Solids* **1998**, *235*, 41–47.
- [80] Johari, G.; Goldstein, M. Viscous Liquids and the Glass Transition. II. Secondary Relaxations in Glasses of Rigid Molecules. *J. Chem. Phys* **1970**, *53* (6), 2372–2388.
- [81] Pankaj, S. *Confined dynamics, side-chain crystallization and long term behavior of nanophase separated poly(3-alkyl thiophenes)*. Martin Luther University Halle Wittenberg, *PhD thesis*, 2011.
- [82] Cohen, M.; Turnbull, D. Molecular Transport in Liquids and Glasses. *J. Chem. Phys* **1959**, *31* (5), 1164–1169.
- [83] Turnbull, D.; Cohen, M. Free-Volume Model of the Amorphous Phase: Glass Transition *J. Chem. Phys* **1961**, *34* (1), 120–125.

- [84] Doolittle, A. K. Studies in Newtonian Flow. I. The Dependence of the Viscosity of Liquids on Temperature. *J. Appl. Phys.* **1951**, 22 (8), 1031–1035.
- [85] Doolittle, A. K.; Doolittle, D. B. Studies in Newtonian Flow. V. Further Verification of the Free-Space Viscosity Equation. *J. Appl. Phys.* **1957**, 28 (8), 901–905.
- [86] Johari, G.; Goldstein, M. Viscous Liquids and the Glass Transition. II. Secondary Relaxations in Glasses of Rigid Molecules *J. Chem. Phys.* **1970**, 53 (6), 2372–2388.
- [87] Ferry, J. D. *Viscoelastic Properties of Polymers*. JohnWiley and sons, USA, 3 edition, (1980).
- [88] Adam, G. Gibbs, J. H. On the Temperature Dependence of Cooperative Relaxation Properties in Glass-Forming Liquids. *J. Chem. Phys.* **1965**, 43 (1), 139-146.
- [89] Huth, H.; Beiner, M.; Donth, E. Temperature dependence of glass-transition cooperativity from heat-capacity spectroscopy: Two post-Adam-Gibbs variants. *Phys. Rev. B* **2000**, 61 (22), 15092-15101
- [90] Babur, T.; Balko, J.; Budde, H.; Beiner, M. Confined relaxation dynamics in long range ordered polyesters with comb-like architecture. *Polymer*, **2014**, 55, 6844-6852.
- [91] Donth, E.J. *Glasübergang*. Akademie-Verlag, Berlin, (1981).
- [92] Serghei, A. Challenges in glassy dynamics of polymers. *Macromol. Chem. Phys.* **2008**, 209 (14), 1415-1423.
- [ 93 ] Pulamagatta, B.; Pankaj, S.; Beiner, M.; Binder, W. Hierarchical Nanostructures in Semifluorinated Norbornene Block Copolymers. *Macromolecules* **2011**, 44 (4), 958-965.
- [94] Hiller, S.; Pascui, O.; Budde, H.; Kabisch, O.; Reichert, D.; Beiner, M. Nanophase separation in side chain polymers: new evidence from structure and dynamics. *New J. Phys.* **2004**, 6.

- [95] Gitsas, A.; Floudas, G.; Butt, H.; Pakula, T.; Matyjaszewski, K. Effects of Nanoscale Confinement and Pressure on the Dynamics of pODMA-b-ptBA-b-pODMA Triblock Copolymers. *Macromolecules* **2010**, *43* (5), 2453-2462.
- [96] Encinar, M.; Guzman, E.; Prolongo, M. G.; Rubio, R. G.; Sandoval, C.; Gonzalez-Nilo, F.; Gargallo, L.; Radic, D. Dielectric and dynamic-mechanical study of the mobility of poly(t-butylacrylate) chains in diblock copolymers: Polystyrene-b-poly(t-butylacrylate). *Polymer* **2008**, *49* (26), 5650-5658.
- [97] Alig, I.; Floudas, G.; Avgeropoulos, A.; Hadjichristidis, N. Junction point fluctuations in microphase separated polystyrene-polyisoprene-polystyrene triblock copolymer melts. A dielectric and rheological investigation. *Macromolecules* **1997**, *30* (17), 5004-5011.
- [98] Floudas, G.; Paraskeva, S.; Hadjichristidis, N.; Fytas, G.; Chu, B.; Semenov, A. N. Dynamics of polyisoprene in star block copolymers confined in microstructures: A dielectric spectroscopy study. *J. Chem. Phys* **1997**, *107* (14), 5502-5509.
- [99] McKenna, G. B. Glass dynamics - Diverging views on glass transition. *Nat. Phys.* **2008**, *4* (9), 673-674.
- [100] Mok, M.M.; Kim, J.; Torkelson, J.M. Gradient copolymers with broad glass transition temperature regions: Design of purely interphase compositions for damping applications. *J. Polym. Sci. Part B* **2008**, *46* (1), 48-58.
- [101] Lee, I.; Bates, F. S. Synthesis, Structure, and Properties of Alternating and Random Poly(styrene-b-butadiene) Multiblock Copolymers. *Macromolecules* **2013**, *46* (11), 4529-4539.
- [102] Beiner, M. About the nature of peculiarities in the segmental dynamics of complex polymeric systems. XVth International Congress on Rheology, Monterey (USA) 2008.
- [Unpublished manuscript]

- [103] Mujtaba, A.; Keller, M.; Ilisch, S.; Radusch, H.; Thurn-Albrecht, T.; Saalwaechter, K.; Beiner, M. Detection of Surface-Immobilized Components and Their Role in Viscoelastic Reinforcement of Rubber–Silica Nanocomposites. *ACS Macro Lett.* **2014**, *3* (5), 481-485.
- [104] Robertson, C.; Lin, C.; Bogoslovov, R.; Rackaitis, M.; Sadhukhan, P.; Quinn, J.; Roland, C. Flocculation, Reinforcement, and Glass Transition Effects in Silica-Filled Styrene-Butadiene Rubber. *Rubber Chem. Technol.* **2011**, *84* (4), 507-519.
- [105] Mark, J.E. *Physical properties of polymers handbook*; Springer, 2nd ed.: Ohio, US, 2007. pp 411.
- [106] Tanaka, Y.; Sato, H.; Saito, K.; Miyashita, K. Determination of Sequence Distribution in Styrene-Butadiene Co-Polymer .1. H-1-Nmr Study of Styrene Oligomers. *Rubber Chem. Technol.* **1981**, *54* (4), 685-691.
- [107] Hofmann, A.; Alegria, A.; Colmenero, J.; Willner, L.; Buscaglia, E.; Hadjichristidis, N. Secondary and segmental relaxation in polybutadienes of varying microstructure: Dielectric relaxation results. *Macromolecules* **1996**, *29* (1), 129-134.
- [108] Zorn, R.; Mopsik, F. I.; McKenna, G. B.; Willner, L.; Richter, D. Dynamics of polybutadienes with different microstructures .2. Dielectric response and comparisons with rheological behavior. *J. Chem. Phys.* **1997**, *107* (9), 3645-3655.
- [109] Wunderlich, B. *Thermal Analysis*; Academic Press, Inc., 1990.
- [110] *ibid*, p. 463.
- [111] Roe, R.J. *Methods of X-ray and Neutron Scattering in Polymer Science*; Oxford University Press; 1 edition, New York, 2000, p. 26
- [112] Grellmann, W. In *Polym. Test*; Seidler, S.,Eds.; HANSER: Germany, 2007;Vol.1, p 92.

- [113] Roe, R.J. *Methods of X-ray and Neutron Scattering in Polymer Science*; Oxford University Press; 1 edition, New York, 2000, p. 196
- [114] Wolff, T.; Burger, C.;Ruland, W. Synchrotron SAXS study of the microphase separation transition in diblock copolymers. *Macromolecules* **1993**, *26* (7), 1707-1711.
- [115] Wunderlich, B. *Thermal Analysis of Polymeric Materials*; Springer, Berlin, Germany, 2005, p. 140.
- [116] Van Krevelen, D.W. *Properties of Polymers. Their correlation with chemical structure; their numerical estimation and prediction by additive group contributions*; Elsevier: Amsterdam, 1997.
- [117] Gaur , U.; Wunderlich, B. Study of Microphase Separation in Block Copolymers of Styrene and a-Methylstyrene in the Glass Transition Region Using Quantitative Thermal Analysis. *Macromolecules* **1980**, *13* (6), 1618-1625.
- [118] Morfin, I.; Ehrburger-Dolle, F.; Grillo, I.; Livet, F.; Bley, F. ASAXS, SAXS and SANS investigations of vulcanized elastomers filled with carbon black. *J. Synchrotron Radiat.* **2006**, *13*, 445-452.
- [119] Mansilla, M.; Rodriguez Garraza, A.; Silva, L.; Salgueiro, W.; Macchi, C.; Marzocca, A.; Somoza, A. Evolution of the free volume and glass transition temperature with the degree of cure of polybutadiene rubbers. *Polym. Test* **2013**, *32* (4), 686-690.
- [ 120 ] Zorn, R.; McKenna, G. B.; Willner, L.; Richter, D. Rheological Investigation of Polybutadienes Having Different Microstructures Over A Large Temperature-Range. *Macromolecules* **1995**, *28* (25), 8552-8562.

- [121] Hofmann, A.; Alegría, A.; Colmenero, J.; Willner, L.; Buscaglia, E.; Hadjichristidis, N. Secondary and Segmental Relaxation in Polybutadienes of Varying Microstructure: Dielectric Relaxation Results. *Macromolecules* **1996**, *29* (1), 129–134.
- [122] Inai, M.; Aizawa, S.; Ito, M. Phase Control of BR/SBR Blends by Silica Particles. *Soft Matter* **2007**, *3*, 64-69.
- [123] Le, H.H.; Keller, M.; Hristov, M.; Ilisch, S.; Xuan, T.H.; Do, Q.K.; Pham, T.; Stockelhuber, K.W.; Heinrich, G.; Radusch, H.J. Selective Wetting and Localization of Silica in Binary and Ternary Blends Based on Styrene Butadiene Rubber, Butadiene Rubber, and Natural Rubber. *Macromol. Mater. Eng.* **2013**, *298*, 1085-1099.
- [ 124 ] Nagaraja, S.M. *Influence of filler network topology and immobilized rubber on reinforcement in natural rubber composites containing different nanoparticles*. Martin Luther University Halle Wittenberg, *Master thesis*, 2015.
- [125] Da Silva, C. A.; Weydert, M.; Budde, H.; Wendler, U.; Menzel, M.; Bartke, M.; Beiner, M. Interrelations between morphology and softening behavior in self-assembled poly (butadiene-*block*-(styrene-*stat*-butadiene)) copolymers. *Rubber Chem. Technol.* **2016**, *In-Press*.
- [126] Semenov, A. N. Theory of Block-Copolymer Interfaces in the Strong Segregation Limit. *Macromolecules* **1993**, *26* (24), 6617-6621.
- [127] Fetters, L.J.; Lohse, D.J.; Colby, R.H. *Physical Properties of Polymers Handbook*; Mark, J.E., Ed.; Springer publisher: Ohio, USA, 1996.
- [128] Russell, T. P.; Hjelm, R. P.; Seeger, P. A. Temperature-Dependence of the Interaction Parameter of Polystyrene and Poly(Methyl Methacrylate). *Macromolecules* **1990**, *23* (3), 890-893.

- [129] Hashimoto, T.; Shibayama, M.; Kawai, H. Domain-Boundary Structure of Styrene-Isoprene Block Copolymer Films Cast from Solution. 4. Molecular-Weight Dependence of Lamellar Microdomains. *Macromolecules* **1980**, *13* (5), pp 1237–1247.
- [130] Mukai, U.; Gleason, K.K.; Argon, A.S.; Cohen, R.E. Poly(dimethylsiloxane)/Nylon-6 Block Copolymers: Molecular Mobility at the Interface. *Macromolecules* **1995**, *28* (14), pp 4899–4903.
- [131] Hempel, E.; Hempel, G.; Hensel, A.; Schick, C.; Donth, E. Characteristic length of dynamic glass transition near T-g for a wide assortment of glass-forming substances. *J. Phys. Chem. B* **2000**, *104* (11), 2460-2466.
- [132] Gordon, M.; Taylor, J. S. Ideal Copolymers and the 2Nd-Order Transitions of Synthetic Rubbers .1. Non-Crystalline Copolymers. *J. Appl. Chem.* **1952**, *2* (9), 493-500.
- [133] Ellison, C. J.; Torkelson, J. M. Sensing the glass transition in thin and ultrathin polymer films via fluorescence probes and labels. *J. Polym. Sci. Part B Polym. Phys.* **2002**, *40* (24), 2745-2758.
- [134] Yin, H.; Napolitano, S.; Schonhals, A. Molecular Mobility and Glass Transition of Thin Films of Poly(bisphenol A carbonate). *Macromolecules* **2012**, *45* (3), 1652-1662.
- [135] Jackson, C. L.; McKenna, G. B. The Glass-Transition of Organic Liquids Confined to Small Pores. *J. Non-Cryst. Solids* **1991**, *131*, 221-224.
- [136] Schonhals, A.; Goering, H.; Schick, C.; Frick, B.; Zorn, R. Glassy dynamics of polymers confined to nanoporous glasses revealed by relaxational and scattering experiments. *Eur. Phys. J.* **2003**, *12* (1), 173-178.
- [137] Ngai, K. L.; Beiner, M. Secondary relaxation of the Johari-Goldstein kind in alkyl nanodomains. *Macromolecules* **2004**, *37* (21), 8123-8127.

- [ 138 ] Lodge, T.P.; McLeish, T.C.B. Self-Concentrations and Effective Glass Transition Temperatures in Polymer Blends. *Macromolecules* **2000**, *33* (14), 5278-5284.
- [139] Hempel, E.; Beiner, M.; Renner, T.; Donth, E. Linearity of heat capacity step near the onset of  $\alpha$  glass transition in poly(*n*-alkylmethacrylate)s. *Acta Polym. Sin.* **1996**, *47* (11), 525-529.
- [140] Kahle, S.; Korus, J.; Hempel, E.; Unger, R.; Horing, S.; Schroter, K.; Donth, E. Glass-Transition Cooperativity Onset in a Series of Random Copolymers Poly(*n*-butyl methacrylate-*stat*-styrene). *Macromolecules* **1997**, *30* (23), 7214-7223.
- [141] Donth, E. Characteristic Length of Glass-Transition. *J. Polym. Sci. Part B Polym. Phys.* **1996**, *34* (17), 2881-2892.

## **Acknowledgement**

I am thankful to God for giving me strength, knowledge and for brightening my paths. Without Him I would not have been able to accomplish this task. I am also deeply grateful to my beloved husband and my family for their unmeasurable love, care, patience and for holding me tight when I was sometimes about to fall. They are my source of inspiration, happiness and reason for always looking ahead.

I am truly fortunate for having Prof. Dr. Mario Beiner as my supervisor during these three and half years of PhD. I will never forget our nice discussions, the personal advice he gave me, the trainings and his immense patience. Although, we have been through many difficulties, I am certain a better supervisor I could not have deserved. It was a great pleasure to share this experience with someone knowledgeable like him and above all humble.

My gratitude also goes to Marc Weydert, my advisor, for always guiding me in my PhD research as well as in the company. Thanks for his coaching and for teaching me so many things like how I can increase my assets. Thank you to Benoit for his technical support and funny conversations.

I am also thankful to my friends from Halle: Sriharish, Micjel, Alfred, Ramona, Annegret, Tamara, Anas and Jacqueline for the wonderful and funny times we spent together. I also want to extend my thanks to my work colleagues from Schopau PAZ for giving me support, affording really nice lunch times and helping when I most needed it.

My deep gratitude also goes to my friends Carlos and Davide for being “pendejos”, who were always keeping me up with their stupid and funny jokes. I wish to pay special thanks to all my colleagues at Goodyear for sharing nice moments at the coffee machine and in the corridors.

I thank the Fonds National de la Recherche for the financial support.

# Curriculum Vitae

## Cecília Aguiar da Silva

### Personal data

**Address:** Rue de Neuerburg 18  
L-1221, Luxembourg

**Date of birth:** 19/12/1986

**Place of birth:** Recife/PE- Brazil

**E-mail:** cecilia\_aguiardasilva@goodyear.com

**Nationality:** Brazilian

**Marital status:** Married

**Languages:** Portuguese (native speaker), English (fluently), German and Spanish (intermediate)

---

### Education

**Since 2013** PhD student in polymer physics at Goodyear Luxembourg Tires S.A / Martin-Luther-University Halle-Wittenberg /Fraunhofer Gesellschaft e.V.  
Supervisor: Prof. Dr. habil. Mario Beiner

**2010-2012** M.Sc. in Polymer Engineering  
Martin-Luther-University Halle-Wittenberg, Germany  
Master thesis approved with grade 1.3 (3.0-1)  
Supervisor: Prof. Dr. habil. Mario Beiner

**2005-2010** B.Sc.in Chemical Engineering  
Federal University of Pernambuco, UFPE, Recife, PE, Brazil  
Undergraduate thesis approved with grade 10.0 (0-10.0),  
Supervisor: Prof. Mohand Benachour

**2002-2004** High School  
Colégio Santa Maria Master, Abreu e Lima, PE, Brazil

---

### Work experience

**Since 2013** PhD student at Goodyear Luxembourg Tires S.A / Fraunhofer Gesellschaft e.V./ Martin-Luther-University Halle-Wittenberg  
Recipient of Fonds National de la Recherche Luxembourg PhD grant's (FNR)  
Subject: Dissipation and reinforcement in composites with self-assembled block copolymer matrices.  
Supervisor: Prof. Dr. habil. Mario Beiner

**2012** Master thesis at Fraunhofer IWM/ Martin-Luther-University Halle-Wittenberg  
Subject: Characterization of oriented block copolymers by rheo-optical vibrational spectroscopy and development of a method to correlate their molecular orientation with their mechanical behavior.  
Supervisor: Prof. Dr.-Ing. R. Weidisch

- 2011-2012** Project work at Martin-Luther-University Halle-Wittenberg  
Subject: Mechanical, rheological and surface properties of thermoplastic polymers modified by polydimethylsiloxane-urea copolymer based masterbatch.  
Supervisor: Prof. Dr.-Ing. H.-J.Radusch
- 2011-2012** Research fellow (student job) at Martin-Luther-University Halle-Wittenberg  
Activities: Preparation of samples and measurements of tensile test, surface tension and rheology.  
Supervisor: Prof. Dr.-Ing. H.-J.Radusch
- 2010-2011** Research fellow at the Leibniz-Institut für Pflanzenbiochemie  
Activities: Synthesis of dendrimers  
Supervisor: Prof. L.A. Wessjohann
- 2009** Trainee in the laboratory of plaster analysis of Roca Brazil S.A.  
Activities: Analysis of plaster samples  
Supervisor: Mr. Mário Alexandre Cunha.
- 2007-2009** Recipient of an Institutional Scientific Initiation Fellowship (PIBIC) of the CNPq (National Counsel of Technological and Scientific Development)  
Subject area: Chemistry, Analytic chemistry  
Activities: Analysis of wine samples  
Supervisor: Dr. A.P. Paim – UFPE – Brazil
- 2006-2007** Recipient of an Institutional Scientific Initiation Fellowship (PIBIC) of the CNPq (National Counsel of Technological and Scientific Development)  
Subject area: Chemistry, Organic synthesis  
Activities: Synthesis of larvicidal compounds  
Supervisor: Prof. R.M. Srivastava – UFPE - Brazil
- 

## Other skills

- Computer skills MS Office and Origin
- Techniques GPC, DSC, DMA, NMR, FTIR, Tensile test, and Contact angle
- Statistics

## Publication

1. Da Silva, C.A.; Budde, H.; Menzel, M.; Wendler, U.; Bartke, M.; Weydert, M.; Beiner, M. Interrelations between morphology and softening behavior in self-assembled poly(butadiene-*block*-(styrene-*stat*-butadiene)) copolymers. *Rubber Chem. Technol.* **2016**, DOI: <http://dx.doi.org/10.5254/rct.16.84842>, *In-Press*.
2. Da Silva, C.A.; Budde, H.; Menzel, M.; Wendler, U.; Bartke, M.; Weydert, M.; Beiner, M. Self-assembled structure and relaxation dynamics of diblock copolymers made of polybutadiene and styrene/butadiene. *RSC Adv* **2016**, 6, 50460–50470.

## **Erklärung**

Hiermit erkläre ich, Cecilia Aguiar da Silva, dass ich die vorliegende Dissertation selbstständig und nur unter Verwendung der im Literaturverzeichnis zitierten Quellen und Hilfsmittel angefertigt habe.

Desweiteren erkläre ich, dass ich die vorliegende Dissertation an keiner anderen Hochschule oder Universität eingereicht habe, noch mich mit einer anderen Arbeit erfolglos um den Doktorgrad beworben habe.

Halle Saale, den Oktober .2016

Cecilia Aguiar da Silva